Terms and Conditions of Use of Digitised Theses from Trinity College Library Dublin

Copyright statement

All material supplied by Trinity College Library is protected by copyright (under the Copyright and Related Rights Act, 2000 as amended) and other relevant Intellectual Property Rights. By accessing and using a Digitised Thesis from Trinity College Library you acknowledge that all Intellectual Property Rights in any Works supplied are the sole and exclusive property of the copyright and/or other IPR holder. Specific copyright holders may not be explicitly identified. Use of materials from other sources within a thesis should not be construed as a claim over them.

A non-exclusive, non-transferable licence is hereby granted to those using or reproducing, in whole or in part, the material for valid purposes, providing the copyright owners are acknowledged using the normal conventions. Where specific permission to use material is required, this is identified and such permission must be sought from the copyright holder or agency cited.

Liability statement

By using a Digitised Thesis, I accept that Trinity College Dublin bears no legal responsibility for the accuracy, legality or comprehensiveness of materials contained within the thesis, and that Trinity College Dublin accepts no liability for indirect, consequential, or incidental, damages or losses arising from use of the thesis for whatever reason. Information located in a thesis may be subject to specific use constraints, details of which may not be explicitly described. It is the responsibility of potential and actual users to be aware of such constraints and to abide by them. By making use of material from a digitised thesis, you accept these copyright and disclaimer provisions. Where it is brought to the attention of Trinity College Library that there may be a breach of copyright or other restraint, it is the policy to withdraw or take down access to a thesis while the issue is being resolved.

Access Agreement

By using a Digitised Thesis from Trinity College Library you are bound by the following Terms & Conditions. Please read them carefully.

I have read and I understand the following statement: All material supplied via a Digitised Thesis from Trinity College Library is protected by copyright and other intellectual property rights, and duplication or sale of all or part of any of a thesis is not permitted, except that material may be duplicated by you for your research use or for educational purposes in electronic or print form providing the copyright owners are acknowledged using the normal conventions. You must obtain permission for any other use. Electronic or print copies may not be offered, whether for sale or otherwise to anyone. This copy has been supplied on the understanding that it is copyright material and that no quotation from the thesis may be published without proper acknowledgement.

Laser Speckle Correlation as a Non-Contact Ocular Microtremor Measurement Technique

By Emer Kenny BSc. (hons), MSc.

A thesis provided to Trinity College, University of Dublin in part fulfillment of the thesis requirements for the degree of Doctor of Philosophy.

Department of Clinical Medicine,

University of Dublin,

Trinity College,

Dublin 2.

Declaration

I declare this thesis to be entirely my own work and not been submitted as an exercise for a degree at this or any other university.

The library may lend or copy this thesis upon request.

Name: Emer Kenny

Date: 3 April 2014

Thesis Summary

Ocular microtremor (OMT) is high frequency, low amplitude fixational eye movement present in all healthy people. It occurs even while the eye appears to be at rest. Benefits of measuring OMT have been proven in a number of clinical conditions. For example, in coma the peak frequency of OMT is known to decline, while for brain stem death, no peak frequency is present.

To date, the most widely used research tool to measure OMT has been an eye-contacting piezoelectric probe technique (PZT). The PZT technique has a number of limitations, including patient discomfort. Ideally, for practical clinical use, a device to measure OMT would be non-contact. The aim of this thesis is to investigate and develop a non-contact method to measure OMT in the human eye.

The technical design of a speckle correlation system to measure OMT is detailed in chapter two. The results of testing the system at OMT-like amplitudes and frequencies are shown and it is verified that the technique is suitable to measure OMT.

The effects on the speckle correlation technique of measuring displacements from a 'non-ideal' surface are investigated in chapter three. It is shown that a calibration error is introduced into the measurement by multiple scattering of light within a surface volume.

The implications of biospeckle, a time-varying form of speckle, are investigated in chapter four. Biospeckle is shown to disrupt the stability of the speckle images over time. However, provided each frame is cross-correlated with the previous frame, the

stability of speckle images captured from the eye are shown to be of a sufficient stability to measure OMT-like displacements.

Chapter five details the results of a pilot study on using the speckle correlation technique on a group of twenty volunteers. The results show that the measurement device was capable of measuring OMT parameters.

Acknowledgements

I want to express my gratitude to everyone who helped in any way for this thesis. In particular, I would like to thank my supervisors Dr. Gerard Boyle and Prof. Davis Coakley. Their support, guidance and encouragement throughout the project was immeasurable.

Thanks to the staff in the Mercer's Institute and the Medical Physics departments of St. James's Hospital, especially Dr. Ciaran Finucane, Dr. Chris Soraghan and Tim Foran, for all their help. Particular thanks to Dr. Niamh Collins for all her time explaining OMT to me.

Thanks to all those who volunteered to have measurements taken, including Nuala Maguire, Ciaran Kenny, David Fitzpatrick and Aoife O'Donoghue.

Finally, I would like to thank my parents, nana and friends for all of their support over the years. Special thanks to my brother, Ciaran, who proof read this thesis and corrected spelling, much like he did with my diary when we were children!

Abbreviation of Terms and Acronyms

DIC	Digital Image Correlation
EMCCD	Electron Multiplying Charged Couple Device
FWHM	Full Width Half Max
GLCM	Gray Level Co-Occurrence Matrix
IM	Moment of Inertia
LASCA	Laser Speckle Contrast Analysis
MPE	Maximum Permissible Exposure
MSAF	Multiple Scatter Amplitude Factor
NR	Newton Raphson
OMT	Ocular Microtremor
PZT	Piezoelectric Technique
THSP	Time History Speckle Pattern

Contents

Chapter 1: Literature Review

Chapter 2: OMT Measurement Using Laser Speckle Metrology

Chapter 3: Investigation of Scattering Influence on Speckle Correlation Technique

Chapter 4: Characterisation of Biospeckle from the Human Eye Sclera

Chapter 5: OMT Measurement *in-vivo* by Laser Speckle Correlation Metrology

Chapter 1

Literature Review

1 Introduction

This chapter reviews the literature relevant to ocular microtremor (OMT) and to laser speckle. The chapter is broken into five main sections. Section 2 reviews the characteristics, clinical relevance and measurement techniques for OMT. Section 3 details laser speckle and statistics to describe speckle. The use of laser speckle in metrology is discussed in Section 4. The dependence of speckle on the material from which it originates is reviewed in Section 5. Finally, Section 6 reviews the literature relevant to biospeckle.

2 Fixational Eye Movements

2.1 Anatomy of the Eye

The review of the anatomy of the eye in this section is mainly adopted from Beers *et al.* [1], unless otherwise stated.

The sclera is the tough, stiff, white outer layer of the eye. It is a dense connective tissue that covers nearly 80% of the eye and serves to protect the inner components of the eye [2]. The sclera provides structural integrity to the eye and maintains the eye's shape.

Due to spatial fluctuations in the refractive index of the scleral tissue, it is opaque to light. It scatters almost all wavelengths of visible light, causing it to appear white.

The sclera is 0.3-1.35 mm thick and consists of three layers; the episclera, the scleral stroma proper and the lamina fusca [3]. Beneath the sclera lies the vascular membrane that consists of a network of blood vessels that supply blood to the eye.

Light enters the eye through the cornea, a transparent section on the front of the eye (see figure 1). The cornea has a diameter of about 10 mm and is transparent, allowing for more than 90% of incident light to be transmitted [2]. Along with the sclera, the cornea also serves as a protective covering for the eye. The cornea helps focus light on the retina at the back of the eye. After travelling through the cornea, light passes through the pupil.

The iris is the circular, coloured area of the eye. It serves to control the amount of light that can enter the eye by dilating the pupil, allowing more light into the eye in a dark environment and less in a bright environment.

The lens is behind the iris. By changing shape, the lens focuses light onto the retina. The retina contains the cells that sense light and the blood vessels that nourish them. Photoreceptors in the retina convert an image into electrical impulses. Linked to each photoreceptor is a nerve fibre. The combination of nerve fibres from the photoreceptors form the optic nerve. The optic nerve carries these impulses to the brain, where they are interpreted.

An ophthalmic and a retinal artery provide blood supply to the eyes. Blood is carried away from the eye by an ophthalmic and a retinal vein. These blood vessels enter and exit through the back of the eye.

Figure 1 shows the anatomy of the eye. The eyelids spread tears over the surface of the eye when blinked. The function of tears is to keep the surface of the eye moist. The lacrimal nerve stimulates the tear glands to produce tears. In the absence of moisture, the cornea can become dried, injured, infected and impenetrable to light.

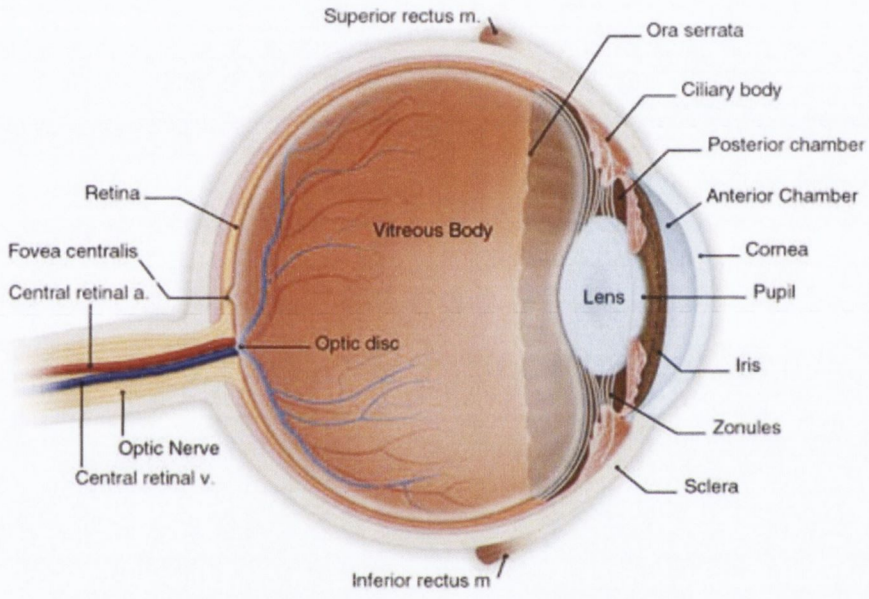

Figure 1. Anatomy of the eye.

The ocular motor system works to direct both eyes towards the object to be viewed. The eye is moved by six extrinsic muscles [4]; four rectus (superior, inferior, medial and lateral) and two oblique (superior and inferior). Figure 2 illustrates these muscles. Every movement of the eye involves all these muscles to some degree. The ocular motor system directs and holds the eye on a target using six different types of eye movement; fixational, vestibular, optokinetic, smooth persuit, saccades and vergence. Each muscle is stimulated by a specific cranial nerve.

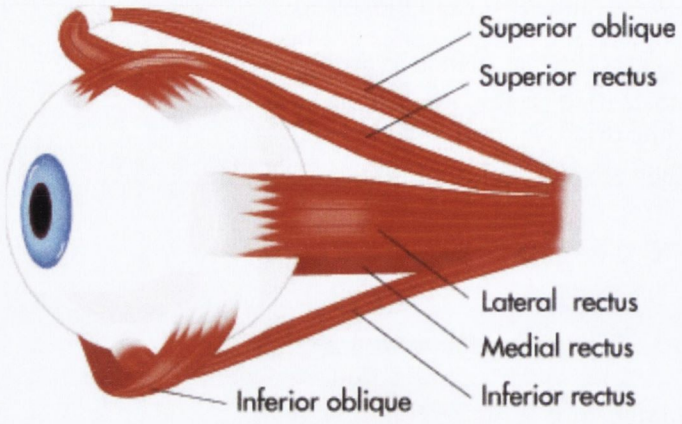

Figure 2. Extrinsic muscles of the eye.

2.2 Fixational Eye Movements

Adler and Fliegelman [5] were the first to describe fixational eye movements in detail. Later experiments by Ratliff and Riggs [6] and Ditchburn and Ginsburg [7] confirmed the existence of the movements. Fixational eye movements are present in all subjects even while the eye appears to be at rest. They are composed of three types of involuntary eye movement; microsaccades, drift and ocular microtremor [5, 8]. The movements prevent visual fading during fixation [8].

Recently, Pansell *et al.* [9] have investigated evidence of a possible fourth fixational eye movement, moving with a low frequency of 0.04-0.1 Hz and amplitude of less than 3.49 mrad. However, the existence of this potential fourth type of fixational movement is yet to be accepted in the literature.

2.2.1 Microsaccades

Microsaccades are the largest, fastest type of fixational eye movement. They have an amplitude of about 1.45 mrad, however, as noted by Martinez-Conde *et al.* [8] the amplitude of microsaccades alone is not a good descriptor because the amplitude of voluntary saccades can be just as small as microsaccades. Microsaccades occur intermittently about 1-2 times a second and their frequency varies between subjects [10, 11]. Microsaccades occur simultaneously in both eyes [12]. A possible role for microsaccades in vision is to correct for the displacement in eye position caused by drifts [12].

2.2.2 Drift

Drift is a slow continuous irregular movement that takes place between microsaccades. It occurs simultaneously with microtremor and has an amplitude of about 290μrad. The frequency of drift is 2-5 Hz [13]. Drift is not thought to be conjugate between the eyes [12].

2.2.3 Ocular Micro Tremor

Ocular microtremor (OMT) is the smallest of the involuntary eye movements. It has an amplitude range of 150-2500 nm (12-216μrad rotational) peak-to-peak. The frequency range of OMT is between 20-150 Hz with an average peak frequency of 84 Hz [14] for a normal subject. It is a non-periodic, continual, high frequency, wave-like physiological tremor [15, 16]. Studies have found no significant difference between OMT measurement in the left and right eye [17] and OMT movement is not conjugate [18]. It is believed that OMT arises from brainstem neurons [13, 16, 19].

2.3 Features of the OMT Signal

Figure 3 shows a typical OMT record of a normal subject. As shown, the OMT record contains 'bursts' of activity with an intervening 'baseline' signal. Bolger [20] noted that almost half of an OMT trace consists of bursts.

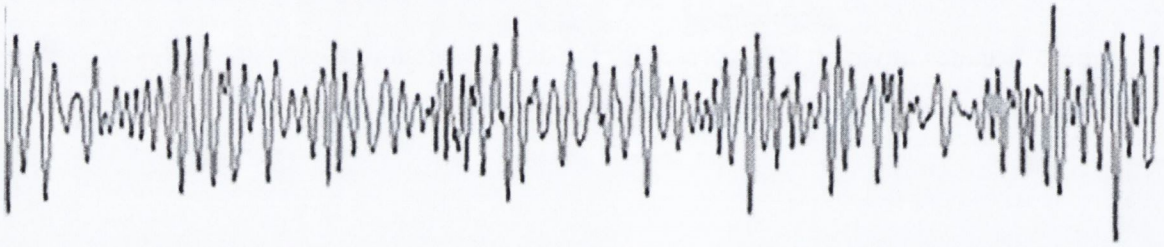

Figure 3. OMT trace from a healthy subject.

The two main identifiers of OMT that have been used in the literature are the OMT frequency and OMT burst/baseline features. Burst/baseline features are assessed in terms of their frequency of occurrence, duration and frequency content. OMT frequency is the indicator of most clinical interest. Several authors have reported various estimates for the frequency of OMT for the open eye, ranging from a mean of 30 to 100 Hz [5, 12-14, 21-23]. Two studies on OMT frequencies for the closed eye found values of 85 Hz [24] (median frequency) and 65 Hz [25] (mean frequency). It is possible that the variation in estimated frequency is due to the various recording techniques used. Bolger *et al.* [14] performed the largest study to date (105 healthy subjects) of OMT frequency in the normal subject and reported a mean value of 84 Hz for the peak frequency, measured using the peak counting technique.

Sheahan [26] described the shape of OMT spectra and identified two main types of shape. Type one spectra have a significant portion of high frequency content, while type two have no significant high frequency peaks. Type one and type two spectra are shown in figure 4.

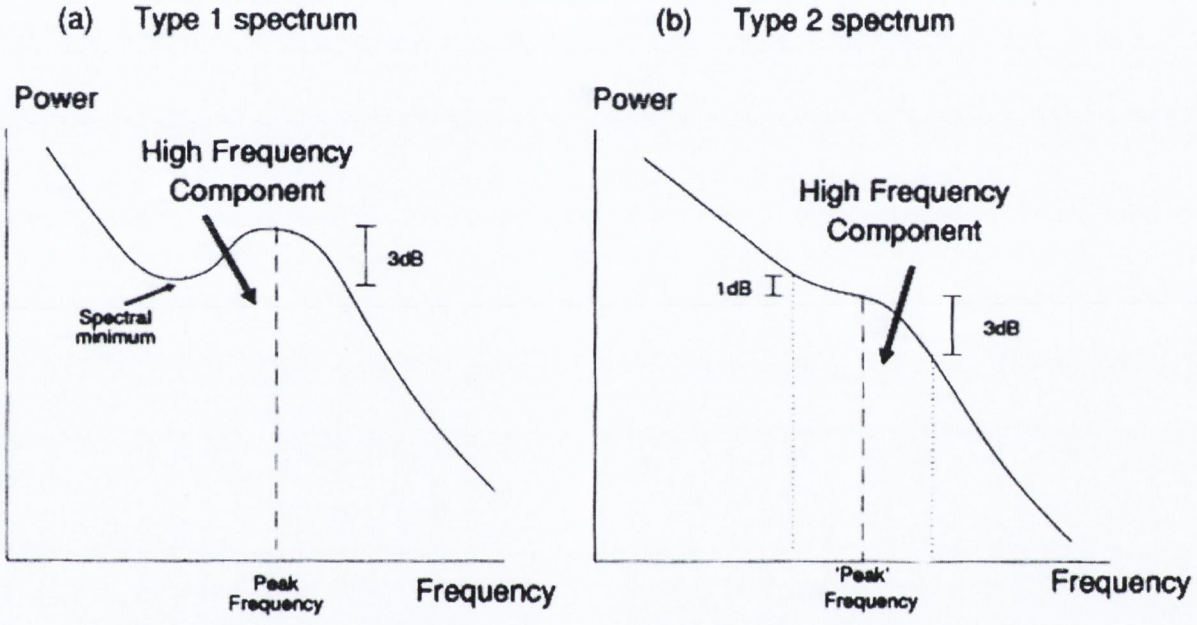

Figure 4. Type one and type two OMT spectra, as defined by Sheahan [26].

The amplitude of OMT is generally not used as an identifier because most OMT research has been performed using a piezoelectric probes (PZT) technique which has a low amplitude accuracy.

Bolger [20] identified six main reproducible parameters to describe the OMT record and help distinguish a normal from an abnormal signal. To calculate these parameters the entire record is analysed, bursts are marked by a trained observer and the remainder of the signal is defined as the baseline signal. The following parameters are then calculated by averaging the segments of burst and baseline in the OMT signal;

1. Number of bursts per second i.e. the number of bursts divided by entire record duration.
2. Mean duration of bursts i.e. the summed durations of burst segments divided by number of individual bursts.
3. Percentage of the record that is baseline i.e. the summed durations of baseline segments divided by total record duration.
4. Frequency content of bursts i.e. the number of peaks per unit time for all burst segments.
5. Mean duration of baseline i.e. the summed durations of baseline segments divided by number of baseline segments.
6. Frequency content of baseline i.e. the number of peaks per unit time for all baseline segments.

The above parameters are, however, subjective since they are inspected visually by an observer and depend on what the observer considers to be a burst within the signal. This manual method of analysis can lead to measurement errors and inter-observer inconsistency has been cited as a source of variance in OMT measurement [17]. Further drawbacks of this method of OMT analysis are that it is time-consuming, not inherently reproducible and that a skilled observer (trained in principles of OMT) is required to examine the data.

As mentioned previously, microsaccades occur intermittently and the frequency of occurrence of microsaccades varies between subjects. Microsaccades disrupt the results of parameters recorded from an OMT signal and need to be removed before signal processing. Because of their inconsistency, a reliable method is needed to remove them. Al-Kalbani [27] investigated methods of automated analysis and feature extraction for OMT signal analysis. In the work by Al-Kalbani, five methods of microsaccade

removal were investigated; a wavelet method, a filtering method, a cutting method, a multiresolution method and an adaptive time-varying filter method. The ability of each method remove microsaccades from OMT data was compared in terms of recovering the OMT signal. The input data used simulated signals derived from PZT measurements, taking 20 OMT traces from normal subjects, as well as 20 OMT traces from patients with neurological diseases. The results found that the wavelet method showed the best performance for microsaccade removal and had the lowest distortion of the OMT signal.

The number of bursts per second (i.e. the peak count) is the most simple, and most commonly used, estimate of OMT frequency. Initial work on a method to automate the peak counting was investigated by Sheahan [26]. Recently, Al-Kalbani [27] developed a custom OMT software analysis package, built in LabView [28]. The software incorporated the wavelet method of microsaccade removal and included a Gabor time-varying filter to automatically identify bursts in a signal. The software is capable of automatically calculating OMT features and returns a frequency spectrum plot of the input signal. The benefit of the automatic feature analysis was demonstrated by its incorporation into the OMT studies conducted by Collins [11].

2.4 Measurement Of Ocular Micro Tremor

Of all forms of eye movement, OMT is possibly the most difficult to measure. The recording of a movement with such small amplitude and fast frequency places a high demand on a measurement system. Although a large number of commercial eye trackers exist, none have the resolution or sensitivity required to measure OMT movement.

The following sections review some of the measurement techniques used to measure OMT. Generally, OMT has been measured in the horizontal plane and with the subject fixating in a 'straight ahead' or 'primary' position.

2.4.1 Contacting Methods to Measure OMT

2.4.1.1 Contact Lens Based Methods

A reflection mirror technique was the first technique used to measure fixational eye movements. Using this technique, a beam of light is reflected by a mirror to a photosensitive detector. Alder and Fliegelman [5] attached the mirror directly to the eye sclera. Ratliff and Riggs [6] performed a similar technique, except they attached the mirror on a contact lens on the sclera.

A scleral search coil technique was implemented by Robinson [29]. For this technique, a coil of wire is embedded in a scleral contact lens placed on a subject's eye. The subject is then exposed to an alternating magnetic field and the voltage generated across the coil is used to measure the eye movement.

A drawback of these methods, aside from their invasive nature, is that the use of the contact lens renders the technique impractical for measurement on a large population. Intrinsic to their viability is that the contact lens correctly fits the subject's eye so that slippage does not occur.

2.4.1.2 Piezoelectric Probe Technique

The piezoelectric technique (PZT) is the most extensively used and validated method to measure OMT. Bengi and Thomas [30] were the first to design a piezoelectric strain

gauge method to record OMT. Work to update the design was performed by Sheahan [26, 31] and, most recently, by Al-Kalbani [27].

Figure 5 shows the PZT system in use. Prior to measurement with the piezoelectric technique, a drop of anesthetic must be placed on the eye and the eyelid is held open either by tape or by surgical eyelid retractors. The PZT probes consist of a piezoelectric element with a piece of rubber attached and are brought into contact with the sclera near the scleral/corneal border using a head-mounted, operator-adjusted mechanism. Piezoelectric materials have the capacity to convert mechanical energy to electrical energy and vice-versa. When the eye moves, it triggers the piezoelectric material to bend. This bending creates a voltage across the material and the voltage is used to measure the eye movement that took place.

The piezoelectric technique provides an accurate representation of the frequency pattern of OMT, but not of the amplitude. As previously noted, studies using this technique quote only the frequency content of the pattern. Al-Kalbani [27] showed the PZT probes to have a variation in amplitude caused by probe loading, i.e. it was shown that the sensitivity of the probes changed with pressure and the way in which the eye reacts to the probe also changes.

Figure 5. PZT system used by Collins [11].

Sheahan *et al.* [17] performed a study on the sources of variance in OMT measurement using the PZT probe technique. The results showed a significant difference between consecutive recordings from one eye, indicating that the set-up contributes some variance to measured OMT frequency. The intra-subject standard deviation ranged from 4-11 Hz between the most and least experienced operator. Recently, McCamy *et al.* [32] discovered that the PZT sensor affects microsaccades in a complex way and that the oculormotor system adjusts to the stress brought on by the sensor by adjusting the amplitude of the microsaccades [32]. Collins [11] reported that the OMT test procedure using the PZT probes could potentially cause phobic or anxiety reactions in subjects. Drawbacks of the PZT technique include the requirement to anaesthetise the eye, as well as patient discomfort.

2.4.2 Non-Contacting Methods to Measure OMT

2.4.2.1 Photography Techniques

Barlow [33] devised a photography technique to measure eye movement. The technique involved placing one drop of mercury on the subject's cornea and another on their forehead. Images of the drops were recorded through a microscope onto film. Movements of both eye and head were measured from the record of the movements of the drop on the cornea, while head-only movements were measured by the drop on the head. The method was sensitive enough to record OMT, but could not measure it accurately [34].

2.4.2.2 Corneal Reflection

The front surface of the cornea reflects part of the light falling it. The reflected image is virtual and referred to as the 'corneal reflex' or 'first Purkinje' image. When the eye rotates, the corneal reflex moves. Eye movements can be detected by tracking the corneal reflex with use either of a film, video camera or photodetector. Eizenman *et al.* [35] used corneal reflection in an attempt to measure fixational eye movements. The eye was illuminated by an infrared laser and the corneal reflex was captured on a photodetector array. The resolution of the system was not adequate to resolve OMT from background noise in the signal, though spectral features of OMT were found upon spectral analysis.

Non-contacting eye movement measurements, such as corneal reflection, are prone to contamination by head movements. Dual Purkinjie Image (DPI) tracking [36, 37] is a more complex corneal reflection technique designed to be sensitive only to eye movements. In this method, both the corneal reflex (the 1st Purjinkie image) and the image formed by the back surface of the eye's lens (the 4th Purjinkie image) are tracked.

During translation of the eye caused by a head movement, the two images displace together, but when the eye is rotated, the two images displace in a different manner. The separation between these images is then exploited to measure eye-only angular rotations. Despite the added complexity involved in this technique to ensure that eye-only displacements are measured, the accuracy of the method when implemented by Cornsweet and Crane [37] was only found to be comparable to that of Eizenman's corneal reflex method.

2.4.2.3 Speckle Interferometry

Boyle *et al.* [21, 38] employed a laser interferometry method for non-contact OMT measurement. The setup for the technique is shown in figure 6. Boyle's system used the eye sclera as a target for two interfering laser beams. The system was tested *in-vivo* on a small sample of 10 volunteers. The results gave a mean frequency of 79.5 Hz and mean amplitude of 728 nm (63 μrad) peak-to-peak. The outcome of this work was that it showed the feasibility of employing interferometry as an OMT measurement technique and the feasibility of using the eye sclera as a target for the laser beams. The in-plane speckle interferometer system had a resolution of 100 nm (8.66 μrad), which is sufficient to capture OMT, but about four times lower than the ideal resolution [26]. The physical bulk of the optics involved in the system design reduced the probability of its practical *in-vivo* application.

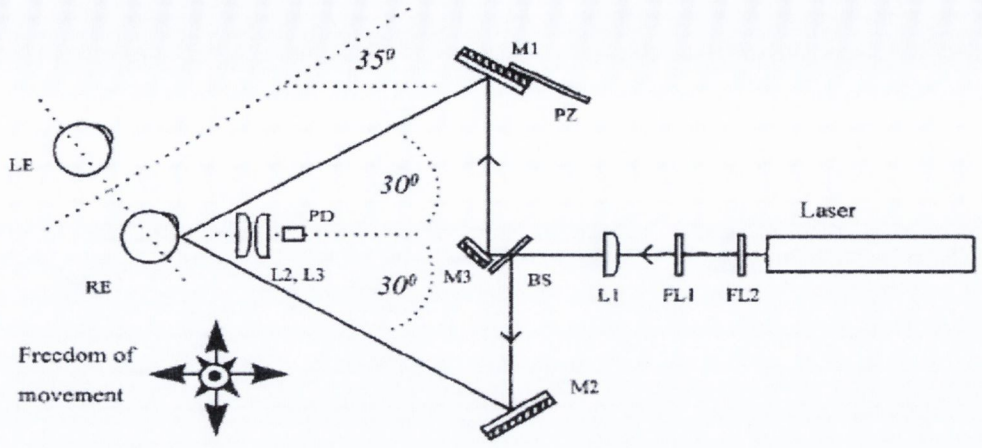

Figure 6. Set-up used by Boyle [38].

To expand the work by Boyle, Ryle *et al.* [39, 40] designed a compact speckle interferometric OMT measurement technique using optical fibers, however, the technique was never tested *in-vivo*.

Neither of the above studies investigated the possible influence of biospeckle [41] on the measurement results. As will be explained in section six of this literature review, biospeckle is caused by phase changes in the speckle from a living surface. Speckle interferometric methods rely on measuring phase changes caused by object motion to infer displacement. Any phase changes due to biospeckle could obscure the measured displacement result.

2.5 Clinical Investigations of Ocular Micro Tremor

The frequency of OMT has been demonstrated to change in a number of clinical conditions.

Coakley and Thomas [42] investigated OMT in 41 healthy and 70 unconscious subjects. An abnormal OMT pattern with an absence of normal burst activity was noted for the unconscious subjects. The average mean OMT frequency for these unconscious subjects was determined to be about half the value estimated for healthy subjects. A low initial frequency was found to be a poor prognosis for regaining consciousness.

In a similar study on OMT and coma, a falling OMT frequency was found to be associated with a poor prognosis and likely death. Conversely, an increasing OMT frequency was associated with a positive prognosis and emergence from coma [43]. A correlation between OMT frequency and the standard method of assessing consciousness, the Glasgow Coma Scale, was demonstrated by Bolger *et al.* [44]

In a study by Coakley and Thomas [45] on six subjects with clinical signs of brain death, all six showed complete absence of ocular microtremor when it was recorded shortly before death. It was argued that OMT could be used as a monitor of brainstem death and viability. A later study by Bolger *et al.* [46] used a larger sample size of 32 patients with suspected brain stem death. The results of this study agreed with those of Coakley and concluded that no OMT activity was found for patients with suspected (and later confirmed) brain stem death.

OMT has shown potential as an indicator of the depth of anesthesia [24, 25, 44, 47]. Changes in OMT frequency have also been noted in cases of Multiple Sclerosis [22] and Parkinson's disease [48]. OMT is thought to originate from the brainstem and, as such, has potential as a measure of brainstem integrity. A conclusive method to indicate brainstem death would have a large clinical significance. The full potential of OMT as a clinical tool is yet to be realised.

2.6 Non-Clinical Factors that Influence OMT

Some studies have been performed on investigating the non-clinical factors that influence OMT measurement.

Bengi and Thomas [49] conducted a study of factors that influence the OMT signal from healthy subjects. They found a change in the frequency spectrum of OMT with eye gaze position. When the eye was adducting (looking towards the nose) a flatter spectrum with an increased frequency content was noted. More recently, Collins [11] also reported on a change in OMT frequency with eye position. The study by Collins on twelve healthy subjects also showed the frequency of OMT to increase with deviating eye position. Notably, a difference in the frequency increase (compared to the frequency in the primary position) between abducting (looking away from the nose) and adducting eye positions was found. An increase of 4.3 Hz was found when the eye was abducting and a larger increase of 9.5 Hz was found while the eye was adducting.

Age-related physiological changes are known to occur in the eye [1]. Bolger [23] investigated the baseline and burst pattern of 72 healthy subjects aged between 21-88 years old. The subjects were split into seven different age groups and OMT signals were recorded using the PZT technique. A small but significant change in frequency parameters (overall frequency, baseline frequency and burst frequency) were found between subjects aged under 60 years and those aged over 60 years.

Collins [11] investigated the effects of caffeine and alcohol on the OMT signal of healthy subjects. The results of the study showed that acute alcohol intoxication led to a small but significant reduction in OMT peak frequency parameters. Similarly, a moderate intake of caffeine also resulted in a small but significant increase in OMT peak frequency.

A small experiment [49] on three subjects found no significant difference between the spectrum of OMT recorded in total darkness and in ambient light conditions.

2.7 Need for New Measurement Device

Due to the invasiveness and difficulties associated with measuring OMT, studies of OMT are far rarer than studies of drift or microsaccades; both of which can be measured using conventional eye tracking systems. Some of the key difficulties and limitations of the methods used to measure OMT to date are that they have been eye-contacting, have only measured OMT in the horizontal direction and have not successfully measured the amplitude of OMT. These issues have restricted a broader understanding of OMT.

The primary disadvantage of the PZT technique for OMT measurement is that it is invasive. Ideally, for clinical use, a high resolution, non-contacting method for OMT measurement is required. A non-contact device for OMT measurement would greatly aid research on the role of OMT in vision. While the role of microsaccades in vision has been widely researched [50], the contribution of OMT to vision is unknown. An understanding of the role of OMT is out of reach at present since it is not possible to measure OMT amplitude during visual tasks.

As already stated, most OMT measurement devices provided reliable, absolute data only on the frequency content of the signal. The amplitude of OMT may, however, have a clinical significance. Coakley et al. [51] measured OMT during sleep and found a relative reduction in amplitude to be the most notable feature of the results. The measured OMT trace in sleep was different to previous findings for subjects in a coma. Coakley postulated that in coma, the amplitude might be normal but that a low frequency dominates the record. Despite this, accurate measurement of OMT amplitude

has proven difficult with the currently available measurement devices and any possible application of OMT amplitude, rather than frequency, as a clinical marker remains unexplored.

OMT studies have focused on the detailed investigation of OMT in the horizontal direction. One study by Bengi and Thomas [49] has reported on both the horizontal and vertical frequency spectra of OMT. As part of the study, OMT recordings of five healthy subjects, fixating in the primary position were taken. A difference between the overall shape of the spectra of the horizontal and vertical component of OMT was observed, though both spectra gave similar peaks in the 70-80 Hz range. Very little else is known about trends in the vertical component of OMT. Ideally, a measurement system would simultaneously record both the horizontal and vertical components of OMT.

Due to the minute size and high frequency content of the signal, the requirements for an OMT measurement system present a technical challenge. Sheahan [26] outlined some of the specifications required for an OMT measurement system. They proposed that a measurement system should have a dynamic range of 25-2500 nm (2-216 μrad), a resolution of 25 nm (2 μrad) and a frequency response (maximum deviation from peak frequency) of 2 dB. Conventional eye trackers are unsuitable for OMT measurement because, due to their technological limitations, they are unable to achieve the resolution required to capture small eye movements in the range of OMT.

Preferably, an OMT measurement device would be sufficiently portable and robust to be used bed-side in a clinical environment.

2.8 Speckle Correlation for OMT Measurement

Optical methods of displacement measurement have the advantage of being non-contact, highly sensitive and capable of a high resolution.

In this work, it is aimed to develop a speckle correlation technique to measure OMT. OMT has never been measured using a laser speckle correlation technique. As will be detailed later, speckle correlation techniques can measure resolutions in the scale required for OMT.

Compared to the speckle interferometry method implemented by Boyle [21, 38], speckle correlation has a simpler set-up. Speckle interferometry requires a second reference beam while speckle correlation needs only one beam. The speckle interferometry used a photodiode to record speckle and hence only captured one-dimensional displacement. The use of an imaging camera with the speckle correlation technique would allow for two-dimensional OMT measurement and the possibility of measuring both the horizontal and vertical components of OMT. Given its ease of setup and achievable resolution, the technique could work well for practical non-contact OMT measurement.

3 Speckle

3.1 Introduction

Speckle originates from light scattered from a rough surface. Under coherent illumination, a wave reflected from a rough surface consists of contributions from many independent scattering centres. These contributions interfere with each other to form a speckle pattern. The intensity of the speckles in the pattern is given by the algebraic

addition of wave amplitudes. High intensity bright spots result from highly constructive interference, while low intensity dark spots result from highly destructive interference. The random pattern formed by the surface structure is reproducible provided all conditions remain the same. An example of a speckle pattern is shown in figure 7.

Speckle patterns occur only when the illuminated surface is non-specular (i.e. when most of the radiation is scattered rather than reflected). In white (incoherent) light illumination, this effect is unnoticed due to a lack of spatial and temporal coherence.

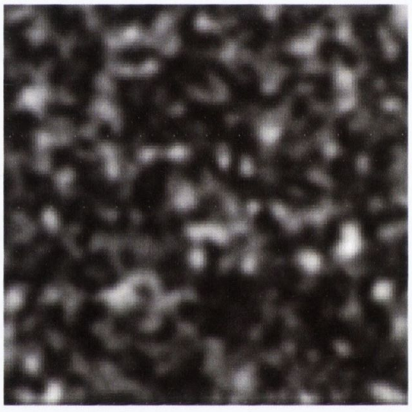

Figure 7. Sample speckle pattern.

3.2 Properties of Speckle

Goodman has provided a comprehensive review of the properties of speckle [52]. The theory in the following section is primarily derived from his work, unless otherwise stated.

Generally there are two types of speckle: (i) objective speckle, formed in free space and usually observed on a screen placed a particular distance from the object and (ii) subjective speckle, formed in the image space of an optical system.

Objective laser speckle (or far-field speckle) has a size approximately equal to the diameter of the illuminating laser beam's Airy disc. The size σ_o of objective laser speckle is related to the width D of the illuminating beam on the object, the wavelength λ and the distance to the observing screen L, such that:

$$\sigma_o = 1.22\frac{\lambda L}{D} \qquad \textbf{Equation 1}$$

The subjective speckle (or imaging speckle) size is dependent on properties of the laser beam and the parameters of the optical system used to record the speckle. It is given by:

$$\sigma_s = 1.22\frac{\lambda z}{D} \qquad \textbf{Equation 2}$$

where z is the lens-to-object distance. The subjective speckle size calculation is often more convenient when given in terms of the properties of a lens. The F-number is the ratio of the lens focal length to the entrance pupil diameter and is given by:

$$F = \frac{f}{D} \qquad \textbf{Equation 3}$$

where f is the focal length of the lens. Substituting for D, the subjective speckle size can be rewritten as:

$$\sigma_s = (1 + m)\lambda F \qquad \textbf{Equation 4}$$

where m is the magnification of the imaging system and λ is the wavelength of the illuminating light. By use of this equation, the F-number of a lens can be used to control the speckle size in an experimental design. Note that for fully developed speckle (explained in the next section), the speckle size is independent of the type of surface being illuminated.

The complex patterns produced by speckle are described using probability and statistics [52, 53]. Statistical properties of speckle can be divided into those of the first and those

of the second order. Statistics of the first order describe the properties of a speckle field at a single point in space or time, these include the intensity probability distribution function $p(I)$ and the speckle contrast C. Second order statistics describe the joint properties of speckle at two points in either space or time, or the properties of a single point in two different speckle patterns. They characterise the size and the distribution of speckle sizes in the pattern. These statistics are usually described in terms of the autocorrelation function of intensity fluctuations.

3.3 First-Order Statistics of a Fully Developed Speckle Pattern

3.3.1 Speckle Amplitude

The speckle phenomenon is mathematically similar to the random walk problem and as such, the mathematical principles of the random walk problem are adopted for interpretation of speckle [54].

Each point on an illuminated surface can be considered to absorb and re-emit light, acting as a source of spherical waves similar to Huygens-Fresnel secondary waves [55]. The complex amplitude of the scattered light at any point in space is given by the sum of the amplitudes from each point on the surface. The light field at a specific point in a speckle pattern is the sum of a large number N of components representing these contributions from all points on a scattering surface. This is analogous to a random walk in mathematics, whereby components consisting of random or known amplitude and of random phase add together, as illustrated in figure 8.

Under illumination by monochromatic and fully polarized light, the complex amplitude of a speckle field is described by a random phasor sum [41, 52] i.e.:

$$A = \frac{1}{\sqrt{N}} \sum_{n=1}^{N} a_n e^{i\phi_n} \qquad \textbf{Equation 5}$$

where a_n and ϕ_n are, respectively, the amplitude and phase of the nth phasor component.

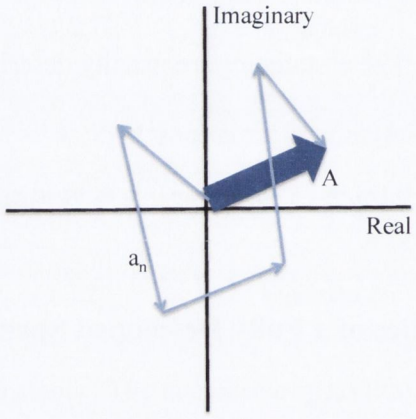

Figure 8. Phasor diagram representing a random walk. Field components a_n add together to contribute to the total field A.

Equation 5 holds true assuming that:

(1) the amplitude a_n and phase ϕ_n of each field component are statistically independent of each other and are also independent of the amplitude and phase of all other field components and

(2) the phases ϕ_n are uniformly distributed on the interval $(-\pi, \pi)$ which means that the surface is rough in comparison to the wavelength,

with the additional hypothesis that the total number of scattering centres N is very large the validity of the central limit theorem is ensured [52].

3.3.2 Speckle Intensity

A 'fully developed' speckle pattern can originate only from the interference of light that is fully polarized in the same direction. In this case, the speckle field itself will then be similarly polarized. For a fully developed speckle field, the probability that the intensity I at any point lies between I and $I+dI$ is given by:

$$P(I)dI = \frac{1}{<I>} exp\left(\frac{-I}{<I>}\right) \quad \textbf{Equation 6}$$

where $<I>$ is the intensity of the speckle pattern, averaged over many points in the scattered field. From this equation, it is apparent that the brightness distribution of a fully developed speckle pattern is governed by a negative exponential relationship. Speckle patterns that obey this criterion are known as fully developed speckle patterns.

Figure 9 shows a theoretical plot of $P(I)dI$. The plot shows that the most probable intensity value for a speckle is black, i.e. there are more dark speckles in a pattern than those of any other intensity.

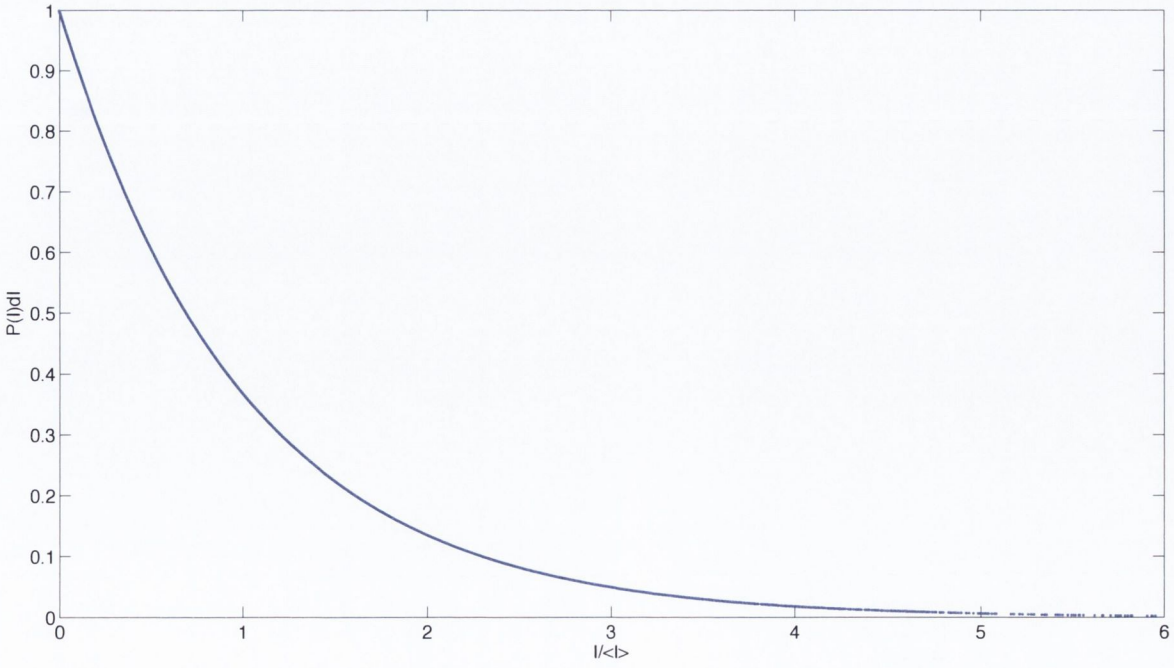

Figure 9. Speckle Intensity Distribution

It can be shown that the mean value of the square of the speckle intensity (i.e. $<I^2>$) is equal to $2<I>^2$ [52] and that the standard deviation of intensity σ_I is given by:

$$\sigma_I^2 = \langle I^2 \rangle - \langle I \rangle^2 = 2\langle I \rangle^2 - \langle I \rangle^2 = \langle I \rangle^2 \qquad \textbf{Equation 7}$$

This equation shows that the standard deviation, σ, of the intensity of a fully developed speckle is equal to the mean intensity $<I>$.

3.3.3 Speckle Contrast

An important quantity when discussing speckle is the speckle contrast, C, of a speckle pattern. Speckle contrast is defined as the ratio of the standard deviation to the mean value of the intensity i.e.:

$$C = \frac{\sigma_I}{\langle I \rangle} \qquad \textbf{Equation 8}$$

A speckle contrast of unity implies a fully developed speckle pattern. A fully reflecting surface will give a speckle contrast of zero and the contrast will increase up to unity as the roughness of the surface increases. In reality, speckle patterns often have a standard deviation less than the mean intensity and this is observed as a reduction in the contrast of the speckle pattern. Speckle patterns of this kind are referred to as 'partially developed' speckle patterns.

Factors which reduce the speckle contrast and result in partially developed speckle include; (i) the addition of a uniform background of light, (ii) the addition of another speckle pattern and (iii) a reduction in the roughness of the surface.

Speckle contrast is velocity and time dependent. If the speckles are moving fast relative to the integration time of the imaging system, they will result in a low spatial contrast and their speckle pattern will appear blurred. For this reason, speckle contrast can be utilised as a rough measure of speckle velocity. For example, if biospeckle activity (explained later) is high in an image, the rapid speckle velocity will result in a blurred, low spatial contrast pattern and the speckle contrast will decrease. The speckle contrast can then be used as a rough measure of the activity in a sample.

3.4 Second Order Statistics of a Fully Developed Speckle Pattern

3.4.1 Time History Speckle Pattern (THSP)

The Time History Speckle Pattern (THSP) is a tool that has been developed to qualitatively analyse a dynamic speckle pattern by observing the time evolution of the speckle [56]. To create a THSP, one column (for example the first column) from each speckle frame in a sequence of successive frames is taken and used to create a new composite image by placing the columns side-by-side in the new image. The x-axis of a THSP shows activity (change in intensity over time). If there is no activity, the pixel intensity does not change with time and the THSP will display straight horizontal lines. Conversely, if there is a lot of activity the change in neighbouring pixel intensities will be fast and the THSP will resemble a speckle pattern. The faster an object moves, the more rapid the speckle pattern intensity varies in time. The THSP can, therefore, be implemented to qualitatively show changes between speckle frames. Examples of a THSP for a sinusoidally moving object and for an object displaying high activity are shown in figure 10.

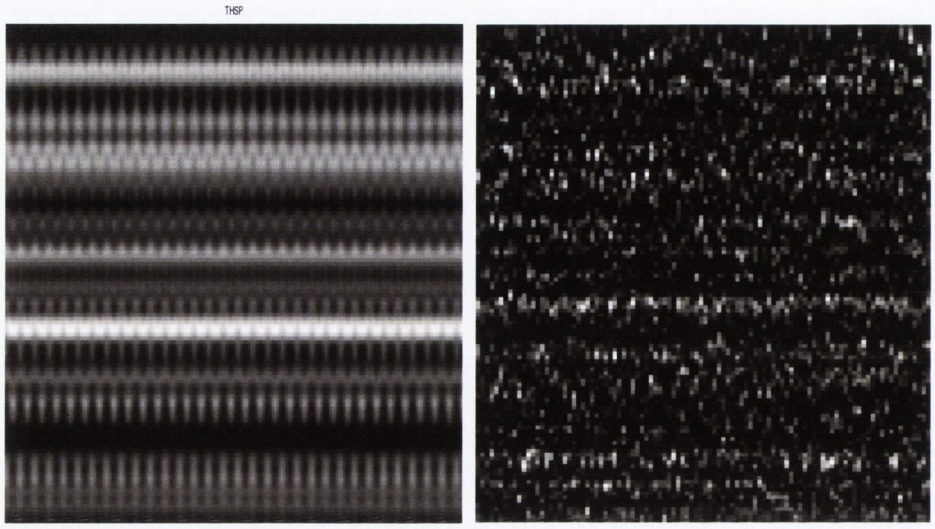

Figure 10. THSP for a series of sinusoidally moving speckle frames (left) and for a speckle frames that show a high activity (right).

3.4.2 Grey Level Co-Occurrence Matrix

Some studies [57, 58] involving dynamic speckle use the grey level co-occurrence matrix (GLCM) and the moment of inertia (IM) to analyse the THSP. An IM equal to zero implies a constant image, e.g. a THSP that shows no change in speckle over time. A high IM implies a high activity (variation in speckle over time). The absolute value of the IM does not provide useful information. It must be compared to a related set of experiments with the same conditions to provide a relative measure. The methods to calculate both the GLCM and IM are detailed below.

A grey level co-occurrence matrix (GLCM) [59] is a statistical method to show how many occurrences of pairs of pixel values are in an image. To create a GLCM the number of incidences of pairings of a certain pixel intensity *i* with pixel intensity *j* in a certain direction are recorded. As an example, consider the following image matrix and its GLCM calculated in the horizontal direction; $M = \begin{bmatrix} 0 & 0 & 1 \\ 2 & 2 & 0 \\ 1 & 2 & 2 \end{bmatrix}$

$$GLCM_M = \text{number of occurrences of pixel values} \begin{bmatrix} (0,0) & (0,1) & (0,2) \\ (1,0) & (1,1) & (1,2) \\ (2,0) & (2,1) & (2,2) \end{bmatrix} = \begin{bmatrix} 1 & 1 & 0 \\ 0 & 0 & 1 \\ 1 & 0 & 2 \end{bmatrix}.$$

For an 8-bit image, the intensities *i* and *j* vary between 0 and 255 and so the GLCM is a 256x256 matrix.

As illustrated in figure 11, the GLCM of an image (e.g. a THSP) that shows no activity (change over time) displays a line through the diagonal of the GLCM image matrix. This is because the occurrences of pixel pairs with the same intensity value over time is large. As the activity in an image increases the number of pixel pairings outside the diagonal increase and the GLCM shows some dispersion.

In order to use the information contained in the GLCM, Haralick *et al.* [59] defined statistical measures to extract textural characteristics of an image. For speckle analysis, the most important of these is the moment of inertia.

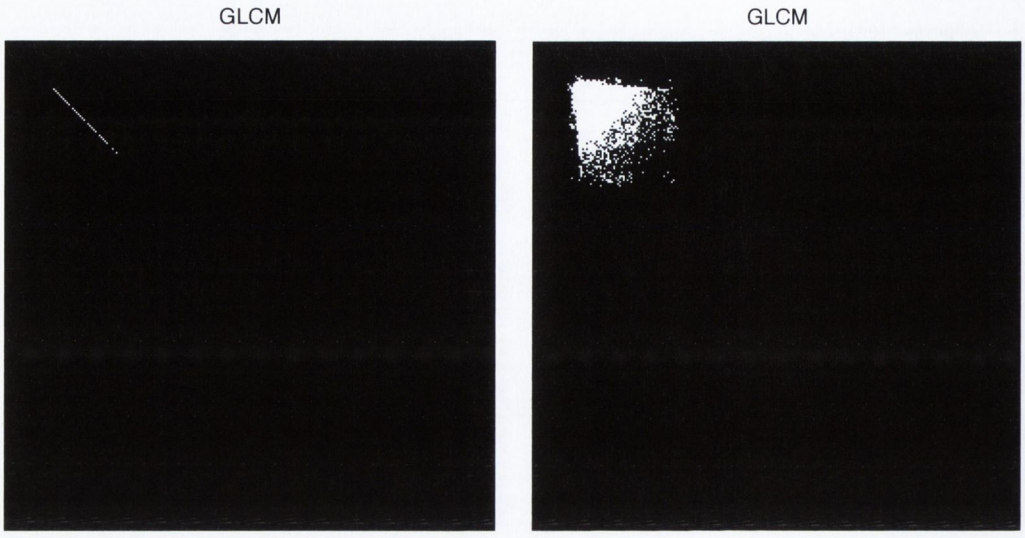

Figure 11. GLCM from a THSP of a series of speckle patterns showing low activity (left) and from speckle patterns showing high activity (right). The image on the right shows greater dispersion due to the higher activity.

3.4.3 Moment of Inertia

A measurement of the spread of values around the principal diagonal of the GLCM can be constructed by the sum of the matrix values times their squared row distance to the principal diagonal i.e.

$$IM = \sum_{i,j} M_{i,j}(i-j)^2 \qquad \textbf{Equation 9}$$

where M_{ij} is the normalized co-occurrence matrix.

Equation 5 defines the moment of inertia (IM) of the matrix with respect to its principal diagonal in the row direction. It is a measure of the intensity contrast between a pixel and its neighbour, over the whole image.

3.4.4 Other Statistics Derived from a Grey Level Co-Occurrence Matrix

Other statistics derived from the GLCM, namely the energy, homogeneity and correlation of the GLCM, not typically used for speckle analysis, are briefly explained here as their properties may be useful to characterise speckle patterns in more depth.

Correlation is a measure of how correlated a pixel is to its neighbour. A value of 1 indicates perfectly positively correlated images, while a value of -1 indicates perfectly negatively correlated images:

$$Correlation = \sum_{i,j} \frac{(i - \mu i)(j - \mu j)M_{i,j}}{\sigma_i \sigma_j}$$

Homogeneity returns a value that measures the closeness of the distribution of elements in the GLCM to the GLCM diagonal:

$$Homogeneity = \sum_{i,j} \frac{M_{i,j}}{1 + |i - j|}$$

Energy returns the sum of squared pixel values of the GLCM, it is equal to unity for a constant image:

$$Energy = \sum_{i,j} M_{i,j}^2$$

4 Speckle Metrology

Early investigations of speckle metrology used it as an alternative to holographic interferometry [53, 60, 61]. While speckle metrology has a range of applications including; velocity measurement [62, 63], stress/strain measurement [64-66] and surface roughness measurement [67-70], the application of most interest in this thesis is speckle displacement. When an object producing a speckle pattern is shifted in some way, the

speckle pattern it produces also becomes shifted. At least two speckle patterns belonging to the object are required to measure displacement, one before and one after the displacement.

Measurement techniques that compare speckle patterns for the purpose of displacement measurement can be broken into two groups; speckle interferometry and speckle correlation.

Speckle interferometry techniques measure displacement by recording the phase difference of scattered light before and after the displacement. The measurement results form fringe patterns. These fringe patterns need to be processed and phase analysis techniques are required prior to final calculation of the displacement. The speckle correlation technique, however, makes displacement measurements based on the intensity of a speckle pattern rather than the phase, i.e. they track positional changes of the speckles in a pattern.

The resolution achievable with both speckle techniques is comparable. Though speckle interferometry measurement requires high stability that is often unachievable in an uncontrolled environment such as a clinic. As previously stated, Boyle *et al.* [21, 38] used speckle interferometry for OMT measurement. The system designed by Boyle *et al.* had limitations, including the physical bulk of the optics. The intention of this thesis is to use speckle correlation as a method to measure OMT. For this reason, only speckle correlation techniques are discussed further.

4.1 Speckle Correlation

Early techniques [71] for speckle correlation involved recording a speckle pattern on a photographic plate before and after a displacement. The doubly exposed 'specklegram' was then optically Fourier transformed by illuminating a portion of the specklegram with coherent light. A fringe pattern would form in the rear focal plane of a positive lens and the period of the pattern was determined by the distance the object moved between speckle recordings.

Sutton *et al.* [72, 73] performed initial studies into digital image correlation. This technique replaced the photographic process and used a video recording system. Since then, advances in both sensor and processor technologies have resulted in studies on digital correlation techniques becoming more widespread [74-79]. Pan *et al.* [80] have conducted a comprehensive review of digital image correlation.

Digital image correlation (DIC) is an image processing technique performed to extract motion measurement from a series of consecutive images. The digital image of a speckle pattern consists of grey level intensity values at each pixel location. The DIC technique measures the similarity of two images in terms of their pixel grey levels. This is achieved by cross-correlating the two image matrices and locating the correlation peak i.e. the location where the two images are best matched. The cross-correlation can be performed in the spatial or the frequency domain. When the peak correlation location between image pairs is tracked over a number of image pairs, the displacement of the speckle over time can be calculated. Using known properties of the imaging system, the speckle displacement in pixels can then be converted to units of displacement of the moving object. Figure 12 displays the cross-correlation profile of two speckle images, taken at time t and time $t+\Delta t$.

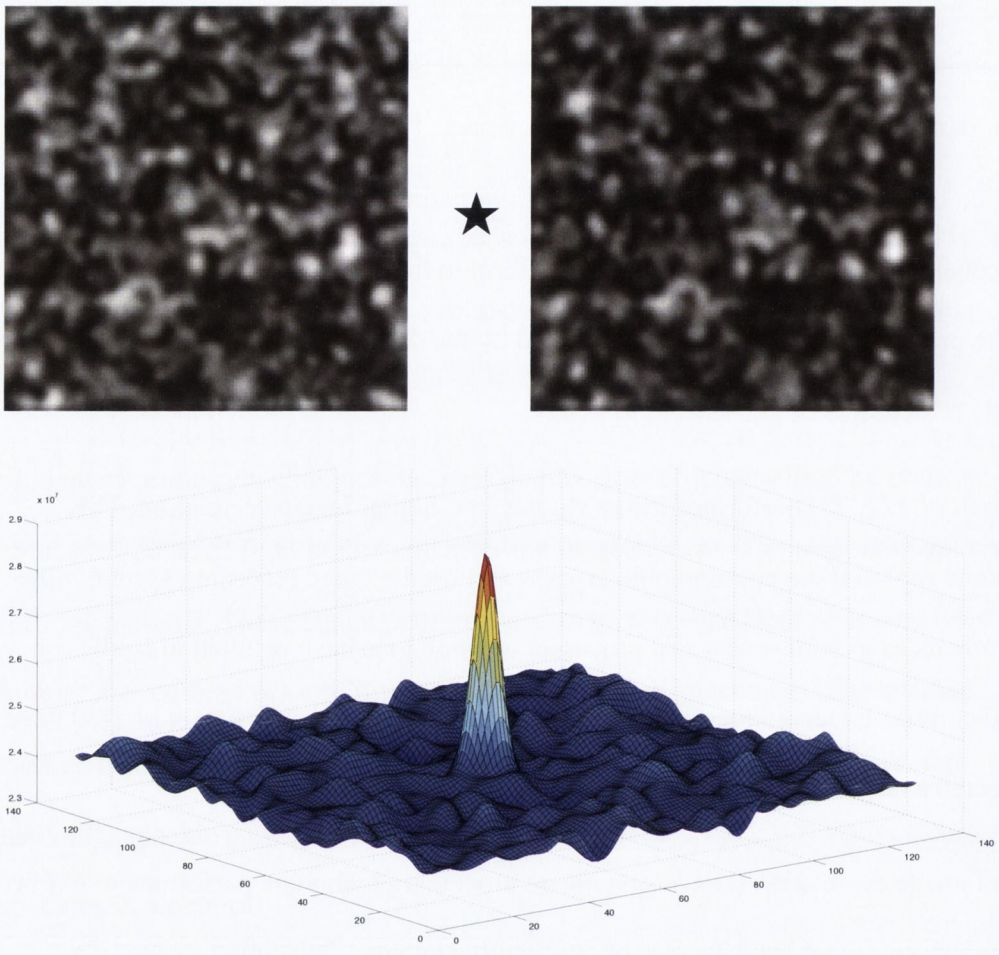

Figure 12. Speckle pattern at time t (top left) and the same pattern at time $t + \Delta t$ (top right). The bottom image shows the cross-correlation plot of the two speckle images. The location of the peak relative to the centre of the plot yields the displacement occurring between the two images.

Digital image correlation methods require the speckle images before and after a deformation to be relatively similar in terms of grey level distributions. However, as the object creating the speckle pattern displaces, some of the speckle observed on a screen will move off the screen as the pattern shifts. This results in a decorrelation between speckle image frames. The decorrelation leads to a reduction in the peak height of the cross-correlation between the images. If the speckle pattern changes completely,

decorrelation will be at a maximum and the cross-correlation method of displacement tracking will break down.

4.2 Speckle Pattern Quality for Digital Image Correlation

It is important that the cross-correlation peak be accurately measured so displacement can be acceptably converted to displacement. Factors that change the shape of the correlation peak, or influence it in some other way, are therefore of concern. For example, a broad peak leads to uncertainty in the exact peak location and therefore to a less accurate displacement. In the following sub-sections, the factors that influence the accuracy of the correlation algorithm are discussed.

4.2.1.1 Subset Size

A subset is an nxn group of elements originating from a larger NxN matrix. The size of the subset can vary. The cross-correlation subset size is a critical parameter in digital image correlation [81]. Generally, in order to obtain a reliable correlation result, the subset size should be large enough to contain a sufficiently distinctive intensity pattern. The subset size should also be large enough to sample a few speckles in order to ensure statistically sound results, although the benefits of a small subset size include a faster processing time.

Lecompte *et al.* [82] investigated the quality of speckle patterns for digital image correlation. In particular they studied the how the size of speckles and the pixel subsets influenced the displacement accuracy. In their work, they found that larger subsets gave the best results. However, the definition of the size of a large subset is objective and they note that the subset size should be chosen with consideration to the expected deformation.

4.2.1.2 Pixel to Speckle Ratio

The size of the speckles compared to the size of the imaging system's pixels influences the accuracy of the displacement measurement. If the speckle size is smaller than the pixel size, variations in intensity will not be resolved and speckle averaging will occur. This will result in a lower speckle contrast and to erroneous results. If the speckle size is much greater than the pixel size then the speckle pattern may not contain enough speckles to provide statistically significant results. The recommended pixel-to-speckle ratio varies in the literature [83, 84]. Lecompte *et al.* [82] argued that to achieve accurate displacement measurements, the speckle size should be chosen to be compatible with the subset size i.e. speckle sizes should be small for small subsets while larger subsets should have larger speckles.

4.2.1.3 Subpixel Correlation Algorithm

Due to the discrete nature of imaging pixel arrays, results of speckle displacement through basic cross-correlation peak tracking are given in integer values. Actual displacement is, generally, a non-integer value. To increase the accuracy and sensitivity of measurements, a subpixel algorithm is required to calculate the exact pixel displacement. The reported accuracy of subpixel algorithms varies in the literature, most studies report a value of 0.05 [85] or 0.01 pixels [86].

The three most common subpixel algorithms in the literature are gradient-based methods [87, 88], Newton-Raphson (NR) methods [89, 90] and curve-fitting methods [78]. Pan *et al.* [91] compared the performance of these three main algorithm types using computer simulated speckle images. The sensitivity and accuracy of each algorithm to successive 0.05 pixel displacements were calculated. The results showed

the NR method to be the most accurate but also the most time-consuming method. Curve-fitting methods, by comparison, were found to be simpler and more computationally efficient.

4.3 Speckle Correlation Techniques

4.3.1 In-Plane Speckle Correlation Technique

Speckle correlation can be used to measure both in-plane [92, 93] (translations normal to the optical axis) and out-of-plane [94-97], (rotational or along the optical axis) displacements. Speckle is more sensitive to motions along the optical axis than it is to in-plane motions [52].

Feiel *et al.* [65] developed a laser speckle technique to measure in-plane displacements from an object. In their experimental setup a two-point imaging geometry is implemented. The laser used in their experiment was 632.8 nm 10 mW HeNe laser. An f=50 mm lens was used to image the scattered light onto a CCD camera. An aperture stop was placed at the back focal plane of the lens in order to minimize speckle decorrelation and improve depth of focus by creating a telecentric system. Using this technique, Feiel *et al.* proved decorrelation to be the strictest limitation on using large magnifications. The technique was found to have a displacement sensitivity of 50 nm (4 μrad).

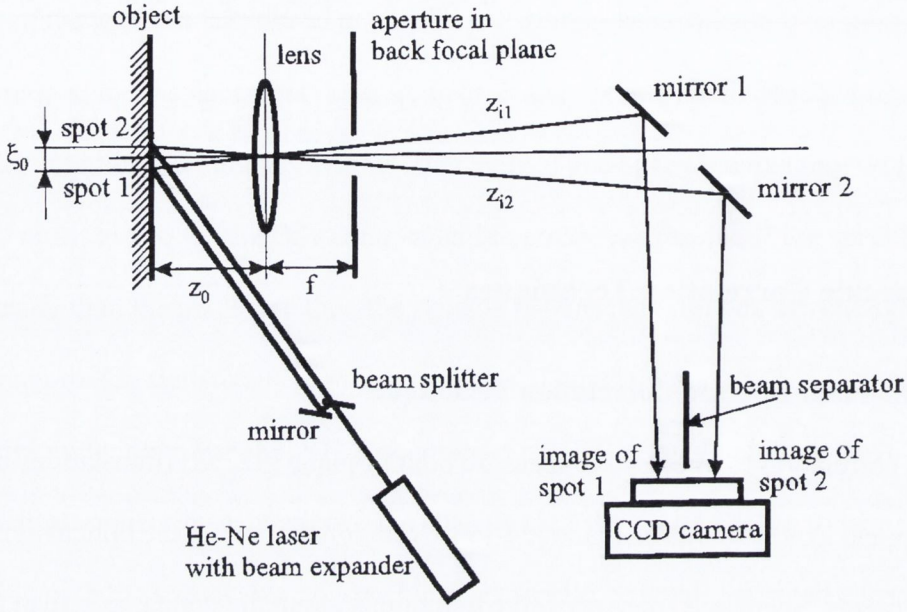

Figure 13. Experimental setup used by Feiel *et al.* [65].

4.3.2 Out-of-Plane Speckle Correlation Techniques

Figure 14 illustrates the geometry of a technique to measure tilt. The technique was first proposed by Tiziani [95] and was since adopted by Goodman [52]. For this technique, illuminating light is incident on a rough surface at an angle ψ_i. The speckle generated by the surface is recorded in the focal plane of a positive lens of focal length f. The angle of the central ray from the surface to the focal plane is ψ_r. A small angle ($d\phi$) tilt in the surface results in a rotation of the speckle pattern in the direction of tilt. This angle is given by $d\theta = \left(1 + \frac{cos\psi i}{cos\psi r}\right) d\phi$ [52]. If the tilt direction is parallel to the x-axis, then the speckle pattern, observed in the focal plane, translates a distance of $x_0 = f\tan(d\theta)$. Given small angles of ψ_i and ψ_r translated distance becomes $x_0 = f\tan(2d\theta)$.

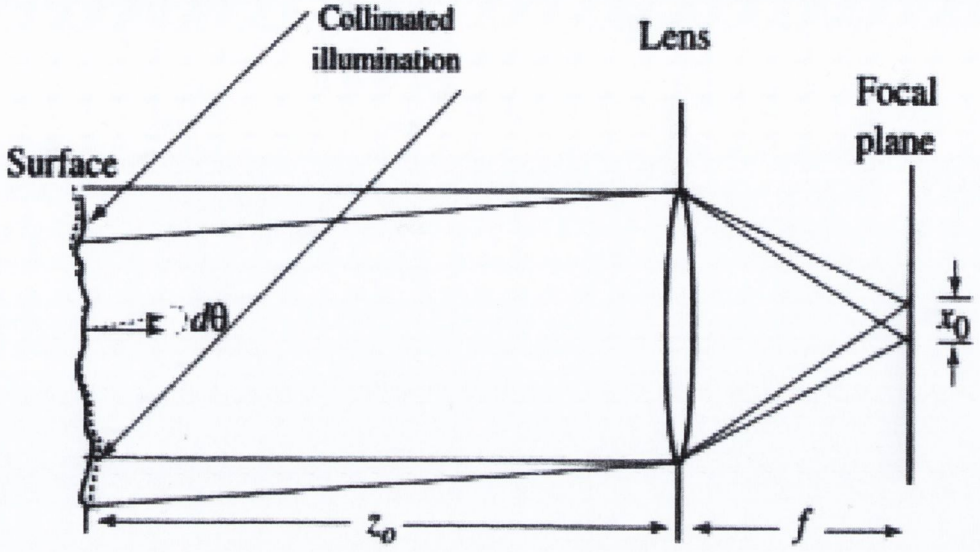

Figure 14. Geometry of a technique to measure tilt [52].

Rose *et al.* [96, 97] have proposed a more simple method of measuring angular speckle rotations. In their set-up, outlined in figure 15, light from a single laser beam illuminates a rough object through a beam splitter. Speckle from the target surface is recorded by an image sensor in the focal (i.e. Fourier) plane of the lens. The importance of imaging in the Fourier plane is that, by implementing it, the rotational displacement of the object is linearly mapped to the speckle displacement and is dependent only on the pixel size and lens focal length. The use of the beam splitter forsakes any dependence of the technique on incoming angle. Furthermore, in the study, Rose *et al.* showed the technique to be invariant to longitudinal or transverse motions of the object. These motions were shown to cause speckle decorrelation but not influence the angular displacement measurement. The sensitivity of the technique was reported to be approximately 5 μrad.

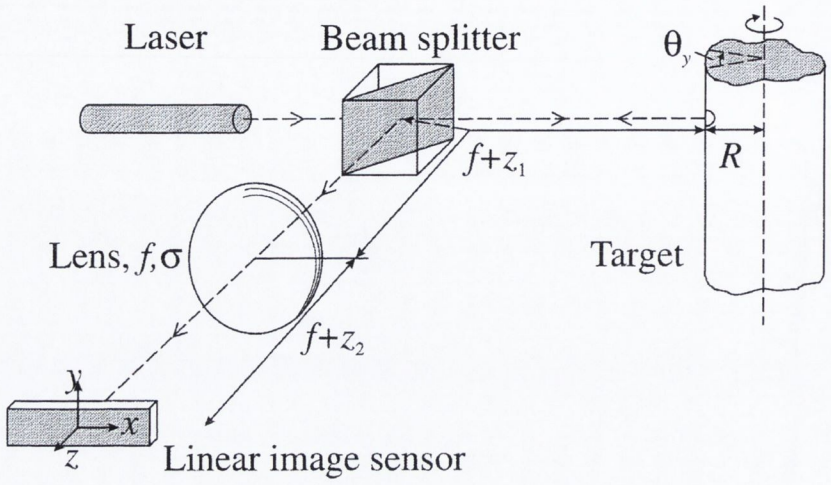

Figure 15. Angular rotation measurement setup used by Rose *et al.* [96, 97]

5 Speckle Dependence on Target Material

Using the Fourier plane technique described by Rose *et al.* and provided the speckle field obeys the assumptions outlined in section 3.3.1 and that the surface from which the speckle originates does not alter the polarization of incident light, the speckle reflected from it will essentially be independent of the surface properties. If, however, the surface does not adhere to the statement above, then the properties of the speckle pattern depend on the surface properties [53].

Sjodahl and Larsson [98, 99] used laser speckle correlation to study the changes in paper when it was exposed to a humid environment. They commented on the volume scattering nature of paper resulting in a rapidly changing speckle structure with small microstructural changes in the scattering volume.

5.1 Surface v Volume scattering

A fully developed speckle pattern consists of similarly polarized light [54]. When light penetrates a surface, multiple scattering can occur within the volume. Multiple scattering within the volume causes light to lose its original polarization and become randomly polarized. Hence, materials into which the light penetrates and is multiply scattered, depolarize the light and do not generate a fully developed speckle pattern. Figure 16 illustrates multiple scattering of incoming light in a volume.

Factors which influence the change in speckle polarization include the incident polarization state, the size and shape of the scatterers, the concentration of the scatterers and the refractive index of both the scatterers and the surrounding medium [100]. In the case of linearly polarized laser light, the speckle pattern emerging from a volume scattering object will consist of speckle that has retained its original polarization state, plus a component from randomly polarized heavily scattered light. Light which emerges in the orthogonal plane consists only of randomly polarized light.

Briers [101] has shown the surface scattered speckles to have a large angular dependence on the incoming light and to occur at angles near the optical axis. Volume scattered speckles, however, were shown to have a weak angular dependence and to emerge over a range of angles.

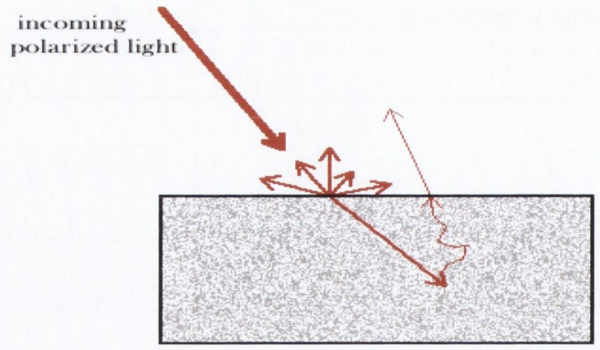

Figure 16. Incoming polarized light becomes scattered at a surface and multiply scattered within a volume.

A volume scattering material will depolarize the incoming light. Briers *et al.* [102] found the speckle pattern from a volume scatterer to be a superposition of two orthogonal speckle fields. The recorded intensity of a depolarized speckle pattern is considered to be the result of the sum of two polarized speckle patterns, one component perpendicular to the incident light and one parallel. In the absence of a polarizer between the object and image plane, both patterns become added on an intensity basis and the speckle contrast is reduced.

The addition of two partially correlated speckle patterns, such as those from two orthogonal polarization states, is detailed by Goodman [52]. The total intensity of such a speckle pattern is simply given by their vector sum [54] i.e.:

$$I(x,y) = |A_x(x,y)|^2 + |A_y(x,y)|^2 = I_x(x,y) + I_y(x,y)$$

I_x and I_y are the intensities of the x and y components of the reflected light and are assumed to be fully developed speckle patterns. A_x and A_y are the complex amplitudes of the speckle field in the x and y direction. I has a minimum contrast of $1/\sqrt{2}$, this occurs when I_x and I_y have equal average intensities.

The sum of M identically distributed, real valued, uncorrelated random variables have a mean value which is M times the mean of any one component and a standard deviation which is $\sqrt{M}$ times the standard deviation of one component [52]. The addition of M uncorrelated speckle patterns on an intensity basis results in a speckle contrast $C = \frac{\sigma}{<I>} = \frac{\sqrt{M}}{M} = \frac{1}{\sqrt{M}}$ [103]. In this case with two orthogonal speckle patterns (M=2) the speckle contrast reduces from unity to $= \frac{1}{\sqrt{M}} = \frac{1}{\sqrt{2}}$. Therefore, a depolarized speckle pattern has a lower speckle contrast than a fully developed speckle pattern. Hence the speckle contrast is lower for volume scattering than for surface scattering.

A surface that gives rise to multiple scattering, such as non-glossy paper, will appear partially or fully decorrelated when viewed through a polarizer rotated through 90 degrees [54]. When the reflection from an object becomes totally depolarized, the speckle contrast of the speckle pattern is $1/\sqrt{2}$, rather than unity.

In a study by Pajuelo *et al.* [104], they noted that the detected value of biospeckle activity was particularly sensitive to the direction of the analyzer that the light passed through prior to reaching the camera. In their case, they used the analyzer in the perpendicular position to increase the proportion of light scattered from inside their test object rather than from the object surface.

5.2 Tissue Optics

Most biological tissues produce strong scattering and are denoted scattering or 'turbid' media [105]. The turbidity of a sample is characterized by its scattering co-efficient μ_s. There is no definitive theory to describe light scattering by biological tissue. The

complex structure of tissue, high concentration of scattering particles, variability of particle size and shape make an optical model cumbersome [2].

When light reaches a biological object it can be reflected, scattered, absorbed or reradiated. The interaction of light with the matter depends on the wavelength of the light and on the structure of the matter. Tissue transparency is maximum in the near-infrared region, allowing up to several centimetres of light penetration [2].

Biological objects typically have a refractive index higher than air [41]. When laser light hits the air/biological object surface, part of the light is reflected and part penetrates into the surface. Absorption and multiple scattering occur within the surface and the laser beam broadens and weakens. Absorption causes a loss in the output light intensity while scattering diffuses the transmitted light in both spatial and temporal directions. Absorption and scattering are characterised by absorption and scattering coefficients for a particular medium and are wavelength dependent.

Biological objects can be separated into two categories; strongly scattering and weakly scattering. Strong scattering results from opaque tissue and fluids such as the eye sclera, skin, brain, vessel walls and blood. Weak scattering arises from transparent tissue or fluids such as the cornea, vitreous humour, aqueous humour and the front chamber of the eye [2].

5.2.1 Speckle Size

The parameters affecting the size of speckles reflected from volume scattering materials have been noted to be different to those from surface scattering materials. As outlined in section 3.2, the size of speckle from a surface is expected to be dependent on the optical properties of the lens, the pixel size and the laser wavelength.

Piederriere *et al.* [106] studied the size of backscattered speckles produced by strong scattering media. In their study they showed that for a given anisotropy co-efficient (a measure of the scatter retained in the forward direction after a scattering event), any rise in scattering co-efficient (probability of a photon scattering in the medium per unit length) widened the speckle size. Similarly, at a given scattering co-efficient, the size of the speckle grew when the anisotropy co-efficient was reduced. Their work showed that the size of speckles in a speckle pattern from a volume scatterer is dependent on the anisotropy and scattering co-efficient properties of the target material.

Xu *et al.* [107] have shown that speckles from inside a tissue have a smaller average size than those produced from the tissue surface. This smaller size is due to the expansion of the laser beam as it penetrates the object. When the light penetrates the surface, it becomes multiply scattered and the light that is scattered back exits through a larger area than it entered. This resulted in a smaller speckle size.

5.3 Methods to Reduce Multiple Scattering

Multiple scattering can be reduced simply by using an alternate laser wavelength or by reducing the size, thickness or scatterer concentration of a sample or. One technique to reduce multiple scattering is by binning [108]. In this technique, if the size of a single scattering speckle exceeds an area of several pixels, its intensity can be represented by the mean intensity of these pixels and the pixels are binned (i.e. grouped together as an average sum) accordingly. The binning results in suppression of the multiple scatter due to filtering out of speckles with a size smaller than the bin. The drawback of the technique is a reduction in spatial resolution.

Refractive index matching (or optical clearing) can also be implemented to reduce multiple scattering. Typically, the technique is used to reduce tissue scattering and increase light penetration through tissue by administration of an optical clearing agent to the tissue [110]. In general, the scattering co-efficient and the anisotrophy of a tissue are dependent on refractive mismatch between cellular tissue components. Refractive index matching through administration of the clearing agent leads to a reduction in the scattering co-efficient.

Lu *et al.* [109] investigated methods to reduce the effects of multiple scattering to aid better results in optical spectroscopy. They compared three of these techniques, namely; subtraction of orthogonal polarization states, use of an added absorber and spatial filtering. In the presence of scattering, the relationship between the attenuation by a sample and the absorption coefficient of the sample becomes non-linear. In the paper by Lu *et al.*, they compared the linearity of an attenuation versus absorption plot as a measure of the performance of the scatter reducing technique. Through this, they found that the subtraction of orthogonal polarization states was the most effective method of reducing multiple scatter. Polarization subtraction is based upon the polarization maintaining property of weakly scattered light. In it, the orthogonal component is subtracted from the component in the original polarization plane. Subtraction of the two components cancels the effects of randomly polarized light and allows polarization maintaining light to be extracted.

6 Biospeckle

The speckle pattern observed from a living object is found to vary in time. This form of speckle is known as biospeckle [41, 111]. In time, the speckles disappear, reappear and

change shape without any significant displacement of their position. Thus, the speckle pattern is time dependent. Often both translational speckle and biospeckle occur simultaneously. Dynamic speckle refers to both translational speckle movement and biospeckle. Translational speckle move as a whole and retain their individual shape as they move, an example would be a speckle pattern from a moving metal surface.

Biospeckle is strongly dependent on the structure and underlying activity of a living surface. Changes taking place on and inside the biological surface cause variations in the phases of the individual speckles which leads to the biospeckle [41]. As was previously mentioned, laser light that hits a biological surface will pass through a number of layers e.g. skin, blood, tissue. How far the laser penetrates into the tissue is dependent on tissue properties, such as the absorption coefficient, and on the wavelength of the laser light. Each layer that the laser reaches will act as a separate scatterer and cause the speckles in the resulting pattern to move and change shape. The overall reflected speckle pattern consists of 'boiling' speckles from each layer the light reached. A cell with high water content has more mobility and causes higher particle movement and therefore faster biospeckle-related changes, as evidenced in seed drying experiments [112].

6.1 Measures and Properties of Biospeckle

Like basic speckle, biospeckle can only be described statistically. Despite the complexity of the time-varying phenomenon some methods have been developed to quantify the temporal variation of biospeckle. Often, combinations of different parameters are used in conjunction to describe biospeckle patterns. Most statistics used to analyse dynamic speckle are based on the speckle contrast, or on second order

statistics evaluated using the THSP. There is no 'gold standard' to accurately describe and quantify the activity of biospeckle.

6.2 Applications of Biospeckle

Biospeckle approaches have been investigated for a range of non-medical applications, including plants [101, 107], fruits [101, 104, 114, 115] and seeds [116, 117]. Most of the detailed work on parameters to define properties of biospeckle originates from research in these areas.

Recently, potential clinical applications of biospeckle have become increasingly popular, though they have not yet been accepted into clinical routine. Optical methods of clinical imaging and measurement, based on analysis of laser light scattered by tissue, is appealing due to the possibility of real time imaging and results. A significant benefit of these methods is their non-contact, non-disturbing nature. The main clinical use of biospeckle is in measurement of tissue perfusion and blood flow mapping [118-122].

Early work on the application of biospeckle to blood flow measurements was performed by Fuiji *et al.* [123]. In their study, they investigated the time-varying properties of biospeckles in terms of their power spectra. The gradient of the power spectral density, expressed by the ratio of the high to low frequency components, was implemented as an indicator of mean velocity. The technique measured blood perfusion at a single point.

Modern methods of speckle-based flow monitoring use a laser speckle contrast analysis (LASCA) technique. This is a full-field, digital technique based on the spatial and temporal properties of speckle and can provide real time imaging. The principle behind

LASCA is that in areas of rapid flow, intensity fluctuations of the speckle pattern are fast and the observed speckle, integrated over the camera exposure time, becomes blurred. To quantify the blurring, the speckle contrast is used. A speckle contrast of 1 implies no blurring and no motion, whereas a value of 0 implies that the scatterers are moving fast enough to blur out the speckle completely.

The LASCA technique was first proposed Briers and Webster [124, 125]. To perform LASCA, the area to be studied is illuminated with laser light, typically a HeNe laser, and the intensity of the speckle pattern is recorded over time. An image is then made by calculating the speckle contrast, C, over a small nxn pixel sub-region of each recorded speckle pattern. The result of LASCA is a false-coloured contrast image representing the speckle contrast averaged over time. In their work Briers and Webster used an exposure time of 40 ms. Even at this relatively long exposure time, they found their measured velocity results for flow of red blood cells in capillaries to be comparable to known values.

To produce a speckle contrast image, it is important to match the sensor exposure time to the correlation time of the speckle fluctuations. This, in effect, will 'freeze' the speckle pattern and produce a high contrast image. Yuan *et al.* [122] performed a study on the cerebral flood flow of rodents and reported the optimal exposure time during speckle contrast imaging to be 5 ms. However, not all studies using LASCA report the exposure time implemented.

A disadvantage of LASCA is the lack of spatial resolution. The contrast is measured over a group of pixels and the larger the nxn region, the more accurate the value for C but the greater the loss in spatial resolution.

Speckle contrast measurements are dependent on the sensitivity of the imaging device. This is problematic since different blood flow images may be obtained for the same blood flow under different imaging device conditions. The images are not general and hence could not be used in clinical and diagnostic situations. One solution to this problem proposed by Yokoi *et al.* [126] was to use a modified temporal contrast factor (MTCF) to suppress the influence of camera sensitivity on the contrast. Despite the high quality blood images that this method provided while suppressing the effects of contrast, its drawback was that it requires calibration of the imaging device prior to imaging each sample.

6.3 Mathematical Speckle Simulation

As a tool to help understand the speckle phenomenon, methods to mathematically generate speckle patterns have been developed [52]. The basic concepts of the formation of speckle pattern are used to produce the speckle patterns.

Time-varying changes in the speckle pattern from a biological object are caused by a large number of interactions between the coherent light and complex biological material. The complicated inconsistency of biological activity results in difficulties in establishing a theoretical model of the biospeckle. However, some mathematical models have been reported [41, 127-130]. Typically, in simulations of dynamic speckle, a phase change between speckle frames is utilised as the main origin of the random changes in speckle over time.

7 Discussion

Ocular microtremor has a proven potential as a valuable clinical tool. The current PZT method widely used to measure OMT is unsatisfactory, mostly due to its eye-contacting nature. Ideally, for clinical use a measurement device for OMT would be non-contact. A non-contacting OMT measurement device would also aid research into the role of OMT in vision.

This work aims to use laser speckle correlation as a technique to measure OMT. Laser speckle correlation is a non-contact, optical method to measure displacements. It has a proven resolution within the OMT requirement range (2-216 μrad). However, reported resolutions have been achieved using inanimate objects, particularly metal. No reports on speckle correlation to measure *in-vivo* eye movements have been found in the literature.

Recording speckle from the eye will necessitate using an eye-safe laser power. Generally, speckle correlation techniques have not been preformed at such low light levels. A high signal-to-noise ratio (SNR) is desired so that speckle images with good speckle contrast (a value close to unity) are produced. Typically, to capture low light images at a high SNR, a long camera exposure time is used. Here, however, the exposure time will need to be short so that the tiny displacements of the eye can be tracked. It is unclear whether the light reflected from the eye sclera will be of a sufficient SNR to record speckle from the eye.

Other eye movements and head movements will act as sources of noise in the measurement technique are. These movements could create some decorrelation between speckle image frames. The effects of these other movements on the correlation

technique will need to be minimized so that they do not cause the measurement system to breakdown.

Speckle from 'ideal' targets, such as metal, generally result in single scattering. Conversely, speckle from any object in which the laser light penetrates the surface, such as the biological surface of the eye, will result in multiple scattering. Multiple scattering alters the properties of speckle. It is unknown what effects, if any, multiple scattering from within the eye surface will have on the proposed speckle correlation measurement technique.

Methods such as polarization subtraction and optical clearing have been implemented in other studies to reduce multiple scattering. Optical clearing would not be suitable for this work as it requires the use of a chemical agent and is typically used to image further into the volume of an object rather than the surface. Polarization may have some use in reducing multiple scattering from the eye since it can be used to select speckle originating from a surface rather than from within a volume. Polarization subtraction, however, would be unsuitable because it would require the use of two image sensors to record both orthogonal polarization planes at once.

The eye is a living surface and, as such, it produces a form of time-varying speckle known as biospeckle. Biospeckle is expected to disrupt the frame-to-frame stability of speckle images captured from the eye and act as a source of noise in the measurement. Most of the literature on biospeckle focuses on speckle imaging techniques, few reports detail speckle metrology in the presence of biospeckle. Whether the translational speckle from OMT movement can be measured in spite of the presence of the random, time-varying biospeckle needs to be determined.

To aid the design of a speckle correlation system to measure OMT, a mathematical model will be needed. The model will allow aspects of the design to be tested without the need to use volunteers. Methods to numerically simulate both speckle patterns and biospeckle and have been reported. Few quantitative measures of biospeckle exist and a method to analyze biospeckle from the eye is required so that numerical biospeckle patterns can be generated with qualities that resemble biospeckle seen *in-vivo*. Furthermore, the model will need to include the effects of multiple scattering. No reports that detail numerical methods to simulate multiple scattering in speckle experiments have been found.

Chapter 2

OMT Measurement Using Laser Speckle Metrology

1 Introduction

Fixational eye movements are present in all subjects even while the eye appears to be at rest. These fixational movements are composed of three types of involuntary eye movements; microsaccades, drift and ocular microtremor [5, 8].

Ocular Microtremor (OMT) is the smallest of the involuntary eye movements. It has an amplitude range of 150-2500 nm (12-216 μrad rotational) peak-to-peak, a frequency range of 20-150 Hz with an average peak frequency of 84 Hz [14] for a normal subject. It is a non-periodic, continual, high frequency, wave-like physiological tremor. Microtremor occurs simultaneously with drift, which is a slow, continuous irregular movement that takes place between the more rapid and intermittent microsaccades.

Clinical use of OMT has been investigated in coma [43], MS [22], Parkinson's disease [48] and depth of anaesthesia [25, 47]. Recent studies have attempted to understand the particular role of OMT in vision [11]. It is believed OMT arises from brainstem neurons [13, 16, 19].

Most measurements of OMT to date have relied on an eye-contacting probe method [30, 31]. Drawbacks of these probes include the requirement to anaesthetise the eye, inter-observer variability, probe influence on the measurement result and patient discomfort [11, 17, 26, 32].

Despite its potential, a full understanding of OMT is incomplete due to the absence of a device to measure it noninvasively. For practical clinical use, a non-contacting method for OMT measurement would be most suitable. Ideally the device would have a high resolution yet be robust enough to measure OMT in a clinical environment. Boyle *et al.* [21] proposed a speckle interferometry method for non-contact measurement of OMT from the eye sclera. The system achieved a resolution suitable for OMT measurement, though the set-up was difficult to implement. A promising outcome of the work by Boyle *et al.* was that it showed the sclera to be an appropriate surface for measuring OMT using speckle based methods. As a continuation of the work by Boyle, Ryle *et al.* [40] developed a speckle interferometry OMT measurement system using laser diodes in order to reduce the physical size of the system. However, again the system was difficult to implement.

In this work, the feasibility of using laser speckle correlation to track OMT from the surface of the sclera is investigated and the requirements for such a measurement system are outlined. Specifically, the application of a laser speckle technique using Fourier plane imaging to measure OMT is investigated. The technique potentially presents advantages over other optical eye movement measurement techniques in terms of resolution, ease of set up and robustness to misalignment. This approach has not been applied previously to eye movement measurement and would represent an important

addition to the relatively limited number of non-contact eye movement techniques available [29, 131], if its utility can be demonstrated. While the basic optical technique has been described elsewhere, it has been validated and applied only for the measurement of relatively simple displacements of inanimate objects, such as small rotation of metal shafts. The eye presents a much more challenging target. To adapt and validate the technique for OMT measurement requires the issues of eye safety, background eye movement and biospeckle to be resolved. The former two issues are addressed in this chapter, as moving to investigate biospeckle effects *in-vivo* initially requires the basic technique to be proven *in-vitro* at eye safe power levels against the known motion of a target. To address eye safety, the technique here is implemented at much lower laser power levels than have been used previously in other applications and a very high sensitivity EMCDD camera is utilised to attempt to compensate for the consequent drop in signal and potential loss of resolution.

OMT takes place against a background of 'contaminating' background eye and head movements. A downside of the fundamental optical technique used here is that it is vulnerable to failure through decorrelation effects for 'large' movements. A series of validation tests are presented here to realistically challenge the proposed measurement approach and to determine if it can be configured to resolve the very low amplitude rotations caused by OMT, despite the necessary restrictions on laser power and the presence of larger amplitude background motion.

As a first approximation, the testing and validation of the laser speckle correlation technique for OMT measurement in this chapter and in the succeeding two chapters will be performed on inorganic materials. First, testing will be performed on a surface scattering material to investigate whether the technique could be applied to measure

angular displacement with the limiting requirements necessary for measuring OMT (eg. low light levels).

Next, the technique will be applied to volume scattering materials. This is an important step as it is unknown what influence, if any, volume scattering would have on the measured displacement. To fully understand and analyze the recorded speckle patterns, a known displacement has to be applied to the target material. Should a biological sample be implemented at this point, extra unknown variables relating to biospeckle would have to be introduced into the measurements, making it difficult to ascertain which movements were taking place due to biospeckle and which were related to volume scattering.

Additionally, in practice, it would be difficult to source a biological sample that (i) truthfully reflects the biological aspects of scattering found in the real eye in-vivo and (ii) is feasible to take measurements from in the lab. For example, sclera samples degrade and dry out quite rapidly.

For these reasons, the approach taken here is to prove the basic feasibility of the system by using inanimate samples to first look at surface scattering, then to study volume scattering on these inanimate samples and finally to move onto the real eye as soon as is reasonably achievable.

1.1 Measurement Requirements

The reported amplitude of OMT varies in the literature. For metrology purposes, most OMT measurements that have been recorded using the contacting probes method give the amplitude in terms of nanometers. For the purposes of this work, these figures are

converted to units of angular rotation of the eye by noting that 87 μrad is equivalent to a 1μm displacement for a typical eye diameter of 23 mm.

1.1.1 Frame Rate

The frame rate of a camera attempting to capture speckle moving at OMT frequencies must obey the Nyquist sampling theorem. To do this, the sampling frequency (f_s) must be greater than or equal to twice the highest frequency contained in the signal i.e. for OMT measurement the frame rate must be $\geq 2(150$ Hz). In the case of living tissue such as the eye, biospeckle will be present in the signal captured by the camera. At present, the rate of biospeckle motion in the eye is unknown and so a higher sampling frequency than that required for OMT alone would be beneficial. A frame rate of 500 Hz (500 frames per second) is high enough to obey the Nyquist theorem and avoid aliasing of the OMT signal.

1.1.2 Dynamic Range and Resolution

Generally a dynamic range of 2-216 μrad (25-2500 nm peak-to-peak) and system resolution of 2μrad has been found to be adequate to track the OMT signal [21, 26, 31]. Although this dynamic range is sufficient to capture OMT, when a large intermittent microsaccade or other movement occurs, a momentary saturation arises in the measurement. More recent studies have used a dynamic range of 2 μrad- 9.52 mrad (25 nm – 110 μm) [11, 27] so that other fixational movements could also be recorded. In a contacting probe measurement system, the system dynamic range and resolution are critical parameters.

In a speckle correlation system, dynamic range will be determined by the maximum allowable frame displacement relative to a reference frame taken at the start of the measurement. A large frame-to-frame displacement will cause a decorrelation in the measurement and reduce the accuracy. Some intermittent resetting of the reference frame could be tolerated in response to large movements. This would be apparent as a discontinuity in the measured movement trace. However, at a minimum, the system needs to tolerate the expected frame-to-frame displacement. Therefore some *a priori* knowledge of estimates for how large these displacements might be is needed in order to design a system capable of measuring OMT against a background of other movements.

1.1.3 Influence of Other Eye Movements on Measurement

Other eye movement can lead to decorrelation of the speckle correlation images. Table displays the amplitude, frequency and velocity ranges estimated from the literature for each of the fixational eye movements. Drift and microsaccades, have an amplitude of about 290μrad and 1.45 mrad respectively. Drift has a frequency of 2-5 Hz and, as previously mentioned, occurs simultaneously with OMT. Microsaccades are more rapid and sporadic and occur approximately twice every second. An imaging system recording speckle from the eye would capture the net displacement of the eye surface resulting from all three fixational movements. Post processing of the images must therefore include a filtering method to separate the OMT signal from the other eye movements.

	Amplitude (μrad)	Frequency (Hz)	Maximum Velocity (mrad/s)	Maximum Rotation per frame at 500FPS (μrad/frame)
OMT	12-200 peak - peak	~80	50	101
Drift	290	2-5	9 [8]	18
Microsaccade	1450	1-2	637 [8]	1274

Table 1. Characteristics of the fixational eye movements. Velocity estimates are based on the amplitude and frequency (unless referenced).

1.1.4 Influence of Body Movements on Measurement

Unwanted head movements can occur during eye movement measurement. These can have a negative influence on the accuracy of measurements since the eye globes participate in the compound movements of the head. Natural functions such as breathing and heart rate, can affect these head movements. Head movements vary in amplitude between measurements and between subjects and so it is difficult to establish their amplitude. To stabilise the head while recordings are being taken, a headrest may be used. It has be shown however, that standard ophthalmic headrests do not eliminate all head movement and amplitudes in the range of ±9 mrad (±100μm) at 2-3 Hz are still possible with their use [132].

In a clinical environment a portable handheld measurement device would be the ideal solution in cases where the patient is not mobile and cannot place their own head in a headrest. Shaking of the hands while holding the device would add additional noise to the system. The outstretched arm has a natural tremor of 4-17 mrad (50-200μm) in amplitude with a frequency of 7-12 Hz [26, 133].

	Amplitude (mrad)	Frequency (Hz)	Maximum Velocity (mrad/s)	Maximum Rotation per frame at 500FPS (μrad/frame)
Free Head	31-39 [132]	2-3	368	736
Headrest	9 [132]	2-3	85	170
Hand	4-17 [26, 133]	7-12	641	1282

Table 2. Characteristics of other body movements that may influence OMT. Velocity measurements are calculated based on the amplitude and frequency.

1.1.5 Required Frame-to-Frame Measurement Ability

In order to determine the required frame-to-frame measurement ability of the system, the likely displacement per frame of all movements that may influence the OMT signal must be calculated. It is clear that the dominant components are likely to be microsaccades in a head rest device. Treating the above velocities as vectors, the maximum possible angular velocity will occur for a situation where all velocities are in the same direction. In this case, the maximum velocity would be

(OMT + drift + microsaccades + head) = (50 + 9 + 637 + 85) mrad = 781 mrad/s.

At the proposed frame rate of 500 FPS (see section 1.1.1), the maximum possible displacement per frame is estimated to be 1.56 mrad.

Including motion from a handheld device the maximum velocity would increase to 1422 $mrads^{-1}$ and the maximum possible displacement per frame would increase to 2.84 mrad. From these figures, it is apparent that hand movement would become the

dominant motion in a measurement system. The velocity and displacement of the total movements almost double when hand movement is included. At present, the measurement device is designed to be table mounted and so further calculations will be derived for a non-handheld device.

The unwanted eye, head and hand movements have frequencies below that of OMT, and so a filter may be implemented to remove them with signal processing. The filtering process would not work however, if the frame-to-frame decorrelation caused by the head and hand movements is large. The effects of this possible decorrelation must therefore be investigated and quantified.

1.1.6 Summary of Required Parameters

Resolution	2 μrad
Dynamic Range	2 μ – 9.52 mrad
Frame Rate	500 FPS
Frame-to-Frame Measurement Ability (Minimum)	1.56 mrad

Table 3. System requirements for a speckle correlation OMT measurement system.

1.2 Fourier Plane Measurement Technique

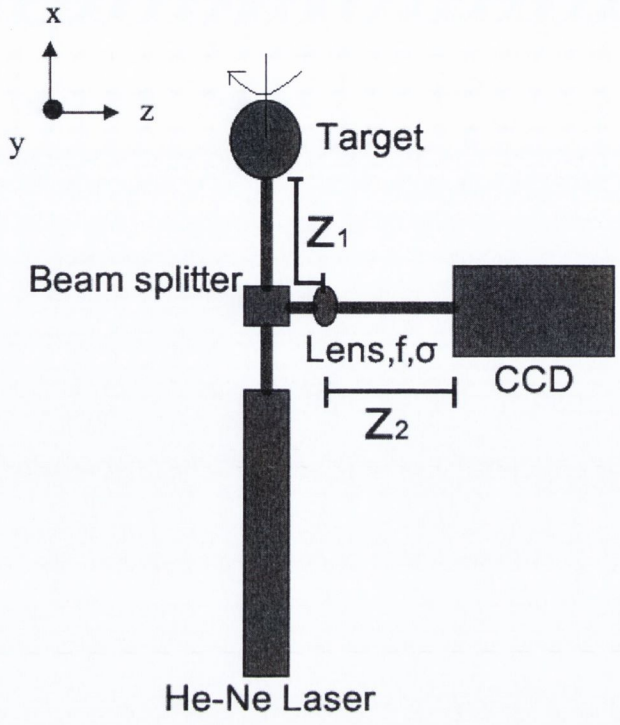

Figure 17. Set-up for Fourier plane measurement technique.

Figure 17 shows the arrangement used by Rose *et al.* [96, 97] for angular speckle displacement measurement. Light from a collimated laser beam is directed through a beam splitter to a target where it is then reflected back to an image sensor placed in the Fourier plane (i.e. $z_2 = f$) of a lens with aperture σ. The out-of-plane angular rotation (θ) of the object is transformed to a linear displacement (p_x) in the Fourier plane of a lens. An image sensor placed in the Fourier plane records the speckle patterns over a certain time. The speckle images are then post-processed using digital image correlation to measure the linear displacement between speckle images. This linear displacement is then converted to angular rotation of the object using the simple equation:

$$\theta = \frac{p_x}{2f} \qquad \textbf{Equation 1 [96]}$$

Speckle techniques recorded in the imaging plane are dependent on a number of variables such as the lens focal length, working distance, numerical aperture, the wavelength of the light and the target shape. An advantage of the Fourier technique implemented by Rose *et al.* is that the angular displacement is dependent only on the linear speckle image displacement and on the lens focal length (f), hence the set-up of the system is much less stringent than that of an imaging plane technique.

Other advantages in terms of precise OMT measurement with this technique are the proven range and sensitivity that can be achieved. In their paper, Rose *et al.* report a resolution of 5μ radians for the technique; this is close to the ideal OMT system resolution of 2μ radians. Further, the method has been proven to be insensitive to target shape and to target distance (z_1). The latter is important to OMT measurement since it would allow for simple set-up of the equipment without a rigid working distance. A fundamental advantage of the technique designed by Rose *et al.* is that their system is sensitive only to rotation. This is significant for OMT measurement as it would imply that the method is robust and insensitive to any left/right or back/front motion of the subject as the measurement is being taken.

1.3 Design Parameters

Using the Rose method, as described above, there are only three variables in the set-up; the beam radius r_s, lens focal length f and lens aperture σ. In the following section the influence of these parameters on the design of the system will be discussed with an aim to find optimized values for an OMT measurement system and to calculate the theoretical dynamic range of our system. Laser power constraints due to eye safety are also discussed.

1.3.1 Illumination source

A highly coherent HeNe laser source was chosen for this set-up, primarily due to the ease of set-up. Additionally, the laser source can easily create interference effects. It is noted that less coherent laser sources, such as a diode laser, could be implemented instead and it would be interesting to investigate the device with such diode. Indeed, another advantage of using a laser diode would be the reduction in the physical bulk of the optical set-up.

The apparatus was arranged such that the laser illumination was collimated at the target surface. Since the HeNe laser is collimated, less optics are needed to use it this way. This is important in attempting to keep the overall bulk of the system to a minimum.

Having the laser collimated at the target surface means that the distance of the laser source to the eye will not be important as the same illumination conditions will be present at all distances using the collimated beam. This helps with ease of set-up and consistency of measurements.

Furthermore, the theory outlined by Rose et al. for this technique assumes a collimated beam and this form of illumination gives the rotational sensitivity seen with the technique.

1.3.2 Lens Focal length

$$\mathbf{f = \frac{p_x}{2\theta}} \qquad \textbf{Equation 10 [96]}$$

Equation 2 shows how the measured pixel displacement, p_x, and angle, θ, are related to the chosen lens focal length, f. As outlined in section 1.1, the desired resolution of an OMT measurement device is 2 µrad. Assuming that a displacement of 0.05 of a pixel of

the image detector is detectable by the system [134], to achieve a resolution of 2 μrad the focal length of the lens in millimeters must be at least 300 mm.

Due to the low light levels in this experiment, it would be prudent to use a smaller focal length lens in order to keep the target to lens to camera sensor distance shorter and hence collect more reflected light at the sensor. An f = 150 mm lens was considered to be a good compromise between achievable resolution and reflected intensity, reducing the estimated resolution to 4 μrad.

1.3.3 Beam Radius

$$\rho_0 = \frac{\lambda f}{\pi r_s} \qquad \textbf{Equation 11 [96]}$$

The equation governing the speckle size, ρ_0, is given in equation 3. From this equation we see that the beam radius, together with the wavelength and lens focal length have a direct effect on the speckle size.

The average size of the speckles in a pattern will influence the performance of a sub-pixel displacement algorithm. Bruck *et al.* [89] suggest a speckle size of two to three pixels in order to achieve good correlation results. When the speckle size is less than two pixels, the actual speckle location and its light intensity value become more uncertain. However, in their study Rose *et al.* roughly match the speckle size to the pixel size and achieve adequate results.

To achieve a speckle size that is at least as large as one pixel, using a focal length of f =150 mm as derived above, the beam radius must not be larger than 1.26 mm for a 632.8 nm laser.

Using the lateral sclera as a target, the beam diameter must be able to fit within the accessible space on the sclera. For a typical adult eye the available space is approximately 4 mm. Therefore a beam radius of up to 2 mm would fit on the sclera.

A small beam radius is desirable because it will provide a higher signal-to-noise ratio and a higher speckle size. For this reason, it was opted not to adjust the actual beam radius of the laser used in this experiment and the given radius was 0.6 mm. This beam radius is well within the available space on the sclera.

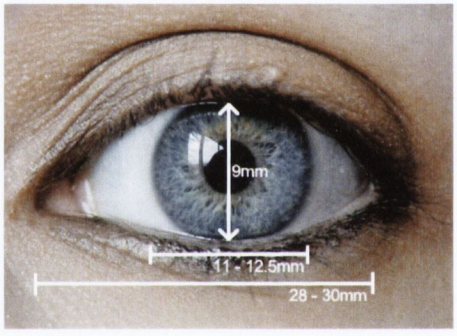

Figure 2. Dimensions of the eye

1.3.4 Aperture Size

$$D_{sp}(\theta) = e^{\left[-(R\theta)^2\left(\frac{1}{r_s^2 F}+\frac{8f^2}{R^2\sigma^2}\right)\right]} \qquad \textbf{Equation 4 [96]}$$

Equation 4 shows how the lens aperture, σ, influences the degree of speckle decorrelation D_{sp}. Assuming fully developed speckle ($F = 1$), to achieve a decorrelation factor of 0.9 or higher for a maximum possible angular displacement of $\theta = 1.56$ mrad (as derived in section 1.1) with a lens focal length of f=150 mm, then the lens aperture

must be greater than or equal to 2.04 mm. For our set-up we chose a standard optic size of 25 mm.

1.3.5 Dynamic Range

Large movements will decorrelate images from frame-to-frame. This will impact the dynamic range. The ceiling on the dynamic range achievable by the system is set by simple optical geometry and can be determined using equation 1. From this, the angular displacement required to translate a single speckle across the image sensor can be calculated. For a lens focal length of 150 mm and a 128x128 image sensor with a 24 μm pixel pitch the angular displacement required to displace one speckle fully across the sensor is 10 mrad, resulting in no correlation between pre and post displacement speckle patterns. Therefore, in a scenario where each frame is correlated with an original undisplaced reference frame, the maximum achievable dynamic range for our system is 10 mrad.

1.3.6 Laser Power

The laser power used in an OMT measurement system must be restricted to a safe level and yet be high enough to achieve a reasonable signal-to-noise ratio at the imaging detector. Ideally the laser light would be visible so that alignment of the laser with the eye sclera is easily achievable. In this study, a visible red helium neon (632.8 nm HeNe) laser was chosen for the OMT tracking device.

Laser safety standards classify lasers by their hazard potential, which is based upon their optical emission. The maximum permissible exposure (MPE) is the level of laser radiation to which a person may be exposed without hazardous effects or biological

changes in the eye. MPE levels are determined as a function of wavelength and exposure time and are expressed in either joules per metre squared (Jm^2) or watts per metre squared (Wm^2). Generally a shorter wavelength or longer exposure time results in a lower MPE. Limits for the safe exposure of eyes and skin to laser radiation are given by the International Electrotechnical Commission (IEC 60825-1) [135] and by the American National Standards Institution (ANSI Z136.1) [136, 137]. Both standards agree in MPE values and using these, the MPE for a direct intra-beam viewing of a 632.8 nm wavelength laser for 10 s exposure time to an eye with a 7 mm pupil diameter was found to be 388.65 μW. It should be noted that this value is for an exposure to the retina, however, in normal use we are aiming the laser at the sclera and hence there is less risk of retinal eye damage.

1.3.7 Summary of Design Parameters

Lens Focal Length	150 mm
Beam Radius	0.6 mm
Aperture Size	25 mm
Laser Wavelength	632.8 nm
Laser Power	136 μW

Table 4. Parameters chosen to achieve a resolution of 4 μrad and dynamic range of 4 μ-10 mrad.

2 Methods

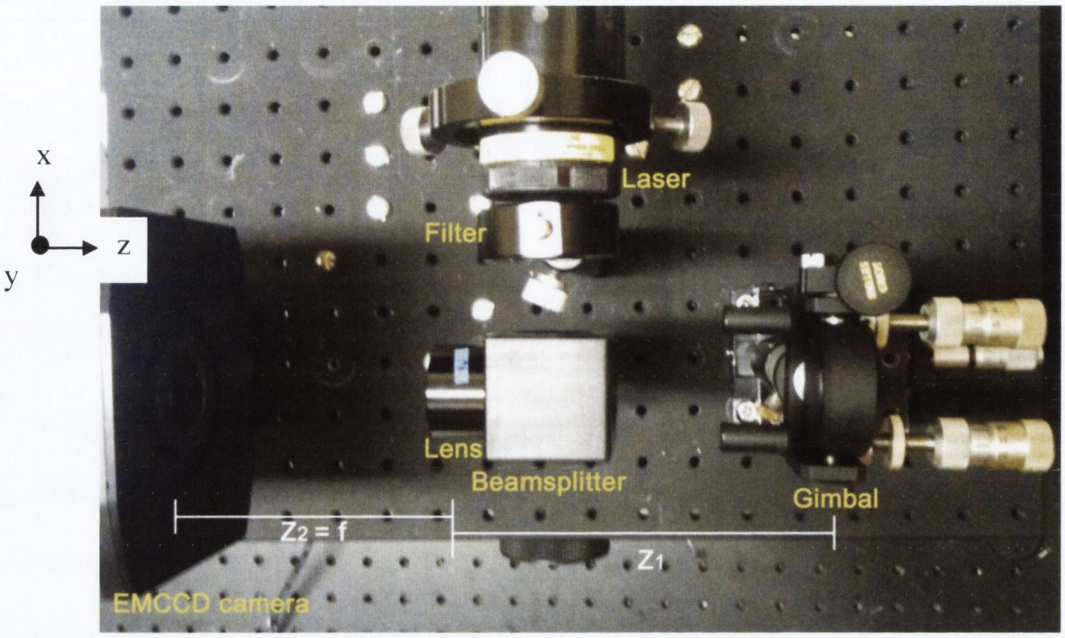

Figure 3. Experimental set-up.

In the following experiments, we aim to demonstrate the feasibility of using the speckle correlation method for measuring the rotation of objects with OMT-like movements. The proposed measurement system must be tested at eye-safe laser levels for its ability to meet OMT measurement specifications in terms of accuracy, resolution, range and robustness to larger eye movements. To perform these tests both an OMT simulator and a manually adjusted gimbal were used to simulate the moving eye. A piece of cardboard was inserted into the gimbal to act as the target material and, similarly, another piece of the same cardboard was attached to the plastic of the simulator.

The optical set-up for the experiment is shown in figure 3, the EMCCD sensor is placed in the Fourier plane of the lens i.e. at $z_2 = f$. The target is illuminated by a 632.8 nm plane polarized HeNe laser which is reduced down to an eye-safe power of 139 μW by the use of a neutral density filter and a beamsplitter. The speckle pattern generated on

the target is collected by an EMCCD camera (Cascade 128+, Roper Scientific [138]) operating at 500 Hz with a 128x128 array of 24 μm pixels and a 100% fill factor. A 5 second (2500 frames) reading is taken for each measurement. The 8-bit digitized speckle images are then sent to the numerical software package Matlab [139] for processing. The analysis procedure is shown in figure 4.

During the processing each displaced speckle-image frame is cross-correlated with the original reference speckle-image frame. The full 128x128 pixels are used for every image during the cross-correlation analysis. To increase the accuracy in finding the exact correlation peak, and consequently the speckle displacement, the location of the cross-correlation peak is calculated with a sub-pixel algorithm. The subpixel correlation method used in this experiment is based on the curve-fitting method as described by Hung *et. al* [78]. The change in correlation peak location over time is used to calculate the pixel displacement of the speckle images.

Using equation 1, the calculated pixel displacement, p_x, is converted to the measured angular displacement, θ. To remove noise outside the desired frequencies, the signal is then filtered using a digital Butterworth filter of order five with a bandwidth of 20 – 150 Hz. A peak detection algorithm is used to measure each peak and trough in the recovered signal. To find the amplitude of the signal, each trough is subtracted from each peak and the mean value is taken to be the peak-to-peak amplitude of the measured signal. To calculate the frequency content of the signal a periodogram is utilised to estimate the power spectral density.

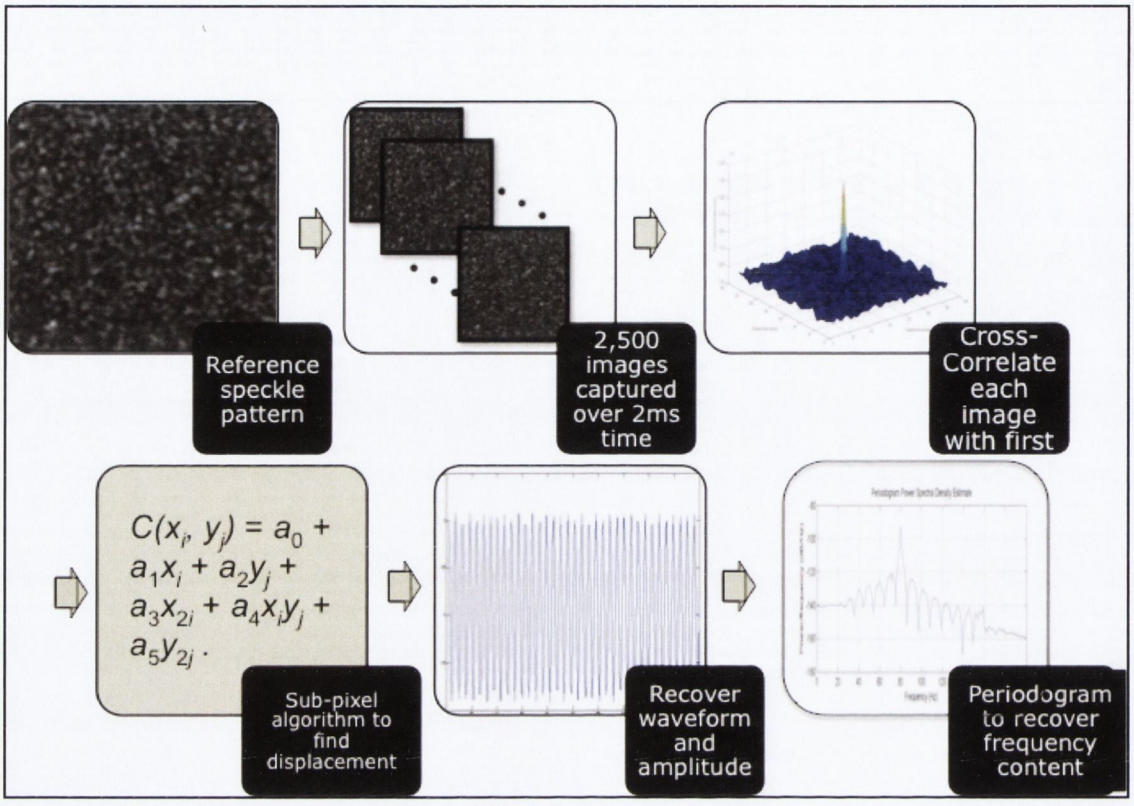

Figure 4. Analysis procedure.

2.1 Simulator Tests

An OMT simulator was used to test the measurement resolution, amplitude response and frequency response of the system. The simulator replicates OMT movement in terms of typical frequencies and amplitudes. It was first designed by Sheahan [26] but has since been revised and updated (see appendix for calibration). A picture of the simulator is shown in figure 5. The two outer piezoelectric bimorphs of the simulator displace in response to an applied voltage and the inner bimorph is used as a reference for calibration. The bimorphs are attached to a piece of plastic on one end. As the bimorphs bend the attached plastic tilts at an angle that is proportional to the applied voltage.

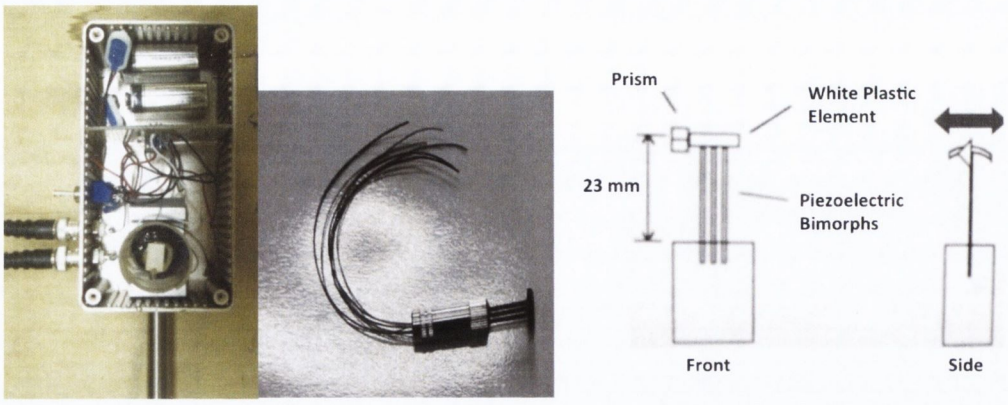

Figure 5. OMT simulator. The small prism attached to the plastic disk is used during calibration of the simulator.

2.1.1 Amplitude Response at OMT Rotation Angles

The amplitude response of the proposed set-up was tested first with varying frequency and then at various input amplitudes.

To test the amplitude response with varying input amplitude, the simulator was driven at the typical mean OMT frequency of 80 Hz and at OMT like amplitudes ranging from 4-197 μrad peak-peak in steps of 20 μrad. The experiment was repeated five times.

The lowest measureable amplitude that was recovered is given as the resolution of the system.

2.1.2 Frequency Response

To test the frequency response a signal generator was used to drive the simulator sinusoidally with frequencies in the OMT range ranging from 10 to 150 Hz in steps of

10 Hz at an amplitude of 197 μrad peak-peak. 197 μrad was chosen since it was the maximum amplitude achievable with the frequency generator.

2.1.3 Robustness to Set-Up

Next, an investigation of the impact of the z-axis (the optical axis) location of the target on the accuracy of the system was performed. Using a linear translation stage, the distance between the simulator and the lens was altered in steps of 1 mm up to a maximum allowable translation of 50 mm. An angular displacement of 197 μrad and frequency of 80 Hz was applied and measured at each step before the simulator was displaced again.

2.1.4 Toleration to Linear Displacement During Measurement

To investigate the toleration of the system to a linear z-axis displacement during measurement, the translation stage was used to create a 3 mm displacement along the axis while the simulator was running. Experimentally, 3 mm was found to be the most repeatable distance at which the translation stage could be displaced by hand during the 5 s recording time. The experiment was performed at an OMT-like amplitude of 87 μrad. An 80 Hz sine wave signal was used to drive the simulator over a period of 5 s while the simulator was moved along the translation stage by hand. Each translated speckle image was correlated with the original undisplaced reference frame.

Next, the toleration of the system to an x-axis displacement was investigated. In this case a linear displacement of 50 μm was applied by hand using the translation stage. The simulator was again set to run at 80 Hz and 87 μrad peak-to-peak. 50 μm (4.3 mrad)

was chosen since it is within the expected measureable displacement of the system (10 mrad).

2.2 Gimbal Tests

A gimbal (Melles Griot, 07MAD701) was implemented to test the amplitude response of the system over a range of angles larger than those achievable with the simulator. The gimbal, shown in figure 6, has an azimuthal resolution of 50 μrad and was used to rotate the target around the y-axis.

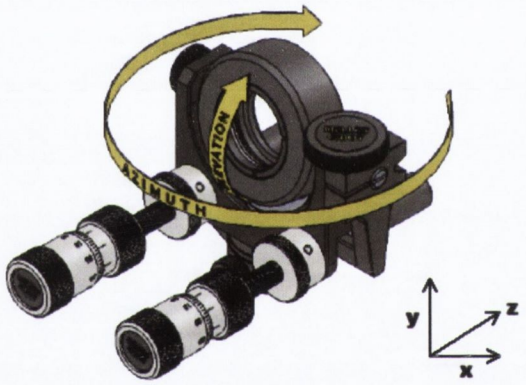

Figure 6. Gimbal Configuration.

2.2.1 Large Angle Amplitude Response

To test the amplitude response of the system at larger angular displacements within the dynamic range of the system, the gimbal was rotated at the following frame-to-frame angular displacements 0.2, 0.25, 0.5, 0.75, 1, 2, 3, 4, 5, 6, 7, 8, 9 and 10 mrad. For each angle, the recorded speckle image was cross-correlated with its respective undisplaced reference image and the results were plotted.

3 Results

3.1 Speckle Size

Figure 7 shows a typical cross-correlation peak resulting from the auto-correlation of a generated speckle pattern. Assuming fully developed speckle and using equation 6, the size of the speckle calculated from the full width at half max of the correlation peak was found to be 55.68 μm. This is in close agreement with the theoretical value of 50.36 μm for a beam radius of 0.6 mm and lens of 150 mm focal length.

$$FWHM = 4\sqrt{ln2}\sqrt{F}\rho_0 \qquad \textbf{Equation 6 [96]}$$

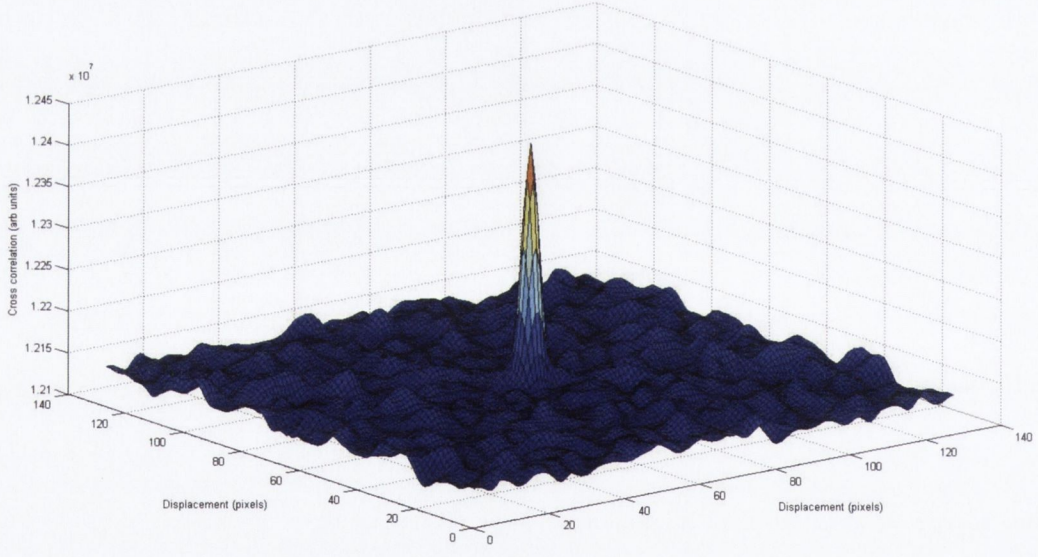

Figure 7. Cross-correlation of speckle pattern.

3.2 Simulator Results

3.2.1 Amplitude Response at OMT Rotation Angles

Figure 8 shows the results of the amplitude response tests using the simulator. As shown in the figure, the measured angular displacements agree well with the applied angular displacement. The mean percentage error was found to be 12%. At a typical OMT amplitude of 87 μrad the percentage error was less than 10%, below 50 μrad the error increased above 10% to a maximum of 33% at 4 μrad.

The results show that the measurement system is capable of measuring angular displacements in the OMT range of 12 - 216 μrad. Further, the system resolution was determined to be at least 4 μrad. This is in agreement with the resolution requirements derived in section 1.3.

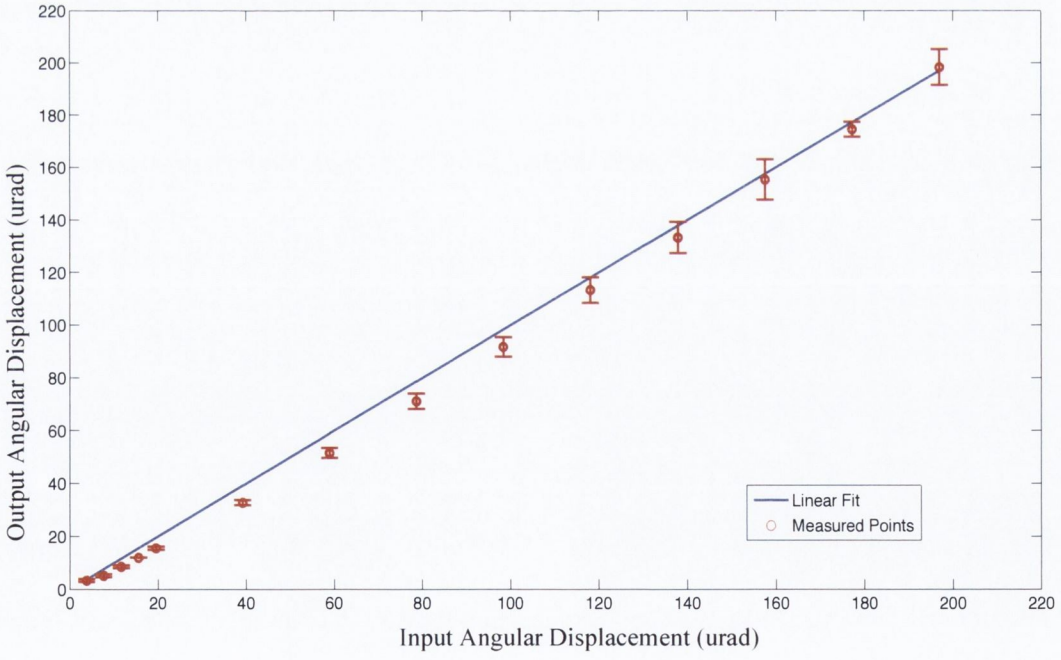

Figure 8. Input vs. output displacement for the simulator at 80 Hz. The error bars show the standard deviation on the measurements.

3.2.2 Frequency Response

The frequency response of the measured signal in the tested OMT-like range of 10-150 Hz was found to be flat to within 0.2 dB, as shown in figure 9.

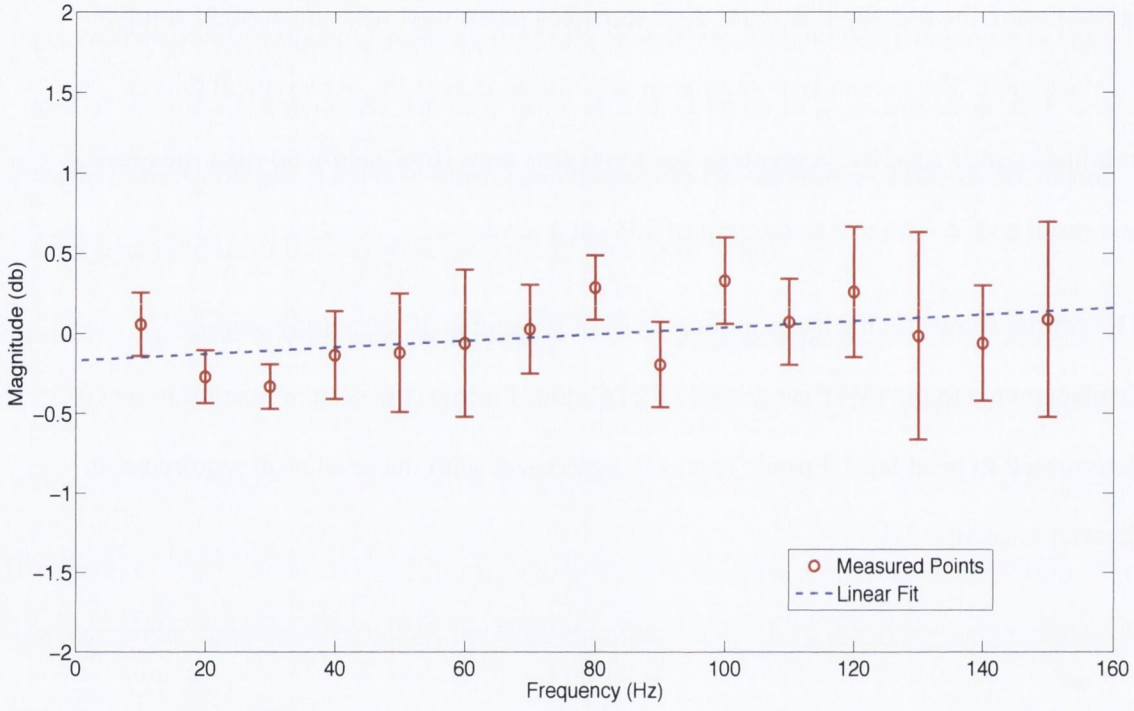

Figure 9. Measured angle against changing simulator frequency. The error bars represent the standard deviation on the measurements.

3.2.3 Robustness to Set-Up

Figure 10 shows the results of testing the response of the system to a 197μrad peak-to-peak 80 Hz displacement at a range of z-axis positions centered at z_1=150 mm ±25 mm. There is no trend in sensitivity to displacement with z position. The mean measured displacement was 192 ±8 μrad. The standard deviation with variable z_1 is similar to the standard deviation seen in figure 8 with repeated set-up at the same z.

These results show no significant difference in the measured angular displacement over the 50 mm range in which the target distance was displaced. This result agrees with the result of Rose *et al.* [96]. The only important distance expected to contribute to the measured displacement is the lens-to-camera sensor distance. As a consequence of the invariance to target distance, all further measurements can be obtained with as short a target distance as possible in order to ensure a strong reflected light signal to the camera.

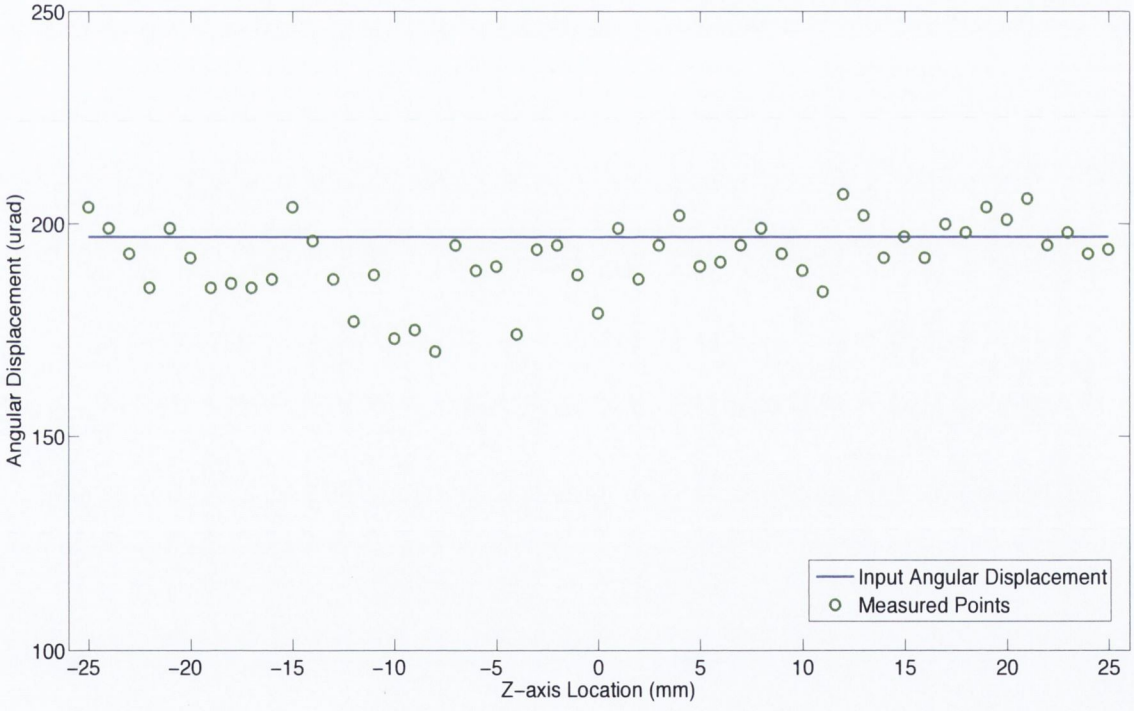

Figure 10. Effect of linear displacement along the z-axis. The zero location of the z-axis is taken as the focal length, i.e. $z_1 = f = 150$ mm.

3.2.4 Toleration to Linear Displacement During Measurement

The influence of a 3 mm linear displacement along the *z*-axis on the measurement of simulator vibration at 80 Hz, 87 μrad was then investigated. The approximate velocity of the linear movement was 600 μm/s. As mentioned previously, the technique is expected to be insensitive to movement along this axis. Figure 11 shows a plot of the unfiltered measured angular displacement. The very slight declining slope of the signal is likely to be due to a contaminating component of x-axis movement occurring simultaneously with the imposed *z*-axis movement.

The mean measured angular peak-to-peak displacement was found to be 77 ±3 μrad with a resulting percentage error of 11.5%. These results are comparable to the previous measurement of the angle when no extra linear displacement was enforced on the simulator. This implies that the system should be capable of tolerating at least 3 mm of linear *z*-axis motion. In our case, this indicates that our system should be able to accept at least 3 mm of linear movement from unwanted sources such as longitudinal head or body movement while still obtaining a recording of OMT.

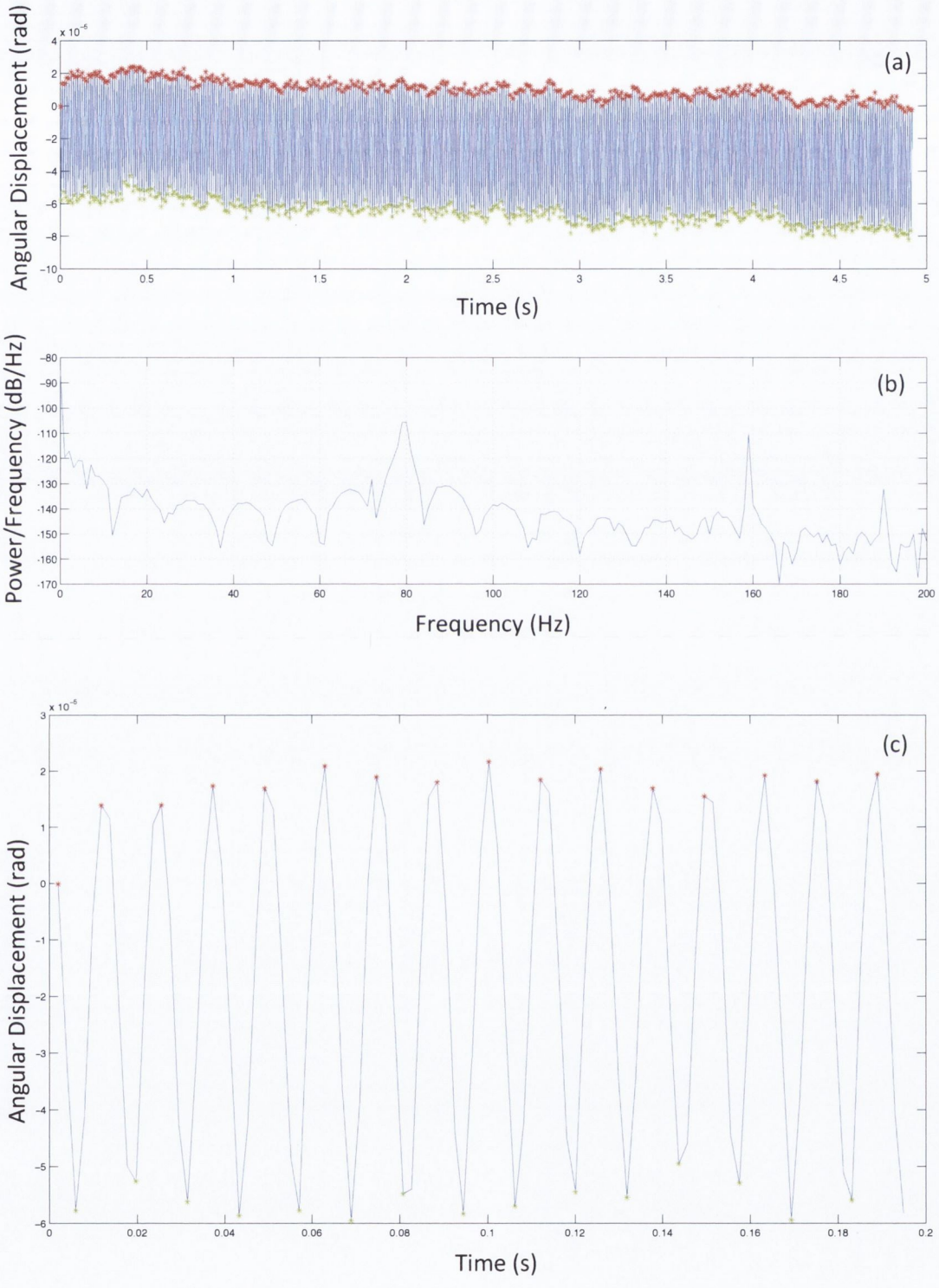

Figure 11. (a) and (b) Measured angular displacement and periodogram for the simulator at 80 Hz, 87 urad with an applied *z*-axis linear displacement. (c) Close up version of the recovered sine wave.

Next, the influence of a 50 μm linear displacement along the x-axis was investigated. As shown in figure 12, it was found that the system could recover the 87 μrad input signal while the movement was imposed on it.

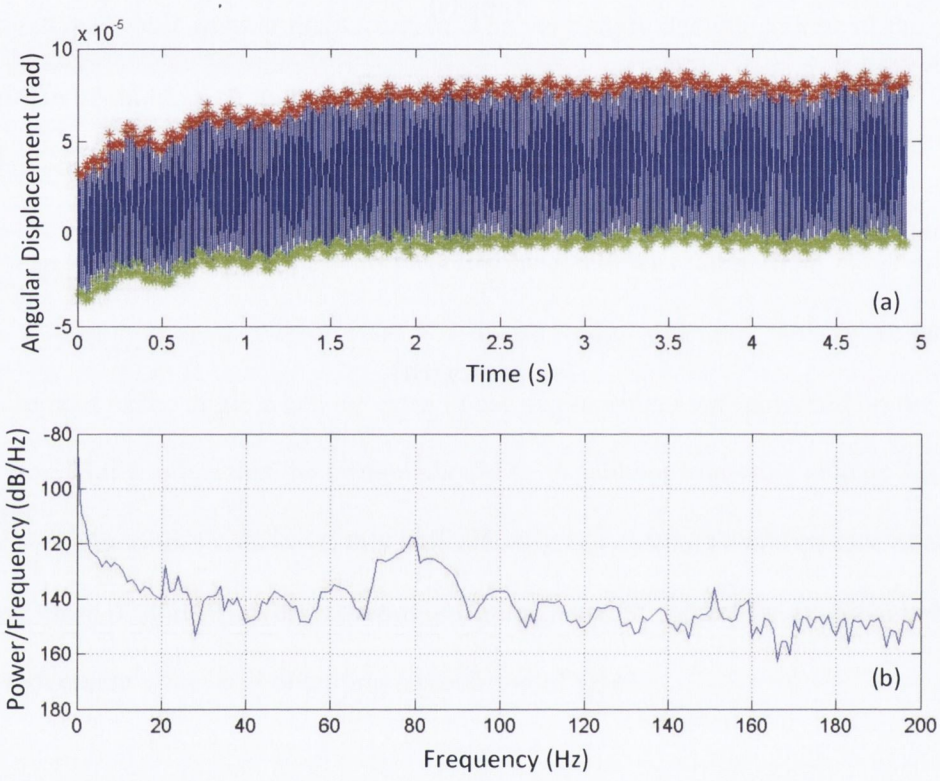

Figure 12. (a) Measured angular displacement and (b) periodogram for the simulator at 80 Hz, 87urad with an applied x-axis linear displacement.

3.3 Gimbal Results

3.3.1 Large Angle Amplitude Response

The results of the larger angle amplitude response test using the gimbal are shown in figure 13. It was found that once a frame-to-frame displacement of 6 mrad was reached the system could not provide an accurate measurement of the angular displacement. This is likely to be a result of a decorrelation between speckle patterns separated from the reference speckle pattern by more than 5 mrad. The system could not measure a frame-to-frame displacement of 10 mrad, which was found in section 1.3.4 to be the theoretical maximum frame-to-frame measurable angular displacement of the system, based purely on optical geometry and ignoring decorrelation.

In an attempt to overcome this difficulty, the cross-correlation algorithm was altered so that each speckle image was cross-correlated with the preceding image. Using this altered algorithm, the system was capable of measuring up to 10 mrad. The mean percentage error on these results was 10.5 ±3% over the range of measurements with a maximum error of 15%.

Both methods of measuring the output angular displacement are compared in figure 13. The measurement results agree well with the input, although the error begins to increase to approximately 10% at 1 mrad. As outlined in section 1.1.3, a microsaccade is expected to create a frame-to-frame displacement of 1.3 mrad. These results show that the system has the dynamic range to measure such a displacement.

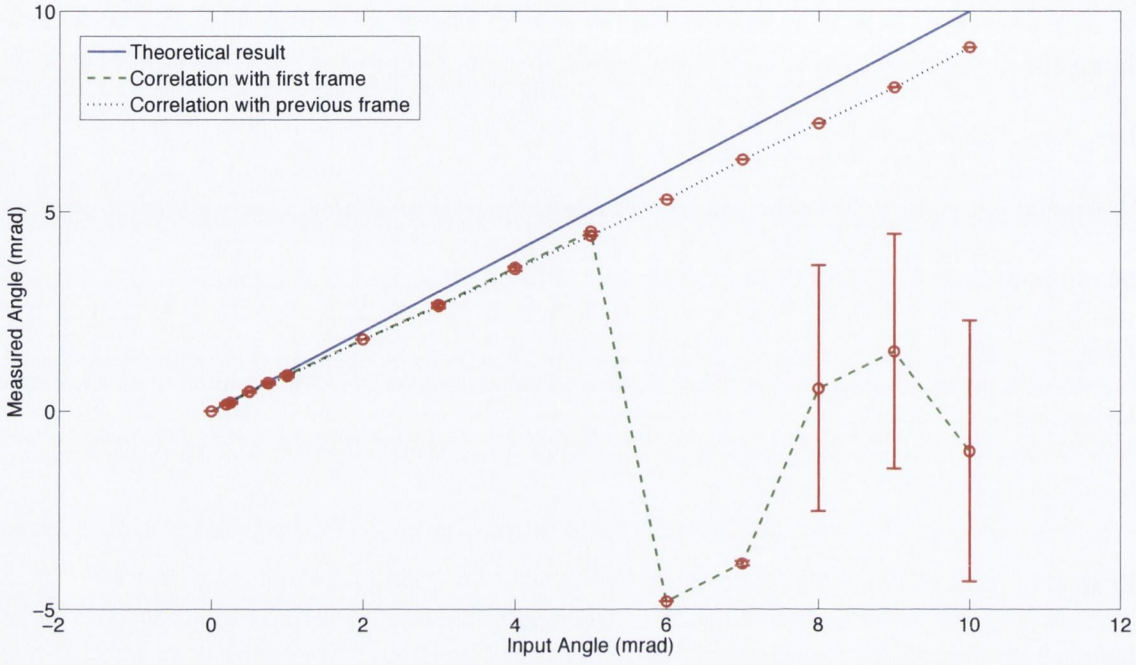

Figure 13. Applied v measured angular displacement of the gimbal in steps of 1 mrad. The dotted line shows the results from correlating each speckle frame with the original undisplaced reference frame. The dashed line shows the result when each frame is correlated with the previous frame.

As an evaluation of the decorrelation between the images, the cross-correlation peak height for image frames correlated with the undisplaced reference frame was measured. The value of the peak height was then divided by the mean correlation matrix floor value to calculate a ratio that could be compared across different image sets. As shown in figure 14, the peak height-to-floor ratio decreased with increasing frame-to-frame displacement. This is to be expected since the frames were becoming progressively more different.

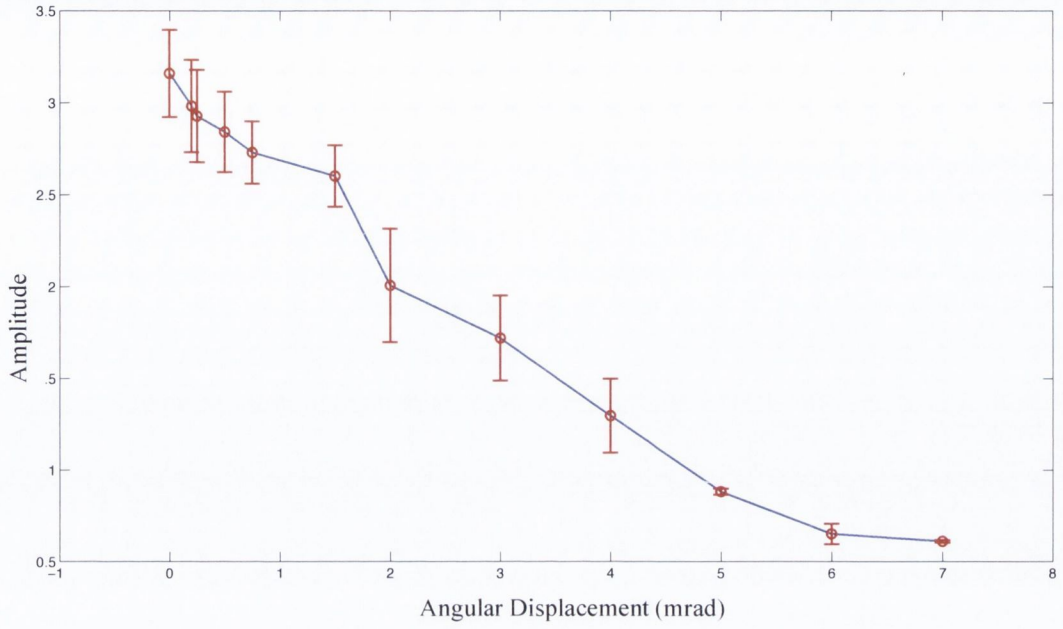

Figure 18. Decreasing correlation peak height to mean floor ratio for increasing frame-to-frame displacement.

4 Discussion

Overall the system was found to be capable of measuring frequencies and angular displacements within the OMT range of 12-216 μrad. Experimentally, the resolution was found to be 4 μrad as expected. This is close to the design requirement for an OMT measurement system.

The amplitude response of the system was found to be insensitive to target locations of up to ±25 mm along the optical axis. This has important outcomes *in-vivo* as it means that there are no strict target distance requirements. It will help ease the set-up alignment, since it is expected that there would be a variance in the target distance as each person places their head in the headrest at slightly different locations.

A linear displacement of the target during measurement of an OMT-like angular rotation at 80 Hz along the optical axis of up to 3 mm was found not to influence the measurement results. This insensitivity is important as it implies that angular displacements of the sclera can still be measured even if the head moves linearly during the recording.

Angular displacements larger than those of OMT were also investigated. It was found that the system was capable of measuring frame-to-frame angular displacements in the order of microsaccades (1.3 mrad) and in the order of the total expected frame-to-frame displacement from all eye and head movements (1.56 mrad).

The accuracy of the frame-to-frame displacement began to diminish at 6 mrad. The maximum expected frame-to-frame displacement is 1.56 mrad. 5 mrad sets a limit as to how much displacement can be tolerated relative to a reference frame. As discussed previously, the maximum expected angular frame-to-frame displacement for a handheld device would be 2.84 mrad, this falls within our measurable range and so the speckle correlation system could theoretically be suitable for such a handheld device.

5 Conclusions

A novel non-contact method for measuring ocular microtremor was reviewed. The parameters required for accurate measurement and methods to achieve them by implementing a speckle-based measurement of angular rotations were discussed. A resolution of 4 μrad and dynamic range of 4-5000 μrad was achieved with the system. It was shown that decorrelation due to other head/body movements will not be large

enough to have a detrimental effect on OMT measurement and that its signal should be recovered from a background of these movements.

Future work should include the effects of measuring speckle from living objects since this would involve a secondary type of boiling speckle known as biospeckle [41, 56, 107, 140]. Biospeckle will cause the speckle patterns to change in time. It is expected that this random time varying speckle will occur together with the wanted translational speckle from OMT movement. Biospeckle will decorrelate the speckle images and be a source of noise in the images. The rates of biospeckle from the human eye sclera have never been quantified nor has their influence on eye movement ever been investigated. To separate OMT related speckle pattern movements from biospeckle movements, the properties of *in-vivo* biospeckle from the sclera will need to be investigated. Further optimization of the proposed optical system may be required to overcome this biospeckle obstacle.

Chapter 3

Investigation of Scattering Influence on Speckle Correlation Technique

1 Introduction

Laser light reflected from an optically rough surface produces a pattern of bright and dark spots known as a speckle pattern [52]. Speckle correlation is used to measure an object's displacement by comparing two speckle patterns from the object, one before and one after the displacement. Chapter two detailed the design of a speckle correlation system to track eye movements in the amplitude range of ocular microtremor (OMT). The optical set-up used a Fourier plane imaging technique [96, 97] to measure rotational angular displacements. The performance of the speckle correlation system was tested and verified using an approximately singly scattering surface. A singly scattering surface is a simplified model of what is expected *in-vivo*. In an *in-vivo* situation, which features the eye sclera as a target for laser light, the laser light is expected to be multiply scattered by the scleral tissue.

The scattering that produces speckle can originate either from the surface of an object or from within the object's volume [52]. A rough metallic surface provides a good approximation to surface scattering. Surface scattering materials that singly scatter

polarized light, give rise to fully developed speckle patterns and have the corresponding speckle intensity distribution [52].

Volume scattering occurs when light penetrates a surface and undergoes multiple scattering before emerging from the surface. In cases of volume scattering, a material-dependent component of surface scattering also exists. Volume scattering is observed from inanimate objects such as paper [52] and from living objects such as biological tissue [141]. Materials that give rise to multiple scattering do not generate a fully developed speckle pattern [142].

The statistics of a speckle pattern depend on whether or not the illuminating light is polarized. Fully developed speckle patterns arise only from light that is fully polarized. Multiple scattering results in depolarized speckle. Since the speckle is not polarized, the basic assumptions of fully developed speckle [52] are broken. The speckle statistics, for example the speckle size, then become dependent on (amongst other things) the microstructure of the object from which the light is scattered [53].

If polarized speckle is observed through a polarizer, the speckle pattern will appear to have the same structure when the polarizer is rotated through orthogonal polarization states, though it will vary in intensity [52]. However, if the speckle is not polarized, two orthogonal states of a polarizer will result in a different speckle pattern structure observed for the same conditions of illumination [54].

Speckle patterns from a volume scattering material are notably different to speckle patterns produced by a simple single scattering surface. In volume scattering media, the speckle size is affected not only by the scattering co-efficient, but also by the scatterer dimension [143]. Single scattering has an effective beam width equal to the actual incident beam width, whereas multiple scattering widens the effective beam width.

Speckle from multiple scattering has been described as arising from a 'larger fuzzy halo' around the incident beam [144]. In a study by Xu *et al.* [107], they verified that the speckle size is determined by the size of the effective laser beam on the target material's surface, rather than the actual beam size. In their work, Xu *et al.* also demonstrated that the size of the effective beam diameter increases with depth of penetration into a material.

A larger effective beam width is associated with a smaller speckle size. Speckle patterns from a material into which light penetrates are composed of different sized speckle; (i) large speckles originating from light scattered from the surface and (ii) smaller speckles produced by light emerging from the inner volume of the material [111]. Xu *et al.* [107] described speckle from a living object as consisting of stationary surface speckles and speckles resulting from the movement of scatterers within the object. The observed speckle pattern, at a given time, can be thought of as an interference of surface speckle and volume speckle.

The theory of speckle metrology for speckle generated by volume scattering is less developed than that for surface scattering. For the most part, experiments involving speckle displacement measurements in the literature have been performed using singly scattering objects such as metal. Some research into speckle from multiple scattering materials has been performed by Semenov *et al.* [145]. In their work, they found that accurate measures for speckle translation from a multiple scattering material could be made, provided that surface scattering prevailed over the volume's multiple scattering. Given that multiple scattering is a random process, Semenov *et al.* theorized that even a tiny displacement of the multiple scattering material would cause phase changes between the internal scatterers in the material. Changes in the phases of scatterers are

known to result in a form of time-varying speckle and the speckle appears to 'twinkle' [111].

In this work, multiple scattering will be considered since, in a real *in-vivo* study using a 632.8 nm HeNe laser, the laser light is expected to penetrate the scleral surface. As noted by Briers *et al.* [111] multiple scattering leads to different speckle statistics than those for surfaces that give rise to fully developed speckle. The aims of the work in this chapter are (i) to examine the changes in speckle statistics caused by multiple scattering and (ii) to determine the influence of multiple scattering on measurements of angular rotation recorded using the proposed speckle correlation system.

To determine whether multiple scattering has an effect on the measured displacement, different target materials with various absorption and scattering properties are investigated. In addition, a mathematical model of the impact of the volume scattering component on displacement measurement is constructed.

The structure of speckle patterns observed from the volume scattering target materials are expected to be dependent on the polarization state of the backscattered light.

1.1 Tissue Optics

The optical properties of biological tissue determine the spatial and temporal characteristics of the laser speckle it produces. Tissue is an optically inhomogeneous, absorbing medium with an index of refraction higher than that for air [146]. Exact measurement of the refractive index of tissue and its constituent parts is difficult [2].

Multiple scattering and absorption cause a laser beam to broaden as it travels through a biological tissue [146]. Laser propagation in a tissue, such as the eye sclera, depends on

the absorption, scattering and refraction properties of the tissue, the cells and the cell parts that make up the tissue. The size, shape and density of tissue's cell components together with the polarization of the laser light all influence the propagation of the laser light in the tissue.

When laser light reaches a tissue, it becomes partly scattered, absorbed and refracted [41]. The absorption and scattering co-efficient of a material are both wavelength dependent. Absorption causes a decrease in the intensity of the light returned from the tissue. Using the eye-safe low laser powers required for the proposed speckle correlation system in this work, the reduction in intensity caused by absorption is expected to put a further stress on the image sensor and reduce the signal-to-noise ratio of the speckle images. Nonetheless, it is the scattered light that is of interest for speckle techniques. Multiple scattering diffuses the originally coherent laser light in both the spatial and temporal domains, effectively causing the coherent laser beam to become incoherent after travelling a few millimeters in the medium.

There are two classes of scattering tissue [141]; (i) strongly scattering tissue, mostly originating from opaque tissue, for example skin, blood and the sclera and (ii) weakly scattering tissue, originating from transparent tissue, for example the cornea and lens of the eye [141].

1.2 Mathematical Speckle Simulation

Speckle is a random phenomenon and therefore can only be described statistically. Goodman [52] has described the statistical properties of speckle. In his work, an optically rough, diffuse surface is considered to be formed by a set of scattering centres.

If the surface is illuminated by a coherent light source, each scattering centre n will give rise to an electric field of amplitude a_n and phase φ_n at a given point. It is assumed that

1. The amplitude and phase values are statistically independent of each other and of the amplitude and phase of all other field components.
2. The phases are uniformly distributed on the interval ($-\pi$, π), meaning that the surface is rough in comparison to the wavelength of the light.
3. The total number of scattering centres, N, is large so that the central limit theorem is obeyed.

The amplitude A of the total scattered light field at a given point is the sum of the N components representing the contributions from the different scattering centres i.e.:

$$A = \sum_{n=1}^{N} a_n e^{i\varphi_n} \qquad \textbf{Equation 1}$$

Based on this approach, Goodman developed an algorithm for numerically generating fully developed speckle patterns [52]. In the algorithm, a speckle pattern is assumed to consist of the sum of individual Gaussian speckles, which are distributed randomly over a pixel array. To generate a single speckle pattern, firstly an MxM array of complex numbers with unity amplitude and randomly distributed phases between 0 and 2π is created. This matrix is then Fast Fourier transformed in accordance with equation 1 to create an amplitude field. The power spectrum is then found by multiplying the result by its complex conjugate, creating a speckle intensity pattern. The final matrix represents the speckle field in the observation plane.

The observed speckle pattern depends not only on the motion of the scatterers but also on the parameters of the optical set-up and image sensor used to capture the speckle. For the optical configuration used here [96, 97], the linear displacement of surface speckle

depends only on the angular displacement of the object, detector pixel size and the lens focal length i.e. $\theta = \frac{dx \,.pixel\ size}{2f}$ where dx is the linear displacement in pixels.

2 Methods

2.1 Scattering From the Simulator

To test how the measurement technique responds to different target materials, the various materials were firmly attached to the plastic surface of the OMT simulator (detailed in chapter two) and used as a target for the laser beam.

Initially the white plastic surface of the simulator was used as the target. The simulator was set to move in a sine wave motion at 80 Hz with an amplitude in the OMT-like range of 5-197 μrad. Measurements were taken in steps of 20 μrad peak-to-peak.

The equipment was set-up as illustrated in figure 1 using an f=150 mm lens. The plastic surface of the simulator was used as a target and illuminated by a 632.8 nm plane polarized HeNe laser beam. The power of the beam was reduced down to 180 μW by using a neutral density filter and a beam splitter. A 5 s (2500 frames) video recording of the speckle pattern on the simulator surface was taken at each displacement amplitude using an EMCCD camera (Cascade 128+, Roper Scientific [138]) operating at 500 Hz with a 128x128 array of 24 μm pixels and a 100% fill factor.

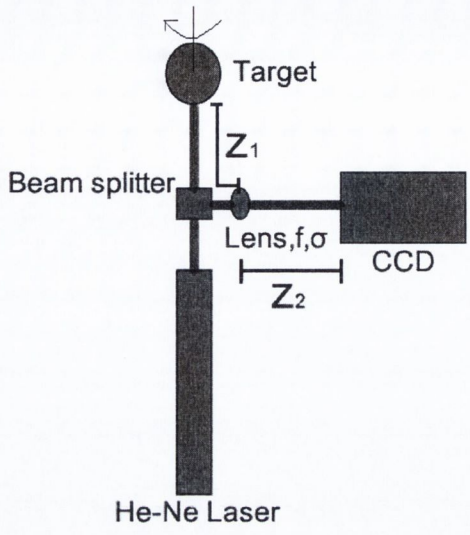

Figure 1. Experimental set-up.

To calculate the displacement between speckle image frames, the full 128x128 pixel array of each speckle image frame was used for processing and each frame was cross-correlated with a reference frame. A curve-fitting subpixel algorithm [78] was used to increase the accuracy in finding the exact correlation peak. The movement of the correlation peak location over time was used to calculate the subpixel displacement of the speckle images. Using the equation $\theta = \frac{p_x}{2f}$ [96, 97], the calculated pixel displacement, p_x, was converted to the measured angular displacement, θ.

To estimate the amplitude of the measured displacement, each trough in the sine wave was subtracted from each subsequent peak and the mean value was taken to be the peak-to-peak amplitude of the measured signal. To assess the frequency content of the signal a periodogram was utilised to estimate the power spectral density.

The experiment was repeated ten times at different target locations so that a unique speckle pattern was tested each time. The procedure was then repeated for metal, wood, polystyrene and cardboard samples attached to the simulator.

The calibration factor for each data set was calculated from the slope of the linear fit to the measured results. The mean calibration factor for each material was then calculated from the average value of these slopes. Bland Altman analysis [147], a statistical tool used to compare two different measurement techniques, was then performed on the data for each material.

2.1.1 Addition of a polarizer

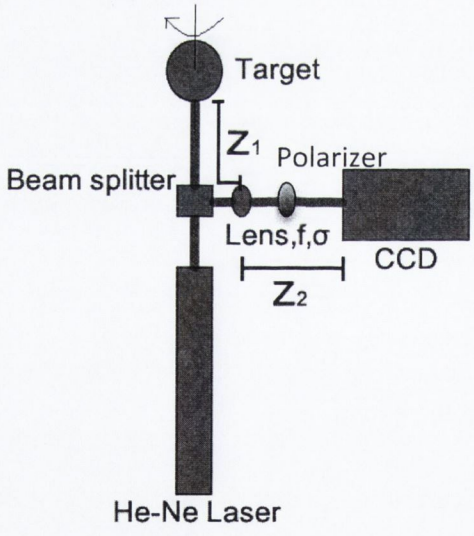

Figure 2. Experimental set-up.

A polarizer was included into the optical set-up to investigate the effects of polarization on the observed speckle patterns and on the measured angular displacement. The polarizer was added so that the reflected light passed from the lens through the polarizer

prior to entering the detector, as illustrated in figure 2. The procedure in section 2.1 was repeated for (i) the polarizer in parallel to the incident laser light polarization and (ii) the polarizer perpendicular to the incident laser light polarization. The experiment was repeated 5 times for each polarization state.

2.2 Scattering from Targets in the Gimbal

A gimbal (Melles Griot, 07MAD701) was used to investigate the scattering effects over angular displacements larger than those achievable with the simulator. The larger angular displacements replicate the amplitudes expected when head movements and other eye-movements are taken into consideration, as detailed in chapter two.

Two different surfaces were used as targets in the gimbal; cardboard and a piece of white plastic, approximately 2 mm thick. It should be noted that the plastic was a different piece of plastic to that used for the simulator. The gimbal has an azimuthal resolution of 50μrad and was used to rotate the target around the y-axis in steps of 50μrad up to a total displacement of 3 mrad. It was noted in chapter 2 section 3.3 that an angular displacement of 5 mrad will cause a decorrelation so large that the measurement technique would break down. 3 mrad was chosen as the maximum displacement since it is above the expected microsaccade displacement (1.45 mrad), but below the 5 mrad decorrelation limit of the system. The observed speckle pattern was recorded at each rotation step.

In an *in-vivo* study, biospeckle will be recorded from the eye. Biospeckle is a time-varying form of speckle that demonstrates random changes in speckle location and speckle shape. In an attempt to avoid potential measurement errors caused by biospeckle, correlation of a speckle frame with the previous frame might be more

suitable than correlation with an original reference frame. Displacement traces were generated both by correlation with an original reference frame and by correlation with the previous frame.

The experiment was repeated ten times for both target materials. Different target locations were used to ensure that a unique speckle pattern was produced each time.

2.3 Simulated Speckle

The aim of the mathematical simulation was to replicate speckle from a volume scatterer, such as plastic, and investigate the influence of multiple scattering on the measured displacement at OMT-like amplitudes. To perform the simulation, two speckle fields were created; one to represent surface scattering and one to represent volume scattering. The two fields were then made to interfere with each other by adding them on a complex amplitude basis. The pixel size and focal length are inputted into the numerical simulation as constants. The procedure to create two numerically generated speckle patterns from a volume scattering material is outlined in figure 3.

To replicate the speckle pattern from surface scattering, a complex amplitude speckle field $S_1(,x,y)$ was generated with a speckle size, σ_s, of 2.1 pixels. Each subsequent scattering field $S_{1+n}(,x,y)$ was made to translate in a manner that imitates motion from the OMT simulator. To do this, a sine wave signal with a frequency of 80 Hz and fixed amplitude within the simulator range (i.e. 4-197 μrad) was generated and used to displace the surface scattering field's matrix.

As stated, the speckle size of volume speckle is smaller than that of surface speckle. Therefore, the speckle size of the secondary, multiple scattering, volume field $V_n(x,y)$

was given a smaller value of σ_v =1.5 pixels. It was found experimentally that the combination of σ_s= 2 and σ_s =1.5, gave a final speckle size of σ_f= 1.6 pixels, which agrees with the value found for the plastic surface.

The volume field was not made to translate. In accordance with the conclusions of Semenov *et al.* [145], the field was, however, given a small phase change between frames $V_n(x,y)$ and $V_{n+1}(x,y)$. This resulted in time varying speckle. The phase change was controlled by the parameter, $\sigma\Delta\varphi$. $\sigma\Delta\varphi$ represents the standard deviation of the phase change between two frames. To create a new phase matrix for every new frame $V_{n+1}(x,y)$, $\sigma\Delta\varphi$ it is multiplied by a matrix of random number prior to being added to the phase matrix of frame $V_n(x,y)$.

A multiple scatter amplitude factor (MSAF) with a value between zero and one was used to scale the volume scattering field prior to addition with the single scattering field. The MSAF defines the fraction of the total speckle field that is composed of a volume scattering component relative to a surface scattering component and represents the ratio of the mean amplitudes of the fields.

As stated, to create the final speckle field $T_n(x,y)$, the two speckle fields were added on an amplitude basis, using their complex number form. This total field was then multiplied by its complex conjugate to create a speckle intensity image $I_n(x,y)$.

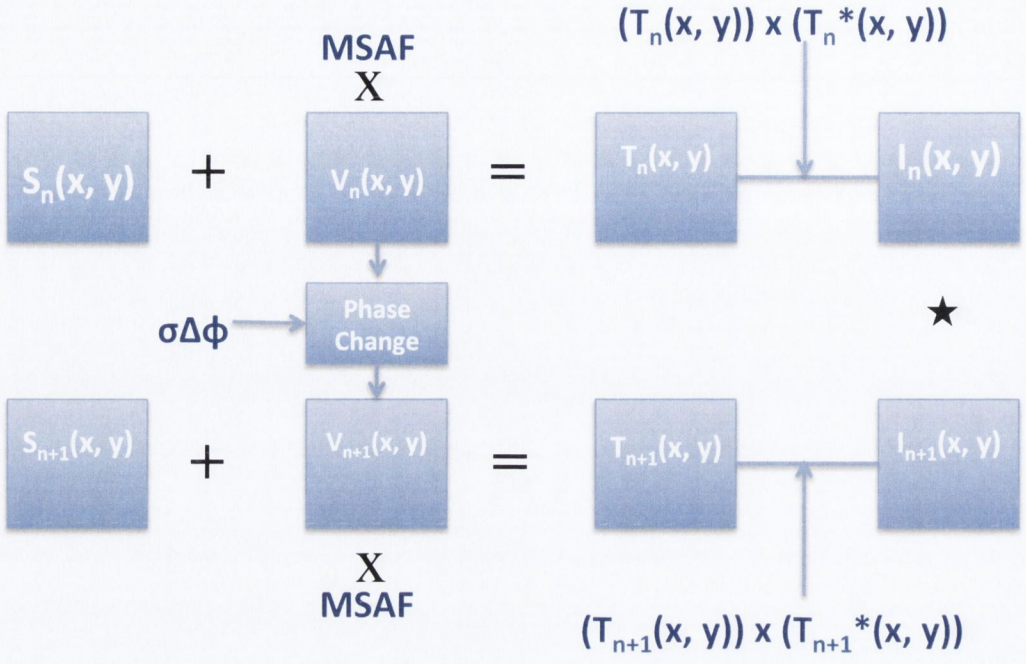

Figure 3. Formation of simulated speckle images to be cross-correlated.

The simulated speckle was first used to investigate whether the degree of correlation between multiple scattering fields had an effect on the measured displacement of the final speckle image. To do this, the multiple scattering's speckle field was given a phase change between image frames by using a phase change parameter, $\sigma\Delta\varphi$. Briefly, a value of $\sigma\Delta\varphi = 1$ indicates total decorrelation and randomness between multiple scattering fields. Conversely, a value of $\sigma\Delta\varphi = 0$ indicates no decorrelation and unchanged fields. The effects on the measured displacement of varying this phase change were investigated at a fixed MSAF value of MSAF =1. The simulation was repeated 5 times for both $\sigma\Delta\varphi = 1$ and $\sigma\Delta\varphi = 0$ so that different initial speckle patterns were tested.

Next, the MSAF value was varied between 0 and 1 in steps of 0.1 at a constant value for $\sigma\Delta\varphi$. By varying the MSAF value and the input angular displacement, the effects on the

measured displacement of varying the amplitude of the multiple scattering field relative to the surface scattering field were investigated.

All codes were written using the numerical software package Matlab [139].

3 Results

3.1 Scattering from the simulator

When using the plastic, polystyrene and wood as target materials, some laser light penetrated through the materials. A diffuse glow was seen surrounding the main incident beam, caused by multiple scattering. Figure 4 illustrates this effect for the simulator's plastic. The radius of the effective beam on the simulator's plastic surface was 4 mm, whereas the actual laser beam radius was 0.6 mm. This penetration and diffuse glow was not observed for the metal or cardboard surfaces.

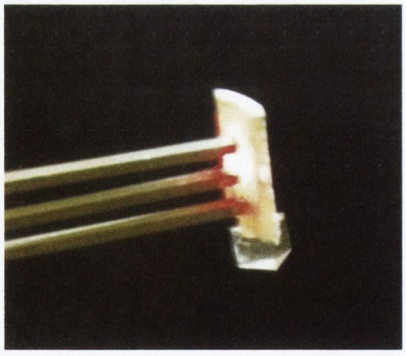

Figure 4. Laser beam penetration through the simulator's plastic surface.

Figure 5 shows five sequential frames for the simulator running at 80 Hz 197 μrad peak-to-peak. With the camera sampling at 500 FPS and the simulator running at 80 Hz, these

five frames represent patterns generated over the full displacement cycle of the simulator. The figure shows that the changes from frame-to-frame are not excessively random. The speckle frames appear very similar and no qualitatively obvious decorrelation is seen. However, when the speckle image frames were played as a movie file, some background 'twinkling' of speckle between frames was noted. The apparent twinkling is suggestive of a degree of speckle boiling present in the speckle image frames. The appearance is qualitatively consistent with the modeled concept of a moving surface, with an unchanging surface speckle field, and a fixed, but possibly boiling, volume scattering field.

The input versus output displacement traces for all materials are shown in figure 6. The tested range of 5-197 μrad is equivalent to a displacement in terms of speckle size of 0.03-1.13 speckles, for a speckle size equal to two pixels. As shown in the figure, the measured displacement from the plastic, polystyrene and wood surfaces are much lower than expected. Each material showed a linear relationship between the measured and expected results over the tested range. The R^2 value was approximately unity for every material.

The various materials gave different calibration factors. The calibration of the materials, determined from the slope of the linear fit to the measured data, were found to be 1.02±0.02, 0.96±0.01, 0.66±0.04, 0.67±0.03 and 0.60±0.03 for non-glossy cardboard, metal, polystyrene, wood and plastic respectively. For each material, the calibration factors were not found to differ radically with different beam target locations i.e. with different speckle realizations. This is exemplified by the low standard deviations in the calibration factors.

The speckle reflected from the metal surface had a strong intensity and some pixels were saturated, this may have influenced the measurement result. As can be seen from the graph, the cardboard and metal surfaces had results closest to the expected results. The plastic surface showed the greatest deviation from the expected results.

As can be seen from the error bars on the graph, at low amplitudes the precision of the measurements were high and standard deviations of 0.32 μrad and 0.71 μrad were calculated for plastic and cardboard respectively. Note that the standard deviations refer to estimates of the mean amplitude (each made over 5 s of data) across the 10 different setups (or speckle realizations), and give a sense of the variation expected from setup to setup for the same material. Beyond about 60 μrad, the spread in measurements grew for both materials but varied between relatively high and low spreads at different amplitudes. The standard deviation for plastic and for cardboard at 197 μrad were 6.14 μrad and 6.73 μrad respectively.

Figure 5. Five sequential speckle frames taken 2 ms apart, using an integration time of 2 ms and using a plastic target on the simulator. The simulator was running at 80 Hz, 197 μrad peak-to-peak.

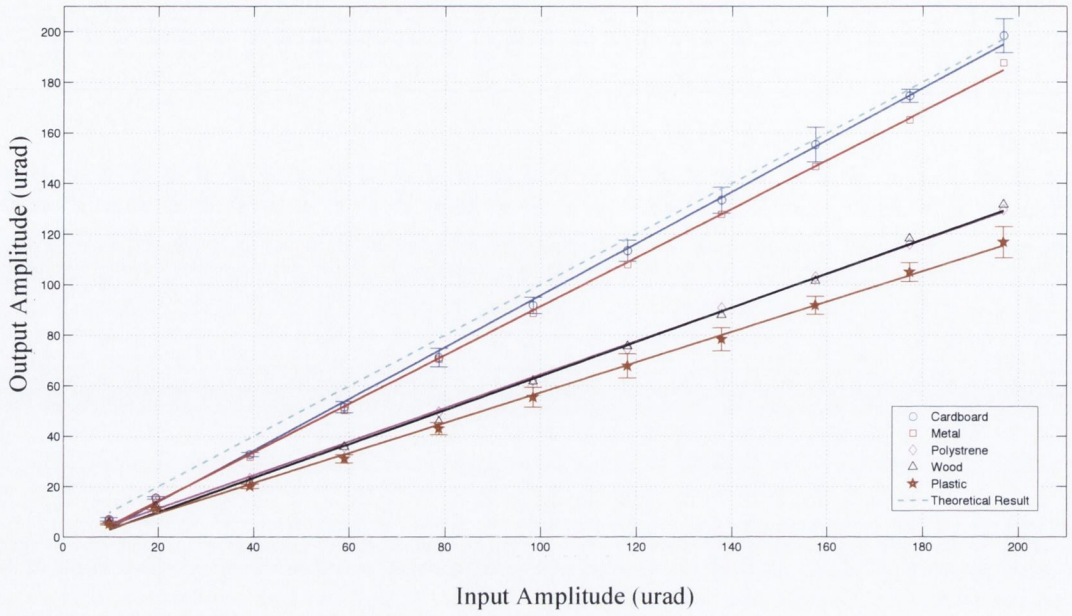

Figure 6. Applied v measured angular displacement for different target materials attached to the simulator. Each frame was correlated with an original reference frame. The simulator was running at 80 Hz and frames were captured at 500FPS with an integration time of 2 ms. The error bars represent the standard deviation between the mean amplitude of each of the ten measurement results.

Figure 7 (a) - (e) displays the Bland Altman plots for the various single and multiple scattering surfaces tested.

In each case, the distribution of the measurement difference was found to be uniform. The non-normal distribution is likely to be a result of both the small sample size and the fact that the sample was not random due to the specific range being investigated. While typically Bland Altman statistics are performed on normally distributed data, some studies, including one by Bland and Altman [148] suggest that non-normality is not a serious concern.

(a)

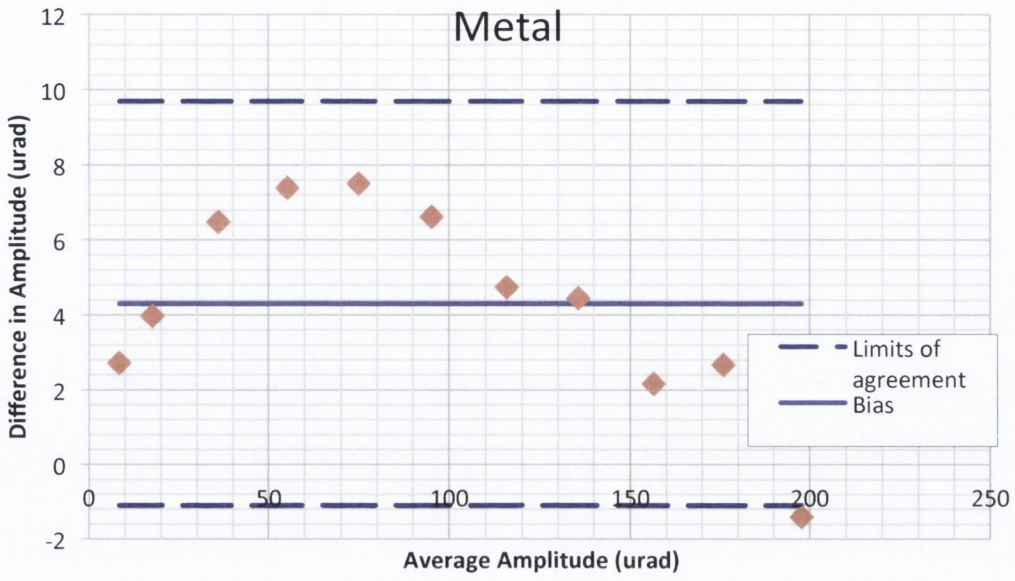
Metal
Difference in Amplitude (urad)
Average Amplitude (urad)
Limits of agreement
Bias
12
10
8
6
4
2
0
-2
0
50
100
150
200
250

(b)

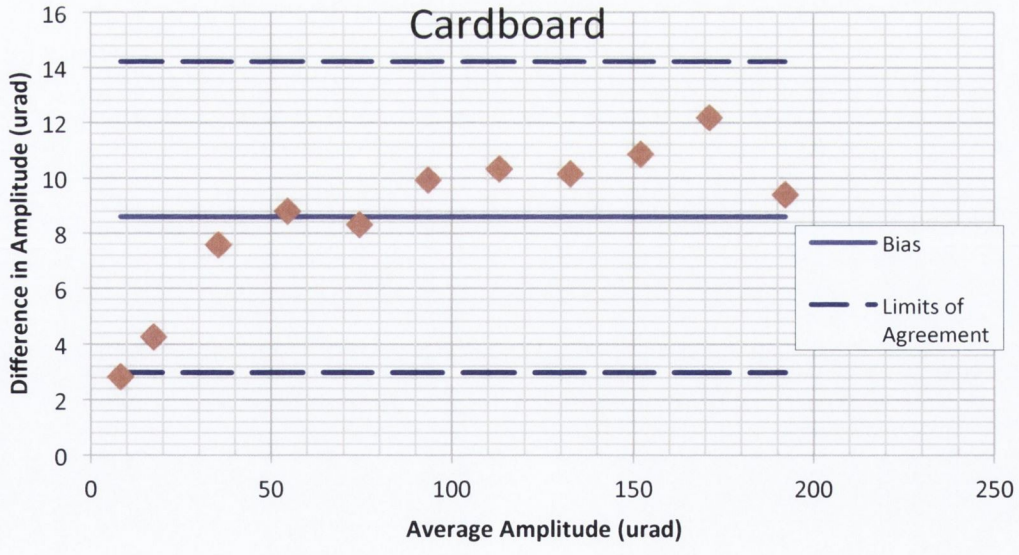
Cardboard
Difference in Amplitude (urad)
Average Amplitude (urad)
Bias
Limits of Agreement
16
14
12
10
8
6
4
2
0
0
50
100
150
200
250

(c)

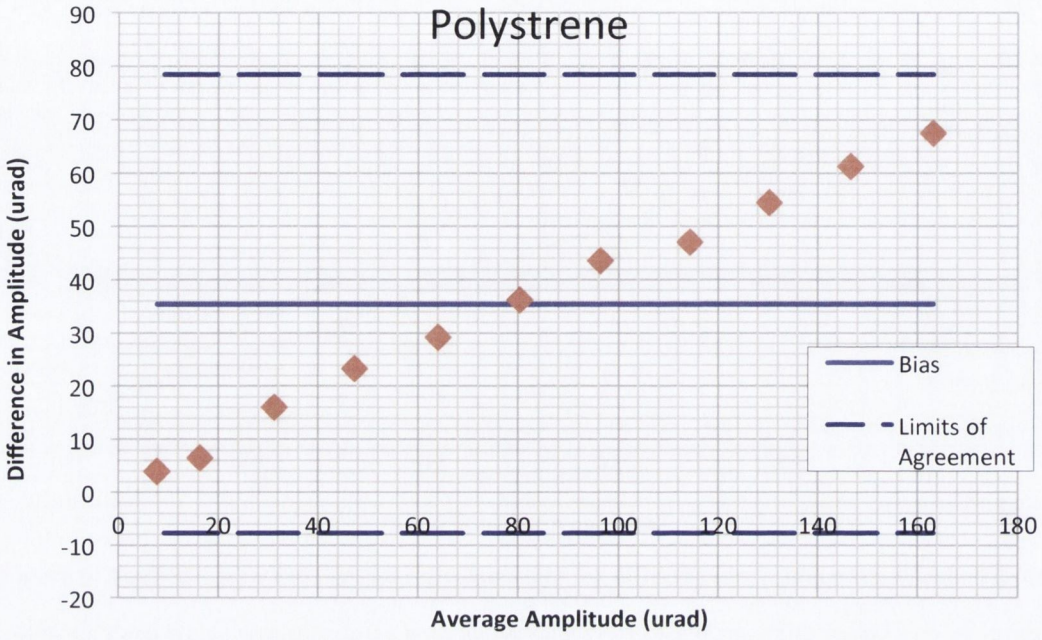
Polystrene
Difference in Amplitude (urad)
Average Amplitude (urad)
Bias
Limits of Agreement
90
80
70
60
50
40
30
20
10
0
-10
-20
0
20
40
60
80
100
120
140
160
180

(d)

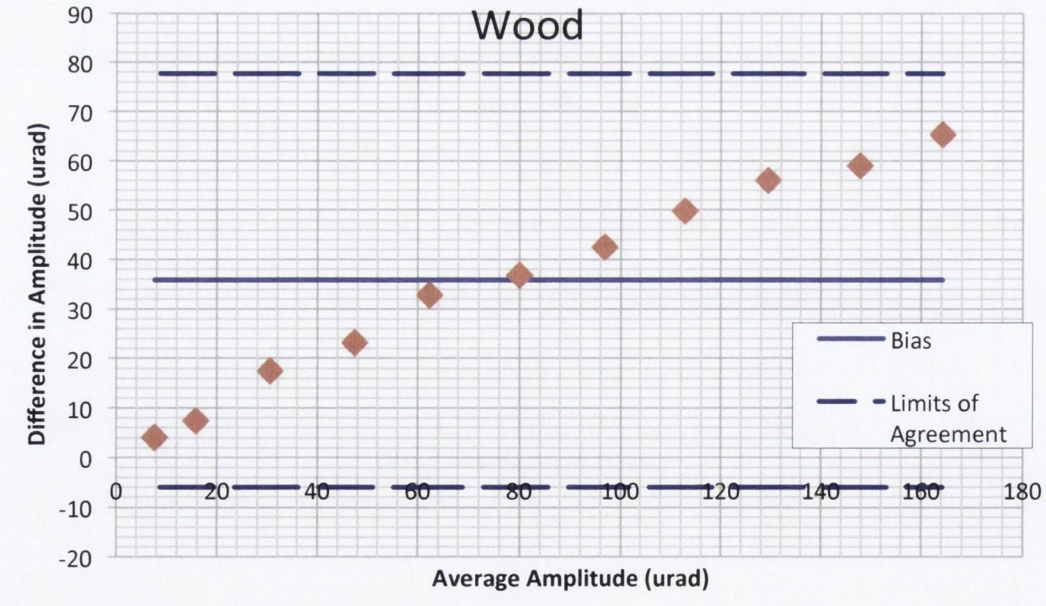
Wood
Difference in Amplitude (urad)
Average Amplitude (urad)
Bias
Limits of Agreement
90
80
70
60
50
40
30
20
10
0
-10
-20
0
20
40
60
80
100
120
140
160
180

(e)

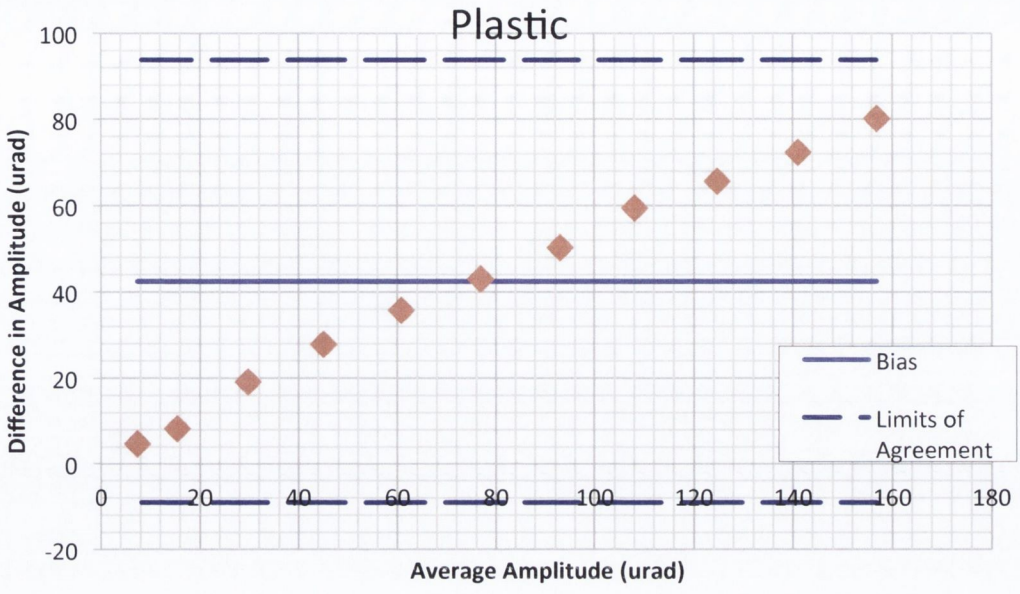

Figure 7. Bland Altman plots for (a) metal, (b) cardboard, (c) polystyrene, (d) wood and (e) plastic surfaces.

The Bland Altman graphs for the multiple scattering surfaces (polystyrene, wood and plastic) display an obvious proportional error for the amplitude. This is consistent with the bias error seen in figure 6.

3.1.1 Addition of a polarizer

Figure 8 shows speckle images taken from the simulator's plastic surface (a) with no polarizer, (b) with the polarizer parallel to the incident laser light's polarization state and (c) with the polarizer perpendicular to the incident laser light's polarization state. The simulator was stationary when the shown images were captured.

As expected from Goodman [54], when the polarizer was rotated from the parallel to the perpendicular state, the speckle pattern changed appearance. The normalized cross-

correlation of images (a) and (b) was highest at 0.71, (a) with (c) was 0.45 and (b) with (c) was only 0.20. These results show that the some of the speckle reflected from the simulator plastic have lost their original polarization state.

Figure 9 shows the result of adding the perpendicular and parallel speckle patterns. It is expected that the weighted sum of intensity patterns of the two orthogonal states will produce a speckle pattern that is equivalent to the speckle pattern seen in the absence of a polarizer. In this case, the sum of the parallel state plus 30% of the intensity pattern from the perpendicular state was found to produce the highest correlation with the pattern found without a polarizer. The normalized cross-correlation between the speckle pattern captured with no polarizer and the pattern generated from the weighted sum of the two orthogonal polarizers was 0.72. This value is higher than the correlations found in the above section.

Figure 8 (d) to (f) show the same measurements for a metal surface. In this case, the observed speckle patterns did not change. This is because the metal surface gave rise to single scattering and resulted in a fully polarized speckle pattern. The only notable change was a lower intensity level for the speckle images with a polarizer. The normalized cross-correlation of images (a) and (b) was 0.91, (a) with (c) was 0.86 and (b) with (c) was 0.97. When no polarizer was included in the set-up, the strong reflection from the metal surface caused some pixels to saturate. The correlation of speckle images with and without a polarizer was slightly reduced from the ideal value of 1, presumably this is due to the aforementioned saturation.

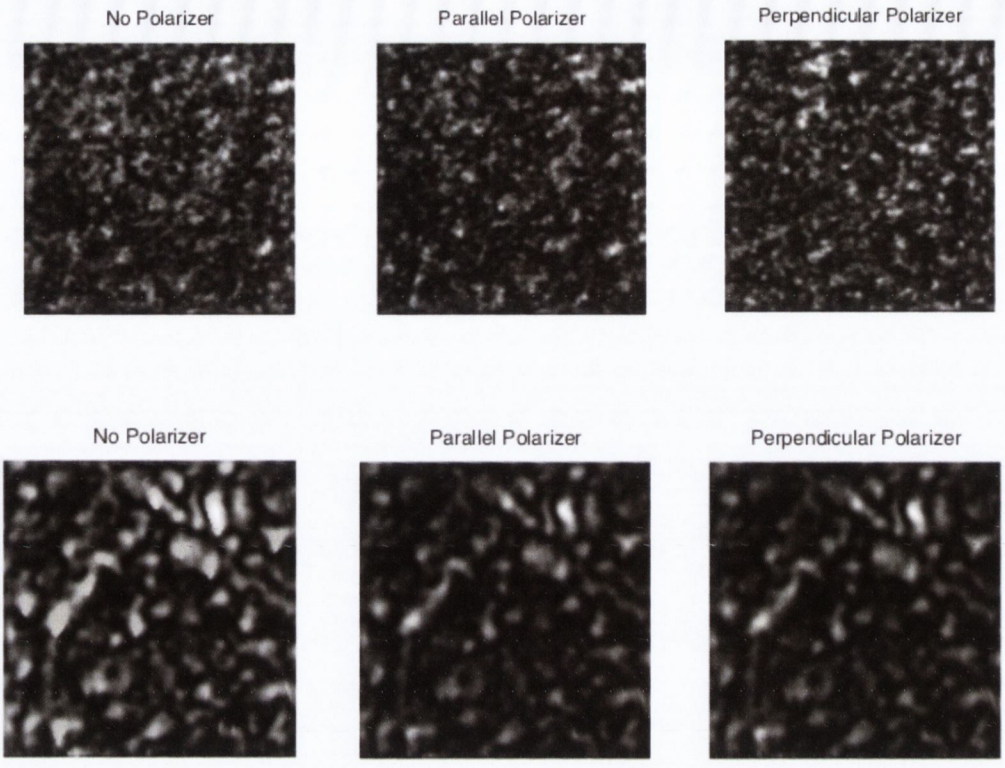

Figure 8. Top: Different polarizations of speckle images captured from the simulator's plastic surface. Bottom: Different polarizations of speckle images captured from a metal surface.

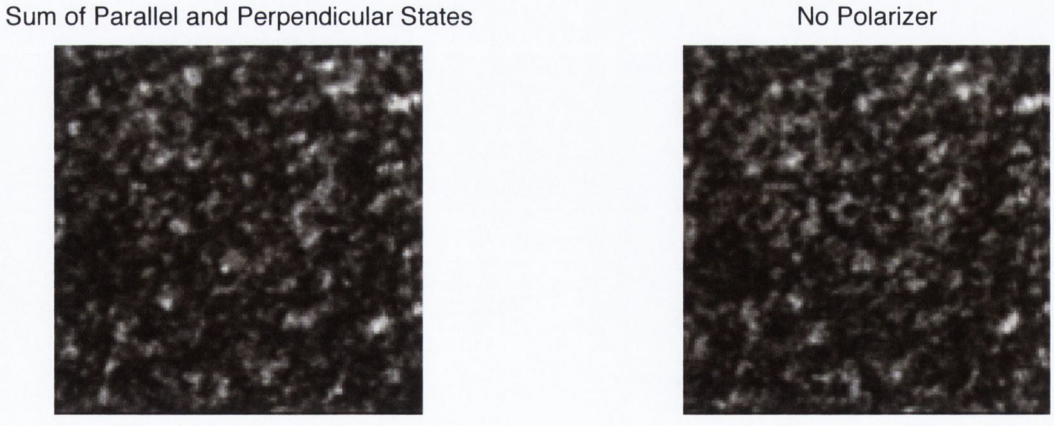

Figure 9. The weighted sum of speckle patterns recorded in the parallel and perpendicular state (left) and the speckle pattern recorded in the absence of a polarizer (right).

Figure 10 shows the measured angular displacement of the simulator with a plastic surface for the case of (i) no polarizer, (ii) the polarizer parallel to the laser light and (iii) the polarizer perpendicular to the laser light. The results show that polarization had little influence on the displacement measurement. The polarizer in the perpendicular state gave the lowest accuracy and a calibration factor of 0.52±0.02. The parallel state gave a similar calibration factor (0.58±0.04) to that without the polarizer in place (0.60±0.03).

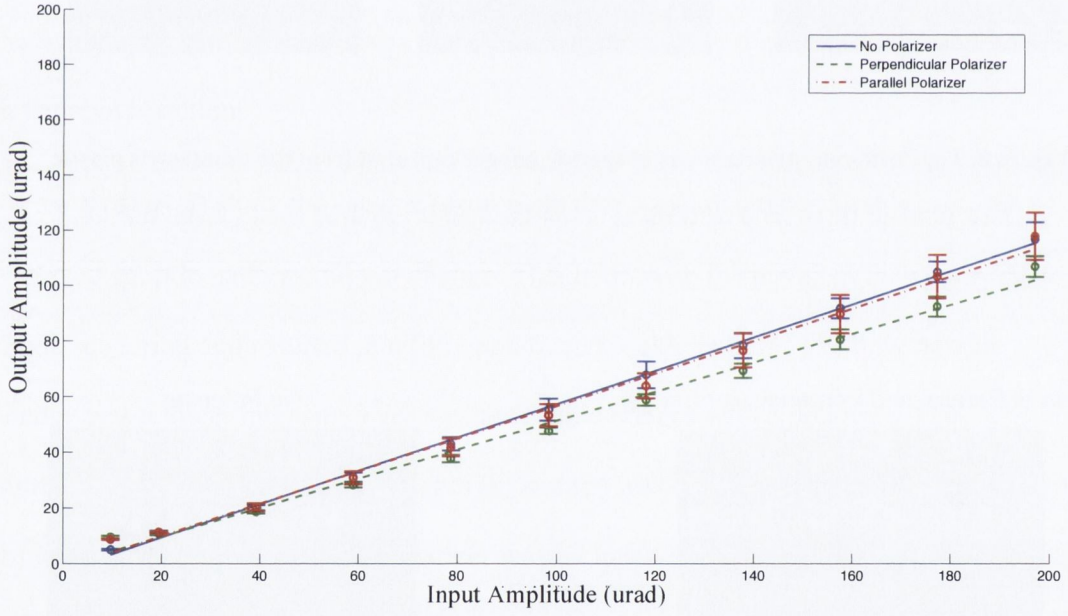

Figure 10. Influence of a polarizer on the applied v measured angular displacement from the plastic simulator surface. Each frame was correlated with an original reference frame. The simulator was running at 80 Hz and frames were captured at 500FPS. The error bars represent the standard deviation between the mean amplitude of each of the five measurement results.

3.2 Scattering from Targets in the Gimbal

3.2.1 Observed speckle pattern

The speckle pattern from the cardboard and plastic surfaces appeared notably different. The plastic surface gave rise to a grainier-appearing pattern, while speckle from the cardboard was smoother, as displayed in figure 11.

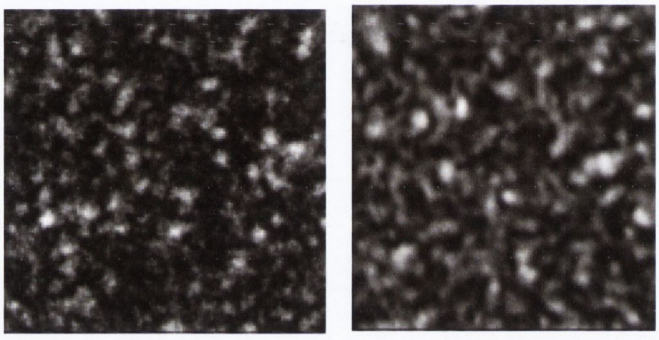

Figure 11. Speckle pattern from plastic scatterer (left) and speckle pattern from cardboard scatterer (right). The image intensities were stretched to fill the full range from 0-255 in order to aid visual inspection.

3.2.2 Speckle Size

The speckle size for the plastic used in the gimbal was calculated from the FWHM of the speckle image's autocorrelation plot to be 1.56 pixels. The speckle size for the cardboard target was 2 pixels. The radius of the effective beam size (including the halo around the main beam) on the plastic was approximately 4 mm. The reduced speckle size for the plastic was a consequence of the increase in effective beam width.

3.2.3 Measured Displacement from Various Targets in Gimbal

The results of measuring the angular displacement of speckle from a cardboard and from a plastic surface are shown in figure 12. Unlike the plot for a small angle displacements using the simulator, no noticeable difference between the curves corresponding to the non-transparent cardboard and the semi-transparent/multiple scattering plastic material can be seen.

Analogous to the results from the simulator, the gimbal results show a linear relationship between measured and set displacements, when the full measurement range is considered. The R^2 values for the cardboard and plastic materials were both calculated to be approximately equal to 1. The calibration factors for the materials, when each frame was correlated with the first frame, were calculated to be 0.91±0.03 for the cardboard and 0.89±0.03 for plastic. In these cases, the percentage accuracy for cardboard was 92±9% and for plastic was 92±14%.

For both plastic and cardboard, the measured displacement had a larger error when each frame was correlated with the previous frame. The calibration factor reduced to 0.70±0.06 and 0.70±0.05 for the cardboard and plastic respectively. The results from the 'frame-to-frame' and the 'frame to first frame' correlation results suggest a possible non-linearity in the amplitude response. For the former, the 50 μrad inter frame displacements yield the calibration factor of 0.7 noted above, as the displacement between frames increases the calibration factor tends towards 0.9. This is illustrated in figure 12(b), where the small amplitude displacement measures made on the gimbal are shown.

For this frame-to-frame correlation, the displacement being measured between each frame was 50 μrad repeatedly. Linear fits to the simulator data show mean measured

displacements of 27.4 μrad and 45.1 μrad, for the plastic and cardboard respectively, at a 50 μrad input.

However, using the gimbal, the mean measurement between frames was calculated to be 34.77±7.15 μrad for plastic and 34.82±6.69 μrad for cardboard. The discrepancy between values measured using the gimbal and using the simulator may be due errors introduced into the gimbal measurements from moving the micrometer screw by hand.

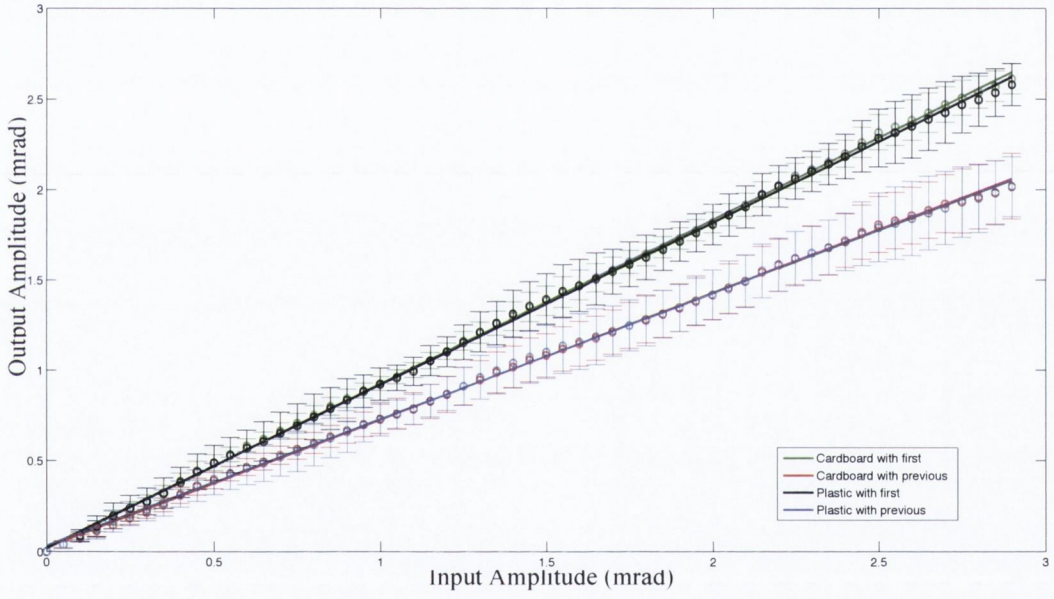

Figure 12 (a). Input displacement versus measured output displacement for two different target surfaces in the gimbal. The error bars represent the standard deviation of all ten measured displacements.

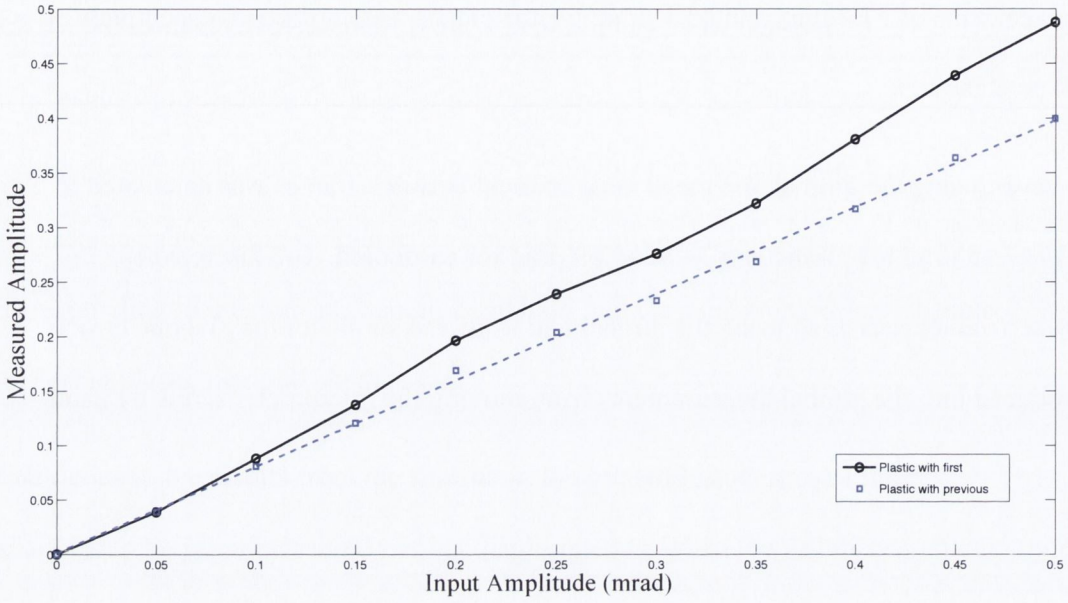

Figure 12 (b). Input displacement versus measured output displacement for plastic target as above. The graph is scaled down to the lower amplitudes where a curve in the measurements can be seen.

3.3 Speckle Simulation

The results of varying the decorrelation between multiple scattering fields, through use of the phase change factor $\sigma\Delta\varphi$ are shown in figure 13. The mean amplitude of each of the five measurement results is shown as points and a linear fit to the data was plotted. The error bars represent the standard deviation between the mean amplitude of each of the five measurement results As can be seen from the figure, the error bars (representing standard deviation) were, generally, smaller for $\sigma\Delta\varphi = 0$ than for $\sigma\Delta\varphi = 1$. The mean of the standard deviation on the measurement results for $\sigma\Delta\varphi = 0$ was 1.39 μrad, while for $\sigma\Delta\varphi = 1$ it was 4.81 μrad. This implies that at high decorrelation, there is a good accuracy in the measurement results but a poor precision. In contrast, when there was no decorrelation, a poor accuracy but a good precision was found. The multiple scattering amplitude factor was kept constant at MSAF = 1 while these results were taken.

For $\sigma\Delta\varphi = 1$, the results demonstrate that a completely decorrelated multiple scattering field has no real effect on the calibration factor when the multiple scatter amplitude factor is set equal to unity. The input versus output displacement trace for this value of phase change showed a slight deviation from linearity with $R^2 = 0.98$. The calibration factor was calculated to be 0.90.

When the multiple scattering field was left constant between frames ($\sigma\Delta\varphi = 0$), the calibration factor was reduced to 0.18. The plot was linear and had a value of $R^2 = 1$.

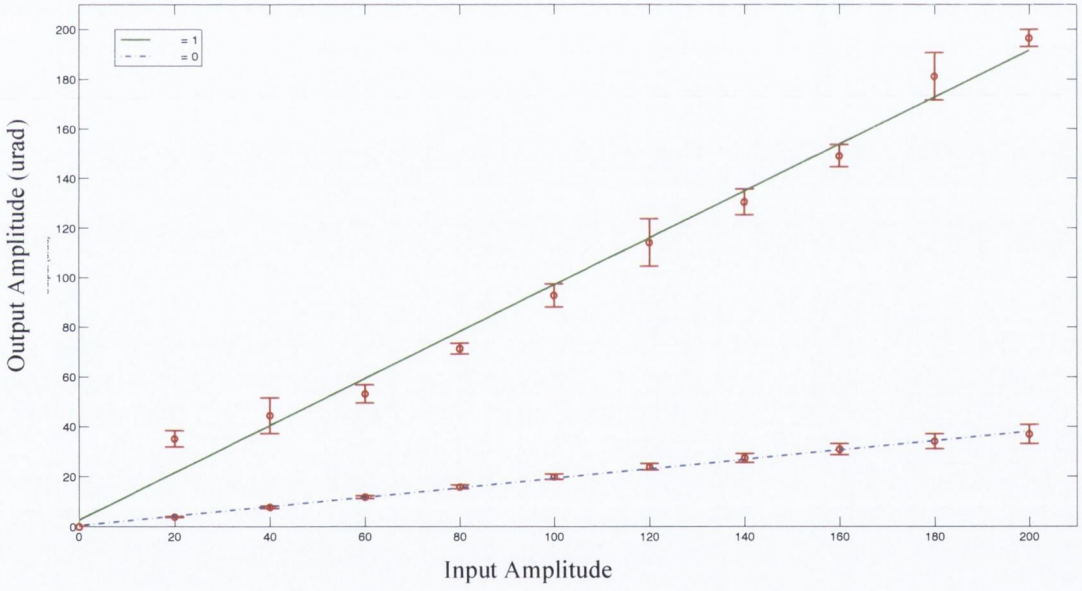

Figure 13. Input v output displacement for simulated speckle. The solid line represents complete decorrelation between the volume scattering image frames. The dashed line represents no decorrelation. The multiple scatter amplitude factor (MSAF) was set equal to unity.

The recovered sine waves found at values of $\sigma\Delta\varphi = 1$, $\sigma\Delta\varphi = 0.1$, $\sigma\Delta\varphi = 0.01$ and $\sigma\Delta\varphi = 0$ are shown in figure 14. For completely decorrelated volume scattering fields ($\sigma\Delta\varphi = 1$), the unfiltered measured simulated waveform gave a peak-to-peak amplitude of 152

μrad. This was a good agreement to the inputted value of 160 μrad, however, it showed some noisy digression from the smooth inputted sine wave. A similar noisy sine wave was found for $\sigma\Delta\varphi = 0.1$. However, at $\sigma\Delta\varphi = 0.1$ the measured average peak-to-peak amplitude of the sine wave signal decreased and was calculated to be 66 μrad. At a value of $\sigma\Delta\varphi = 0.01$, the recovered sine wave showed little variation and the measured peak-to-peak amplitude decreased to 45 μrad. This value of $\sigma\Delta\varphi = 0.01$ represents a small phase change between multiple scattering frames, meaning the frames have a degree of correlation. A value of $\sigma\Delta\varphi = 0$ showed a similar reduction in amplitude and smooth sine wave.

A phase change equal to zero is equivalent to a multiple scattering field that does not change or move between frames. However, it is supposed in this work that the multiple scattering field does vary between frames. For this reason, a phase change of zero was not further considered.

The *in-vitro* results using the OMT simulator display smooth sine waves and so values of $\sigma\Delta\varphi$ that distorted the measured sine wave in the simulated case are not thought to be a good representation of the *in-vitro* results. Based on these considerations, a value of $\sigma\Delta\varphi = 0.01$ was chosen as an approximation to the *in-vitro* results.

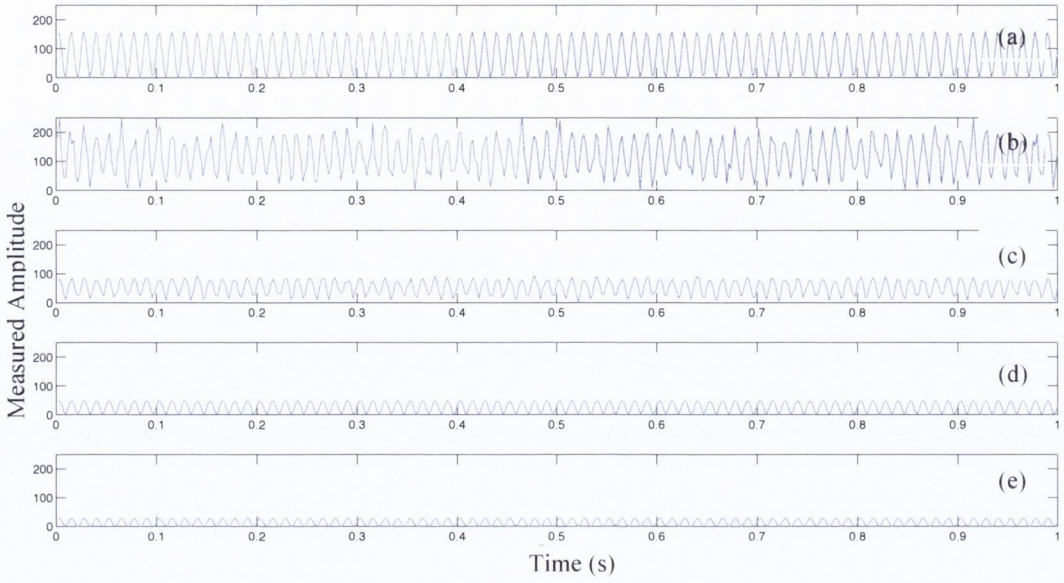

Figure 14. Simulated measured waveforms for different degrees of speckle phase change with MSAF = 1. (a) Input sine wave, (b) $\sigma\Delta\varphi = 1$, (c) $\sigma\Delta\varphi = 0.1$, (d) $\sigma\Delta\varphi = 0.01$ and (e) $\sigma\Delta\varphi = 0$.

Figure 15 shows the displacement results for varying the prominence of the multiple scattering field in the total field. The prominence was varied using multiple scatter amplitude factors between 0-1. For these measurements, a value of $\sigma\Delta\varphi = 0.01$ was used as the phase change factor. This value was shown to result in a smooth output sine wave and in a decreased peak-to-peak amplitude, as found with the *in-vitro* results.

The results of this simulation found that a secondary (multiple scattering) speckle field made to interfere with the primary (surface scattering) field did cause a modulation in the measured displacement. As displayed in the figure, the accuracy of measurement reduced as the amplitude reduction factor (MSAF) became larger, i.e. when the amplitude/prominence of the multiple scattering field became larger. The calibration factors were calculated to be 0.96, 0.96, 0.90, 0.87, 0.77, 0.60, 0.61, 0.31, 0.26, 0.26 and

0.14 for MSAF values corresponding to 0, 0.1, 0.2, 0.3, 0.4, 0.5, 0.6, 0.7, 0.8, 0.9 and 1. All values of MSAF resulted in linear traces.

The measured results from the simulator using a plastic target are also shown on the plot. As can be seen, when the MSAF value was 0.5, the results from the mathematically simulated speckle agreed well with the measured results using the OMT simulator with a plastic target. At this value of MSAF, the calibration factor was 0.6. This is in exact agreement with the calibration factor found for plastic in section 3.1.

On the basis of these results, it is theorized that it is the value of MSAF rather than the degree of change in the multiple scattering field that influences the material-dependent amplitude calibration established from the *in-vitro* results.

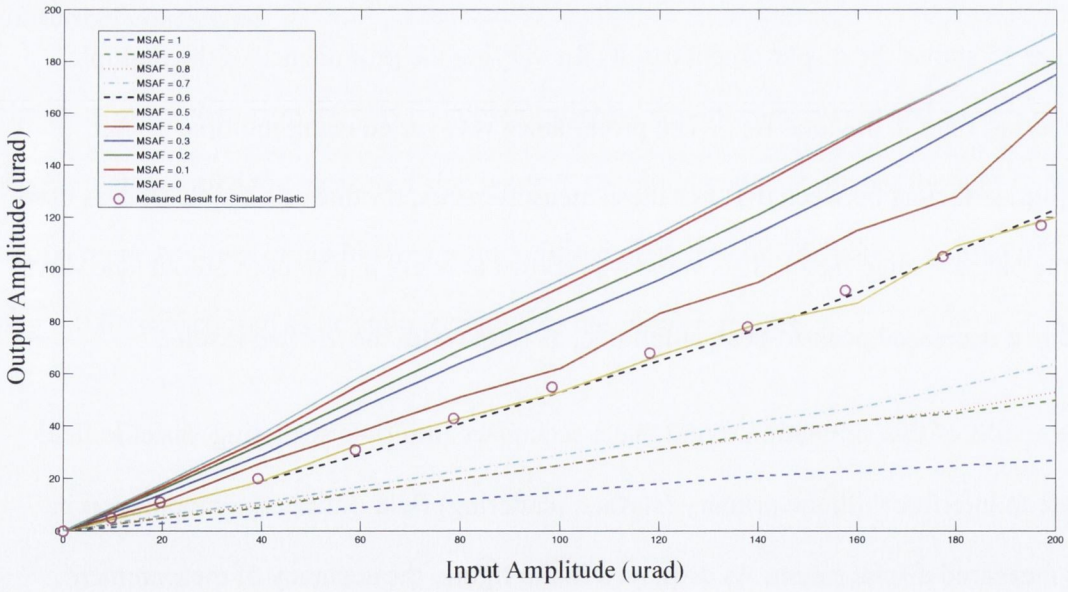

Figure 15. Simulated input versus output displacement at OMT-like ranges for various degrees of added multiple scatter. $\sigma\Delta\varphi$ was 0.01.

Figure 16 shows the measured versus applied displacement for a simulation of angular displacements in the tested range of the gimbal. The multiple scattering field was given an MSAF value of 0.5 since this was found in the above results to closely resemble the measurement results found using the simulator plastic.

Both traces were found to be approximately linear with $R^2 = 0.98$ for each frame correlated with the original reference frame and $R^2 = 1$ for each frame correlated with the previous frame. The calibration factor was found to be 0.99 for each frame correlated with the original reference frame and 0.54 for each frame correlated with the previous frame.

The trace for each frame correlated with the previous frame showed a reduced accuracy, as was found with the experimental gimbal results.

The trace for each frame correlated with the original reference frame shows improving accuracy, curving to match the inputted displacement where the measured frame to reference frame displacement reaches 250 μrad. A similar trend of improvement in measurement accuracy with larger inputted displacement was found in the results in section 3.2.3. The experimentally measured results were not as accurate as the simulated results, however this is likely to be due to an error introduced into the results by manually adjusting the micrometer screw of the gimbal.

It is supposed here that the curve in the measured displacement signal found for the simulated gimbal result is related to relative speckle size and displacement magnitude. To test this hypothesis, the inputted speckle size for both the surface scattering field and the volume scattering field were doubled to $\sigma_s = 4$ and $\sigma_v = 3$ respectively. This resulted in a total speckle size of $\sigma_t = 2.87$. The input versus output displacement results for the simulations are shown in figure 17. As can be seen from the figure, a curve is again

present in the results but at a higher input amplitude. This confirms that the speckle size influences the impact of the volume field on the accuracy of measurement.

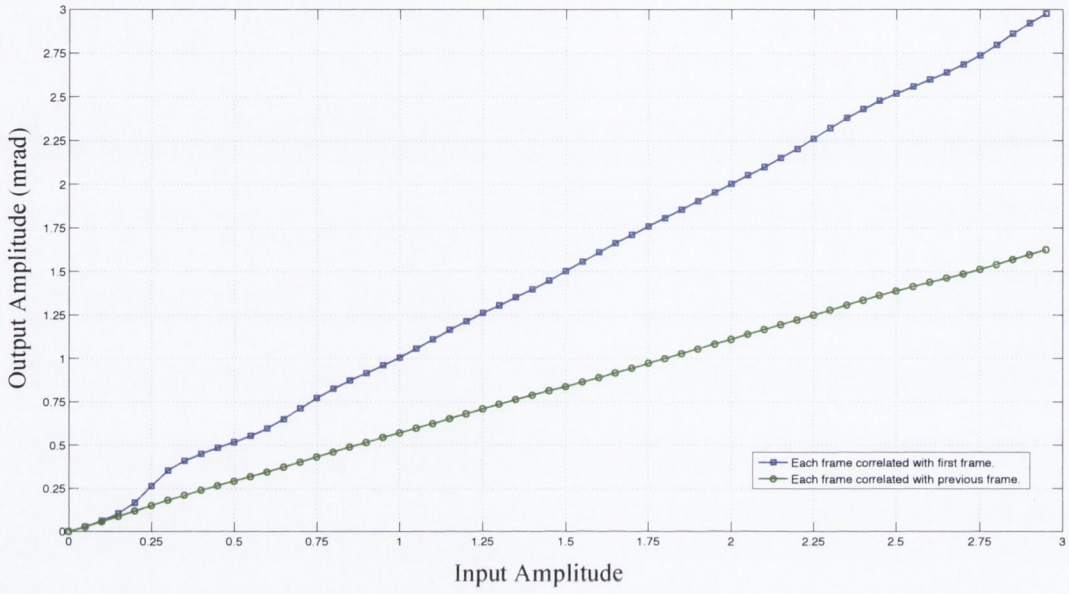

Figure 16. Simulated input versus output angular displacement at angular displacements in the gimbal range. The speckle size was 1.6, $\sigma\Delta\varphi$ was 0.01 and the MSAF was 0.5.

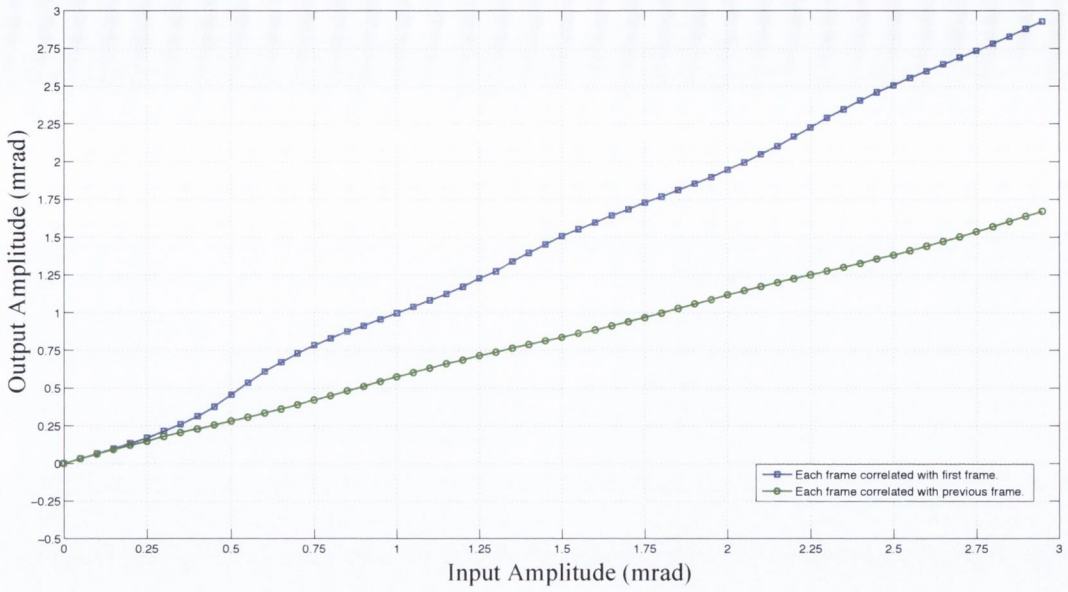

Figure 17. Simulated input versus output angular displacement at angular displacements in the gimbal range. The speckle size was set at the larger value of 2.87, $\sigma\Delta\varphi$ was 0.01 and the MSAF was 0.5.

4 Discussion

Measurement of the speckle displacement from a target that displays multiple scattering is more complicated than that for speckle singly scattered from a surface. For single scattering, the speckle displacement is directly proportional to the scatterer's displacement. In the case of multiple scattering, the measurement of the scatterer's displacement needs additional material-dependent calibration.

The speckle patterns of different surfaces which exhibited either volume scattering or surface scattering were investigated in this work. An OMT simulator was used to displace the materials through angular rotations between (4 – 197 μrad). Materials that gave rise to multiple scattering were found to display a speckle 'twinkling' effect. This

was due to multiple scattering from within the material's volume interfering with the speckle from the material's surface.

The results showed that the measured displacement from the speckle patterns was dependent on the material used. Materials giving rise to surface scattering (metal and cardboard) gave measured displacements that agreed more closely with the expected results than the results of the volume scattering materials (plastic, wood and polystyrene) did. In general there were bias errors that impacted on accuracy, and signal noise that impacted on precision. A 'calibration factor' was estimated to correct for bias errors.

Each material was found to have a unique calibration factor. In the OMT range of displacements (12 – 216 μrad), cardboard was found to have a calibration factor of 1.02±0.02 while plastic had a considerably lower calibration factor of 0.60±0.03. At the range of displacements tested using the gimbal (0.05 – 3 mrad) the calibration factors were 0.91±0.03 and 0.89±0.03 respectively.

A mathematical model was written to simulate speckle from a translating volume scattering material. The model assumed that multiple scattering from a volume results in time-varying speckle, but not in speckle translation. One constraint of the numerical model was that it assumed speckle from volume scattering to have the same statistics as those originating from surface scattering. This is unlikely to be the case in reality.

The influence of the speckle amplitude of the volume scattering field on the simulated measured angular displacement was measured by assigning a multiple scatter amplitude factor (MSAF) to the volume field. It was found that as the MSAF value was increased, the measured angular displacement became increasing lower than the ideally expected result.

Using simulated multiple scattering fields, it was found that, for multiple scattering fields that were totally random (synonymous with totally random phase changes in the speckle) between speckle image frames, the measured peak-to-peak amplitude returned the expected input amplitude. The measured displacement signal, however, showed some noise. In this study it was found that the multiple scattering fields had to retain some degree of correlation between frames in order to replicate the calibration error seen for the volume scattering materials using the OMT simulator.

A qualitative explanation for the impact of the volume field on measurement accuracy and precision can be given. The cross-correlation of two observed speckle image frames will be the simple sum of (1) the correlation of the surface scattering fields and (2) the correlation of the volume scattering fields plus mixing of higher order correlations. In the case where the multiple scattering field between frames is totally random from frame-to-frame, the volume scattering fields will not be correlated and will cause no real influence on the total correlation, other than adding background noise to the peak location. If, however, the two volume scattering fields do have some degree of correlation, their correlation peak will impact the overall correlation sum. If it is supposed that the volume scattering field does not displace, but the surface scattering field does displace with an object's movement, then the summed correlation of (1) the translating cross-correlation peak from the surface scattering fields and (2) the non-moving cross-correlation peak from the volume scattering fields, would result in a net cross-correlation peak that has not translated as much as the surface scattering correlation peak alone. This apparent reduced translation of the speckle images would result in a reduction in the measured displacement and is a likely source of the calibration errors seen in this work using the plastic, wood and polystyrene materials.

The overall aim of the work in this thesis is to measure OMT using the proposed laser speckle correlation system. The sclera is planned as the target for the laser and it is expected that the laser light will penetrate the sclera and result in multiple scattering. It is anticipated on the basis of the work in this chapter that the multiple scattering will cause a calibration error in the results. In addition to the surface-scattered and volume-scattered speckle, another form of speckle, called biospeckle [41], is expected in the eye. Biospeckle is a time-dependent form of speckle and is observed for all living objects. The influence of biospeckle on the proposed OMT measurement system will be investigated in the next chapter.

A limitation of this study was that the measurements were taken using only one laser wavelength. The absorption and scattering properties of a material are wavelength dependent and, therefore, the amount of multiple scattering is wavelength dependent. Similarly, the effects of using higher or lower laser powers were not investigated in this study. A lower laser power may be expected to have a reduced penetration into a material and cause less multiple scattering.

5 Conclusions

In this work, the influence of multiple scattering on the speckle correlation system was investigated using a variety of inanimate, multiple-scattering materials. Each scattering material was observed to give a characteristic calibration factor for the displacement measured using the speckle correlation technique.

It was shown that a mix of volume and surface scattering led to the experimental observations. Weaker calibration factors were associated with higher degrees of volume scattering present in the total scattering field.

From the results of the mathematical model used to simulate volume scattering effects, it is suggested that if the volume scattering field is relatively correlated between measurements, then this volume scattering component will have an effect on the measurement accuracy and cause a calibration error. If however, the multiple scattering is highly decorrelated between image frames, then the volume component appears as noise and affects the precision of the measurements rather than the accuracy.

Chapter 4

Characterisation of Biospeckle from the Human Eye Sclera

1 Introduction

Due to its minute size (12-216 μrad peak-to-peak) and rapid oscillation (approximately 84 Hz), ocular microtremor (OMT) is difficult to record accurately. OMT is a fixational eye movement and has been proven to express characteristic changes in a number of clinical conditions [19, 22, 42-48, 149]. To date, the most popular measurement system to record OMT has been an eye-contacting piezoelectric method [30, 31]. This contacting technique, however, has many difficulties associated with it, including patient discomfort [17, 26]. Ideally, for practical clinical use, OMT would be measured in a non-contact manner.

Chapter two described the technical requirements for a non-contact laser speckle correlation technique to measure angular displacements in the OMT range. The technique records speckle in the Fourier domain following a method to measure rotational displacement proposed by Rose *et al.* [96, 97]. The system performance was verified *in-vitro* and the system was shown to have a dynamic range of 4-5000 μrad, a resolution of 4 μrad and a bandwidth of 250 Hz.

Ideally a target for the speckle correlation technique would exhibit a surface scattering component only. Chapter three investigated the impact of a volume scattering component on the measurement technique. Measurements were taken using 'imperfect' inanimate materials. The volume scattering component of the materials was shown to introduce a measurement error that manifests as a 'calibration' bias error, if the volume scattering was stable between image frames, or as noise otherwise. The eye is likely to have similar volume scattering characteristics to the inanimate subjects. Additionally, temporal stability between image frames captured from the eye is likely to be reduced due to biospeckle and, consequently, the surface component of the scatter reflected from the eye is expected to be unstable. In this chapter, additional considerations in measuring the angular displacements from the sclera *in-vivo* are presented.

Measuring speckle from living objects involves a type of speckle known as biospeckle [41, 56, 140]. Speckle statistics for inanimate surfaces have been studied extensively [53, 54, 60, 61, 103] yet the spatial-temporal statistics of speckle from a biological surface are not so well understood due to their compound nature. A speckle pattern derived from living tissue such as the skin or the eye differs from that observed from an inanimate surface in that the speckles show a spatial-temporal change. Over time, the individual speckles change shape and randomly fluctuate in a manner sometimes referred to as 'boiling speckle', so-called due to their resemblance to the boiling of a liquid. The temporal evolution of the speckle is related to physiological changes taking place on and inside the biological surface. These changes cause variations in the phases of the components of the speckle pattern.

Moving speckle can be categorised into two groups; translational speckle and biospeckle. Translational speckles retain their shape and size as they move and their displacement is directly related to the displacement of the object from which they

originate. Biospeckles appear, disappear and change their shape as they move, making their displacement harder to track. Generally, these two types of speckle occur together.

With the increasing use of lasers in medicine, biospeckle has become more prevalent in research. Most studies of biospeckle in the human body are related to blood flow velocimetry [119, 124, 150]. At present, there are no clinical uses of biospeckle in routine practice. Acceptance of biospeckle techniques are hindered by the uncertainty in quantitative analysis of biospeckle images.

The overall aim of this thesis is to investigate and develop a non-contact method to measure OMT in the human sclera. It is expected that biospeckle will be seen when recording these OMT measurements *in-vivo* in the human eye. Biospeckle has never been characterised in the human eye. The patterns are complex and produced by a variety of unknown variables. The first objective of the work in this chapter is to characterise biospeckle from the human sclera. The second objective of this chapter is to investigate whether biospeckle image frames captured from the human eye *in-vivo* are stable enough to allow displacement of the eye to be measured using speckle correlation. The realisation of these objectives will help ascertain whether OMT can be measured from the sclera.

In this chapter the frame-to-frame stability from biospeckle patterns recorded *in-vivo* are analysed using a quantitative measure. By implementing this quantitative measure, a time scale is estimated for which successive biospeckle frames remain sufficiently correlated, which should allow OMT displacement to be tracked. Speckle patterns from an inanimate surface on an OMT simulator are used as a reference for the levels of correlation achievable over time. The frame stability is mathematically modelled and this model is applied to assess the impact of biospeckle on our proposed technique for

OMT measurement. This will quantitatively ascertain the degree to which biospeckle might limit system performance for OMT measurement.

1.1 Biospeckle in the Eye

Laser light interaction with biological tissue is complex. When laser light interacts with tissue, some portion of its incident energy is Fresnel reflected, some portion is transmitted, some backscattered, some scattered and the rest is absorbed by the tissue. The light that penetrates into a surface such as the eye, is scattered by red blood cells, water and other tissue. As these scatterers move, the biospeckles created by them move and change shape. The higher the mobility of these scatterers, the higher the expected rate of biospeckle activity.

Here, the interest is in the sclera as the target for a speckle correlation-based eye movement measurement system. The thickness of the sclera is non-uniform and in the range of 0.3-1.35 mm [3]. The thickest part is located at the posterior pole [151]. A thin membrane called the conjunctiva covers the sclera. The sclera is almost avascular and so blood supply is minimal. However, beneath the sclera are the highly vascular choroidal and retinal layers. The penetration depth of a 632 nm HeNe laser in soft tissue is approximately 1-2 mm [152], suggesting that the laser light could penetrate beyond the sclera. Each layer of tissue that the laser light passes through is expected to contribute to the overall activity of biospeckle captured from the sclera.

When tracking translational speckle for OMT measurement, biospeckle from the eye will act as a source of noise. The *in-vivo* biospeckle will need to be characterized and post processing techniques on the biospeckle image frames may be required to reduce noise and recover the OMT signal.

1.1.1 Biospeckle Characterisation

There is no gold standard metric to describe or measure biospeckle. No single parameter will define the biospeckle seen from the sclera *in-vivo* and so a multivariate analysis of biospeckle is required.

The following speckle characteristics are commonly found in the literature and can be used to describe biospeckle patterns; grey level histogram, speckle contrast, time history speckle pattern (THSP), grey level co-occurrence matric (GLCM) and the moment of inertia (IM).

The time history speckle pattern (THSP) is a tool that has been developed to analyse a dynamic speckle pattern by observing the time evolution of the speckle [56]. The faster an object moves, the more rapidly the speckle pattern varies in intensity. The THSP can therefore be implemented to qualitatively show changes between speckle frames. In effect, the THSP combines the spatial and temporal features of a series of dynamic speckle images into a single two-dimensional image.

A grey level co-occurrence matrix (GLCM) is a statistical method to show how many occurrences of pairs of pixel values are in an image. The moment of inertia (IM) is calculated from the GLCM. It is a measure of the intensity difference between a pixel and its neighbour over the entire image. The IM has been used in speckle metrology as a tool to quantify the THSP [57]. A high IM implies movement in the speckle frames, relating to a high activity in the sample. The absolute value of the IM does not provide useful information and it must be compared to an analogous experiment with the same variables in order to provide a relative measure.

In this work, three other statistics derived from the GLCM and typically used for texture analysis [59] will be implemented to describe the speckle images. These are the energy, homogeneity and correlation of the GLCM. Correlation is a measure of how correlated a pixel is to its neighbour. Homogeneity returns a value that measures the closeness of the distribution of elements in the GLCM to the GLCM diagonal. Energy returns the sum of squared pixel values of the GLCM, and is equal to unity for a constant image.

1.2 Speckle Correlation Metrology

Digital speckle correlation is a technique wherein a series of speckle images are recorded by a digital imaging sensor and a cross-correlation algorithm is used to calculate the pixel displacement between a reference image and all subsequent images. Using known parameters of the optical configuration used, this measured pixel displacement is converted to units of displacement of the object from which the speckle originates. The cross-correlation algorithm detects both the cross-correlation peak location and the peak height. It is important for the success of the speckle correlation technique that the peak location be measured correctly and accurately.

The displacement of speckle between two image frames is determined by location of the cross-correlation peak of the images. In order to measure displacement using the proposed speckle correlation technique, it is essential that the speckle pattern of the reference image frame and the n^{th} frame remain correlated. It was discussed in chapter two that large movements between two imaged speckle patterns results in decorrelation. Decorrelation can also occur due to changes in the speckle pattern triggered by biospeckle. It is expected that other fixational eye movements (drift and microsaccades) and particulary biospeckle will cause decorrelation between image frames captured

from the sclera. It may be necessary to acquire a new reference image frame at intermittent intervals to maintain correlation stability between the current and reference frame.

Some features of the correlation peak that can be used to ascertain frame-to-frame stability are discussed in the succeeding section. To characterize the correlation peak, some concepts used to evaluate the performance of correlation filters [153, 154] are adopted.

1.2.1 Frame Stability

The larger the *N*x*N* pixel image frame area that is being cross-correlated, the larger the information content in the correlation surface plot. A large image area will reduce the impact of local errors on measurement. For the measurement technique to be feasible, the random changes occurring across the frames due to biospeckle must not be so large as to obscure the global shift occurring between the frames due to displacement.

For cross-correlation displacement tracking to be successful, it is desirable that the correlation peak be sharp and large so that it is distinguishable from background. A sharp peak indicates a good match between images. As image frames become more decorrelated, the cross correlation peak height drops and the width of the peak becomes broader. To quantify this feature, a peak height-to-floor ratio, analogous to a signal-to-noise ratio, can be used. To calculate this ratio, the peak value of the cross-correlation plot is determined and then divided by the average of the background floor value. The decibel value of the peak-to-floor ratio was calculated as:

$$Ratio = 20log\left(\frac{Peak\ value}{Mean\ floor}\right) \qquad \textbf{Equation 1}$$

A high peak height-to-floor ratio indicates better noise (biospeckle) tolerance and a lower probability of error in the measurement results.

1.3 Mathematical Biospeckle Simulation

Chapter three described and tested a model to simulate laser speckle reflected from an inanimate solid diffuse object moving at an OMT-like angular displacement and frequency. Here, the model is further developed in order to replicate the biospeckle effects of laser light that is reflected from the human sclera. The influence of other eye movements are also considered. All codes were written in the Matlab [139] programming language, version R2009a.

The dynamic behaviour of biospeckles result in different spatial-temporal properties to those of ordinary speckle and an adjusted numerical method is needed to describe biospeckle behaviour. Any changes on or within the surface giving rise to speckle will create differences in the relative phases between light scattered from different points on the object. This causes the intensity distribution to change over time.

Mathematical biospeckle generation is based upon the basic formation of an ordinary speckle pattern, however, phase changes are implemented to model the speckle change over time. To model the variation due to changes in the biological tissue, each scattering centre n, with its own unique phase ϕ_n, is given a phase change $\Delta\phi_n$. As with ordinary speckle, the amplitude A of the total scattered light field is given by the sum of the N number of components representing contributions from the scattering centres, i.e.:

$$A = \sum_{n=1}^{N} a_n e^{i(\varphi_n + \Delta\varphi_n)} \qquad \textbf{Equation 2}$$

To simulate the effects of biospeckle, a phase variance model proposed by Rabal *et al.* [41, 129, 155] is followed in this work. In this model, random phase variations are included into the speckle matrix of each generated speckle pattern to simulate the phase change caused by the scattering centres in living objects that lead to biospeckle. Using the model, a scattering centre that results in biospeckle has a phase distribution $\varphi(m, n, k,)$ given by:

$$\boldsymbol{\varphi(m, n, k) = \varphi(m, n, k\text{-}1) + G(m, n, k)\sigma[\Delta\varphi(k\text{-}1, k)]} \qquad \textbf{Equation 3 [41]}$$

Where $m = n = 0, 1, 2, 3, N\text{-}1$ are the pixel co-ordinates of the imaging sensor. $\sigma[\Delta\varphi(k\text{-}1, k)]$, is the standard deviation of the phase changes between frame k-1 and frame k. k varies from 1 to K-1 where K is the total number of biospeckle frames. G is a random NxN matrix with a Gaussian distribution, meaning the matrix has a mean of zero and a standard deviation equal to unity. A new random matrix for G is calculated for every frame in the speckle sequence. The degree of biospeckle is related to the magnitude of the phase changes between subsequent frames i.e. a large phase difference between speckle frames is equivalent to a high degree of biospeckle. Hence, the larger the value of $\sigma[\Delta\varphi(k\text{-}1, k)]$, the more biospeckle that is present in a speckle pattern. Assuming that a constant 'level' of biospeckle is present in a given simulation, then $\sigma[\Delta\varphi(k\text{-}1, k)]$ reduces to the same value $\sigma[\Delta\varphi]$ between each frame. After mathematical manipulation [129], the above equation can be rewritten as:

$$\boldsymbol{\varphi(m, n, k) = \varphi(m, n, k\text{-}1) + G(m, n, k)\sqrt{\ln C(k-1) - \ln C(k)}} \qquad \textbf{Equation 4 [41]}$$

where $C(k)$ is the correlation coefficient of the normalised cross-correlation of the k^{th} frame with a reference frame. The square root term represents the standard deviation of the phase change between two consecutive speckle image frames. For perfect

correlation between all frames, i.e. $C(k) = C(k\text{-}1) = 1$, this term becomes zero and the phases of the k^{th} and $k\text{-}1^{th}$ frame are equal. In this case, where the phase does not change, no change occurs in the speckle pattern and no biospeckle is observed.

It should be noted that the above model assumes no other form of speckle displacement is taking place. If the speckle pattern was not stationary, the correlation coefficient would be reduced due to the speckle displacement as well as due to any biospeckle present.

2 Methods

2.1 In-Vivo

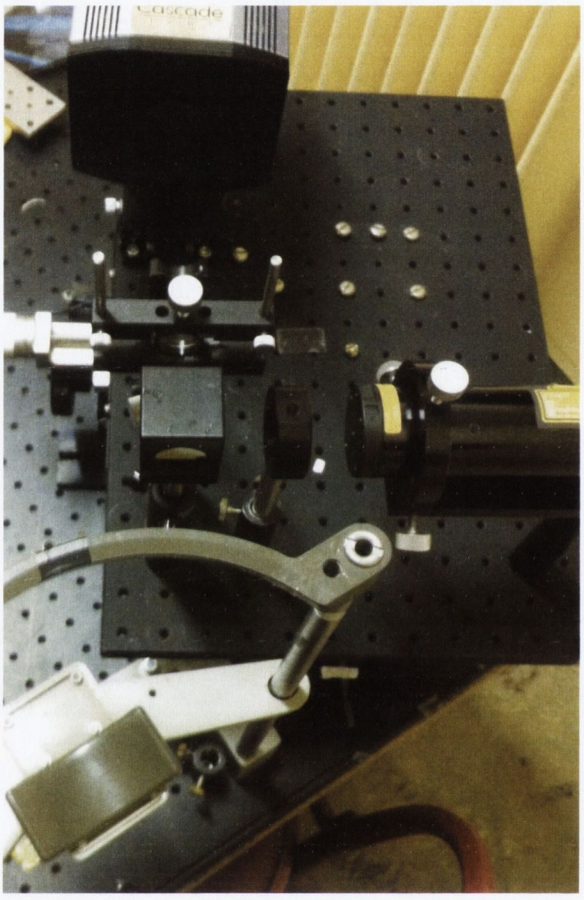

Figure 1. Experimental set-up for *in-vivo* measurement.

The optical set-up, as designed in chapter two, is shown in figure 1 for the *in-vivo* experiment performed here. *In-vivo* speckle measurements were captured from three healthy volunteers. The volunteers (3 healthy females, mean age of 28 years) were instructed to maintain a steady head position while a recording was taken from the sclera of their right eye. Written informed consent was obtained from the volunteers and the protocol was approved by the local ethics committee (St James's/AMNCH Research Ethics Committee).

The sclera of each of the volunteers was illuminated by a 632.8 nm plane polarized HeNe laser which was reduced down to an eye-safe power of 180μW by the use of a neutral density filter and a beamsplitter. The speckle pattern generated on the sclera target was collected by an EMCCD camera (Cascade 128+, Roper Scientific [138]) operating at 500 Hz with a 128x128 array of 24 μm pixels and a 100% fill factor. The EMCCD sensor was placed in the Fourier plane of the lens. A 5 second (2500 frames) reading was taken for each measurement. The 8-bit, uncompressed, digitized speckle image frames were then sent to the numerical software package Matlab [139] for processing.

2.1.1 In-Vitro Comparison

An OMT simulator with an inanimate cardboard surface was used so that the level of stability achievable with biospeckle could be compared to that of a non-biological reference. The procedure above was repeated using the OMT simulator. As previously described in chapter two, the simulator replicates OMT movement in terms of typical frequencies and amplitudes. A cardboard target was attached to the simulator surface and the simulator was set at 80 Hz and 4 μrad peak-to-peak. The amplitude of 4 μrad was chosen to test the correlation, as it is the lowest amplitude that could be tested using the simulator.

2.1.2 Biospeckle Characterisation

The speckle patterns recorded from volunteers *in-vivo* were quantified with use of the THSP, GLCM, IM, energy, homogeneity and correlation of GLCM. The mean values of

the *in-vivo* results were then compared to the values found for the mathematically simulated biospeckle frames.

2.1.3 Frame Stability

The peak height-to-floor ratio was analysed for each of the *in-vivo* speckle videos from the volunteers and for the simulator speckle images.

The mean floor value of the correlation plot was calculated, excluding a 10x10 pixel mask around the correlation peak. This area was omitted since it may contain part of the peak. As outlined in chapter two, the full width half max (FWHM) of the autocorrelation plot of a speckle pattern can be used to find the speckle size (ρ_0) according to $FWHM = 4\sqrt{\ln 2}\sqrt{F}\rho_0$ [96, 97]. From the calculation in chapter two, the speckle size for an 'ideal' speckle surface in this experiment is expected to be 2.1 pixels, giving an expected maximum FWHM of 7 pixels. Therefore, a mask of 10x10 pixels surrounding the peak is expected to be large enough not to contain significant peak information.

Setting the first frame as the reference frame, a log plot of $y = 20log\left(\frac{Peak\ value}{Mean\ floor}\right)$ for correlation of each subsequent frame with the reference frame was plotted.

Data from the *in-vivo* sclera biospeckle frames, collected from all three volunteers, were next used to establish how rapidly the speckle frames decorrelate. First, each frame (k) of the 2500 biospeckle images was correlated with the previous frame (k-1) and the average peak height-to-floor ratio was calculated. The procedure was then repeated for correlation of frame (k) with frame (k-n), where n ranged from 2-10. In total, comparisons were made for delays ranging from 2-20 ms.

2.2 Simulated Biospeckle

To replicate the biospeckle pattern seen *in-vivo*, two speckle matrices were generated in Matlab. An $S_n(x,y)$ matrix was created to represent surface speckle and had a larger input speckle size, $\sigma_s = 2$. The matrix $V_n(x,y)$ was made to represent volume scattering and was given a smaller input speckle size, $\sigma_v = 0.8$. These values were chosen empirically so that the speckle size of the final simulated biospeckle image matched the speckle size seen *in-vivo*. These speckle sizes were inputted to the model in units of pixels

As detailed in the biospeckle generation steps below, the matrices were added together on a complex basis before converting them to a final speckle intensity image, $I_n(x,y)$. The multiple scattering amplitude factor (MSAF), explained in chapter three, was set to 0.5.

The value of the standard deviation of the phase difference between each generated speckle frame, $\sigma\Delta\varphi$, was altered experimentally until it produced speckle that resembled the speckle patterns seen *in-vivo*.

Mathematical speckle was generated following the basic speckle simulation method outlined by Goodman [52]. The following steps were then taken to create a series of time-varying speckle patterns;

1. Two random 128 x 128 phase matrices were created. 128 x 128 was the desired biospeckle image size.
2. An M x M and P x P matrix (representing the matrices $S_n(x,y)$ and $V_n(x,y)$) were filled with zeros. $M = \sigma_s$ x 128 and $P = \sigma_v$ x 128.

3. The $S_n(x,y)$ and $V_n(x,y)$ matrices were filled with values $e^{j\varphi(m,n)}$ where $\varphi(m,n)$ is a random distribution between 0 and 2π.
4. These matrices were then resampled to the desired array size.
5. A fast Fourier transform (FFT) was performed on both matrices to yield arrays representing the complex amplitude speckle.
6. To replicate a fixational displacement, the data in the $S_n(x,y)$ matrix was displaced using the Fourier shift theorem.
7. The $V_n(x,y)$ matrix was multiplied by the multiple scattering amplitude factor (MSAF).
8. The two matrices were added together, resulting in the matrix $T_n(x,y)$.
9. The matrix $T_n(x,y)$ was multiplied by its complex conjugate $T_n^*(x,y)$. This created the first biospeckle intensity image frame $I_{n=1}(x,y)$.
10. New phase matrices were created in accordance with equation 4 by assigning a value to $\sigma\Delta\varphi$, multiplying the result by a matrix of random numbers, G, and adding the product to the previous respective phase matrices.
11. Steps 2 to 9 were repeated until the desired number of image frames, N, were created.

The process that was used to model biospeckle is outlined in figure 2. In the first iteration of the code (n=1), the phase matrix is a random 128 x 128 matrix.

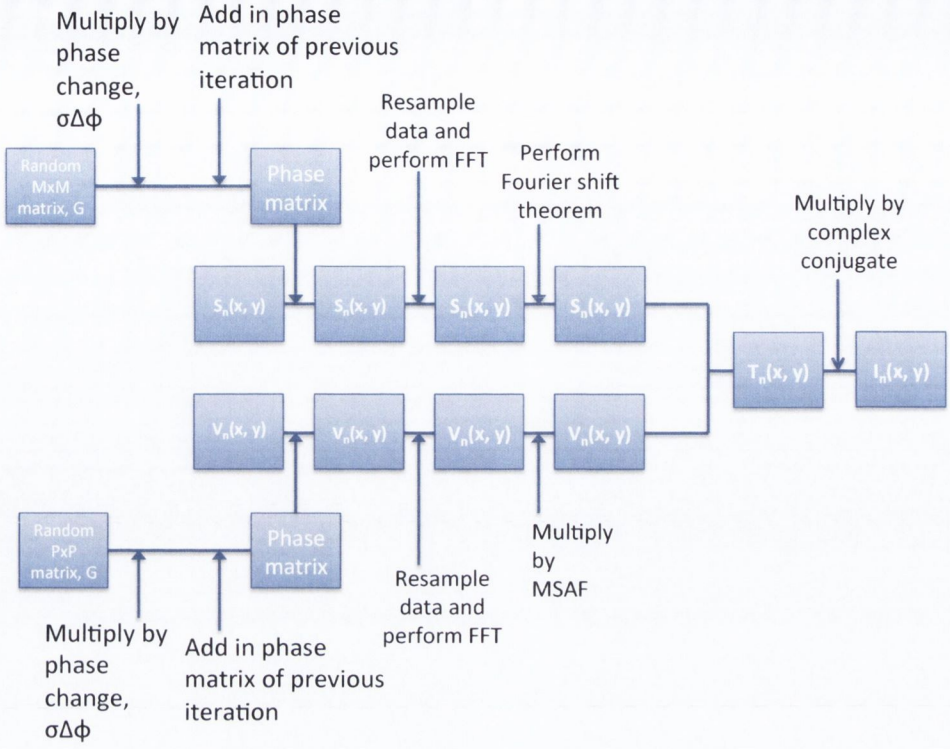

Figure 2. Biospeckle simulation procedure.

To translate the simulated biospeckle pattern, data from fixational eye movements that was previously acquired using a piezoelectric (PZT) probe system [11, 27] was used. In brief, the OMT PZT measurement system records movement via a piezoelectric bimorph. The recorded signal is amplified and digitized. The resolution of the PZT probes is approximately 2 nm and recordings were measured with a 2500 Hz sampling rate. Processing of the original data was performed in LabView [28].

Figure 3 shows an unfiltered trace recorded using the PZT system on a normal healthy adult. After it was inputted to Matlab, data from the unfiltered trace was resampled to replicate the 500 Hz sampling rate used in this experiment by reading every 5^{th} frame. In an attempt to approximate the trace to within the known OMT range, the arbitrary

unit of the PZT amplitude data was rescaled so that a value of 0.1 was made to equal 162 μrad. This resampled, unfiltered trace was then used as the input displacement for the mathematical biospeckle simulation performed in Matlab. The mathematically generated biospeckle patterns were translated across 2500 frames (equivalent to a 5 s recording).

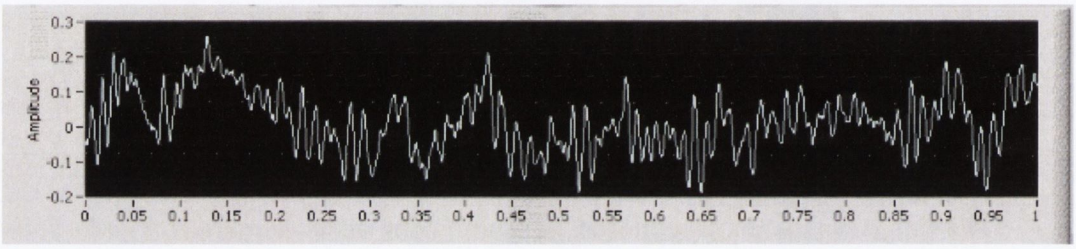

Figure 3. Unfiltered OMT data recorded using the PZT system

2.2.1 Verification of OMT Signal Recovery from Cross-Correlation

The mathematically generated biospeckle frames were used to determine the ability of the speckle correlation algorithm to extract OMT movement from the captured signal in the presence of biospeckle. After the biospeckle frames were generated and translated, they were further processed in Matlab.

During the image processing each displaced speckle image frame was cross-correlated with the original reference speckle image frame. The full 128 x 128 pixels were used for every image during the cross-correlation analysis. To increase the accuracy in locating the exact correlation peak, and consequently the calculation of the speckle displacement, the location of the cross-correlation peak was calculated using a subpixel algorithm. The subpixel correlation method used in this experiment is based on the

curve-fitting method described by Hung *et al.* [78]. The movement of the correlation peak location over time was used to calculate the pixel displacement of the speckle images. The pixel displacement was converted to units of angular rotation of the sclera using the equation

$$\theta = \frac{\Delta pixel}{2f} \qquad \textbf{Equation 5 [96, 97]}$$

A peak detection algorithm was used to locate each peak and trough in the recovered angular displacement signal.

To remove noise outside the desired frequencies, the displacement results obtained from the cross-correlation were filtered using a digital Butterworth filter of order five with a bandwidth of 20 – 150 Hz.

To find the amplitude of the signal, each trough was subtracted from each peak and the mean value was taken to be the peak-to-peak amplitude of the measured signal. To calculate the frequency content of the signal a periodogram was utilised to estimate the power spectral density.

The measured displacement and frequency content were then compared to the input values taken from the OMT PZT measurement system.

3 Results

3.1 In-Vivo

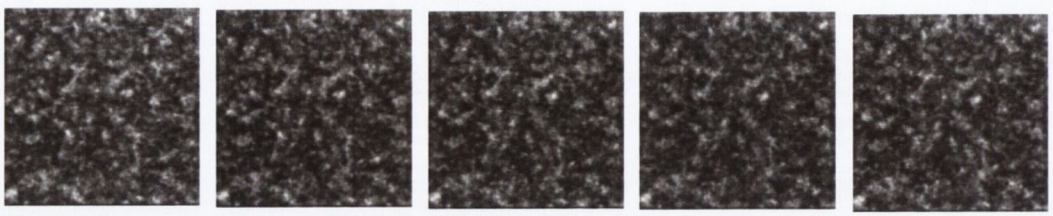

Figure 4. Five sequential frames taken *in-vivo* from the sclera, 2ms apart.

Figure 4 shows five sequential speckle frames taken 2 ms apart from the sclera of one volunteer. An initial qualitative analysis of the frames indicates similar features in each frame and they appear reasonably stable. The speckle size for the example shown was found to be 80 μrad (1 pixel).

3.1.1 Biospeckle Characterisation

The results of the *in-vivo* speckle characterization are presented alongside those of the simulated biospeckle patterns for comparison purposes.

3.1.2 Frame Stability

Figure 5(a) shows a cross-correlation plot calculated between two speckle frames 5 s apart using speckle collected from the simulator with cardboard surface while it was running at 80 Hz, 4 μrad peak-to-peak. Figure 5(b) shows the cross-correlation plot for the same recording, however, each frame was correlated with the previous frame and so

the frames used to generate the correlation plot were taken 2 ms apart. Figures 5(c) and (d) show typical *in-vivo* cross-correlation plots created using frames captured 5 s and 2ms apart.

Both of the plots generated using speckle from the simulator show a clear cross-correlation peak. This demonstrates that even at a very low amplitude (4μrad) and a time difference of 5 s, the speckle correlation algorithm can measure the displacement of an inanimate object.

In figure 5(c) the peak of the correlation plot for the *in-vivo* biospeckle is indistinguishable from background. This denotes that the biospeckle frames become completely decorrelated when they are cross-correlated 5 s apart. The decorrelation is due to temporal changes caused by a combination of actual eye movement, biospeckle and the low contrast associated with the collected images. In the case where each frame is correlated with the previous frame (2 ms apart), the correlation peak for the *in-vivo* speckle images is more distinguishable, less noisy and larger.

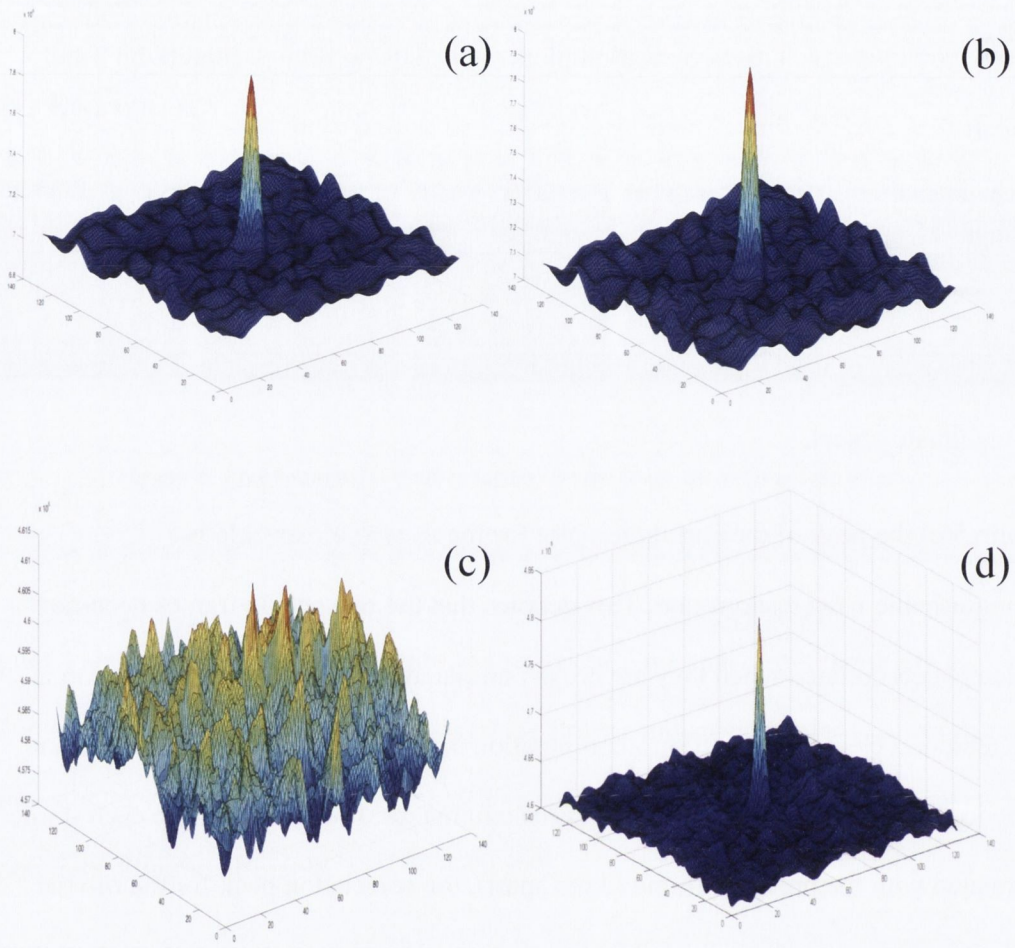

Figure 5. Cross-correlation plots for (a) speckle frames recorded 5 s apart on the simulator running at 80 Hz, 4µrad peak-peak (b) frames recorded 2ms apart on the simulator running at 80 Hz, 4µrad peak-peak (c) frames recorded 5 s apart *in-vivo* and (d) frames recorded 2ms apart *in-vivo*.

Figure 6 shows the results of measuring the peak height-to-floor ratio over time for (i) the simulator at 80 Hz, 4 µrad peak-to-peak with frames measured 5 s apart (ii) the simulator at 80 Hz, 4 µrad peak-to-peak with frames measured 2 ms apart (iii) one volunteer's sclera with frames measured 5 s apart and (iv) the same volunteer's sclera with frames measured 2 ms apart.

As shown in the figure, when each frame is correlated with the previous frame, the peak height-to-floor ratio amplitude is higher than that for each frame correlated with the original reference frame. This is particularly evident for the *in-vivo* case. The simulator results show almost constant correlation peak amplitude with time, implying good correlation peaks and a strong correlation between speckle image frames.

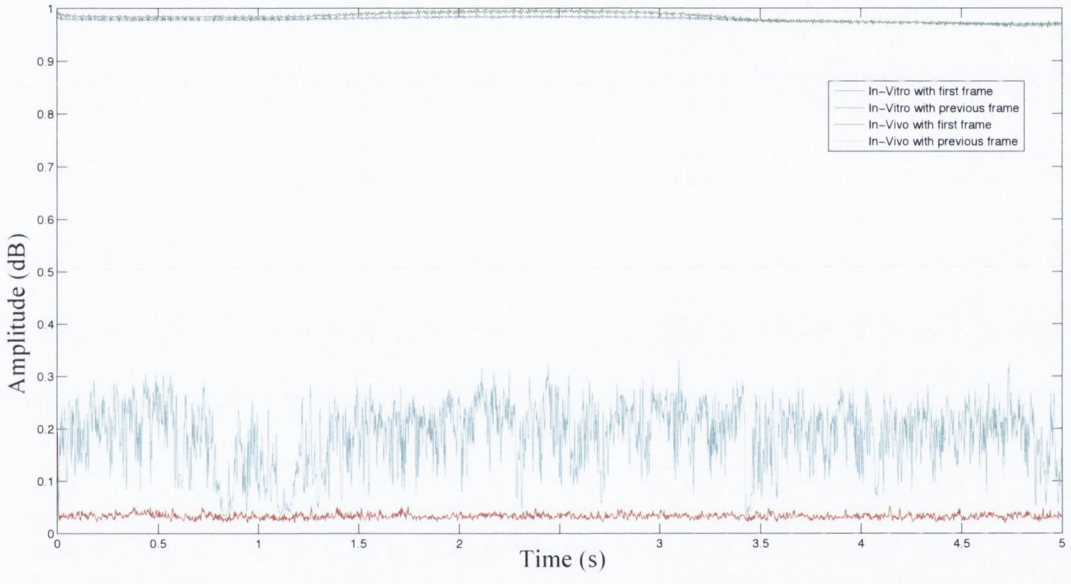

Figure 6. Correlation peak height to floor ratio plotted against time for *in-vitro* and *in-vivo* speckle frames.

The poor amplitude of the *in-vivo* result derived from each frame being correlated with the original reference frame is a consequence of biospeckle acting as noise. Biospeckle causes speckle images to become progressively more different. When each frame is correlated with the previous frame, the image pairs are relatively more similar across the tested range. Each frame correlated with the previous frame gave a mean correlation peak-to-floor ratio of 0.19 dB, an increase of 0.16 dB compared to correlation with an original reference frame.

Figure 7 shows the dependence of the correlation peak height-to-floor ratio on the number of frames between the reference frame and the tested frame *in-vivo* for three different volunteers. As can be seen in the figure, the frames decorrelated rapidly. When the frames were correlated with a reference frame five frames proceeding it (a time difference of 10 ms), the peak height amplitude dropped to a value below 0.1 dB. In comparison, for the inanimate cardboard surface, absent of biospeckle, the peak height-to-floor ratio never dropped lower than 0.97 dB. This demonstrates that the decorrelation effects of biospeckle occur rapidly.

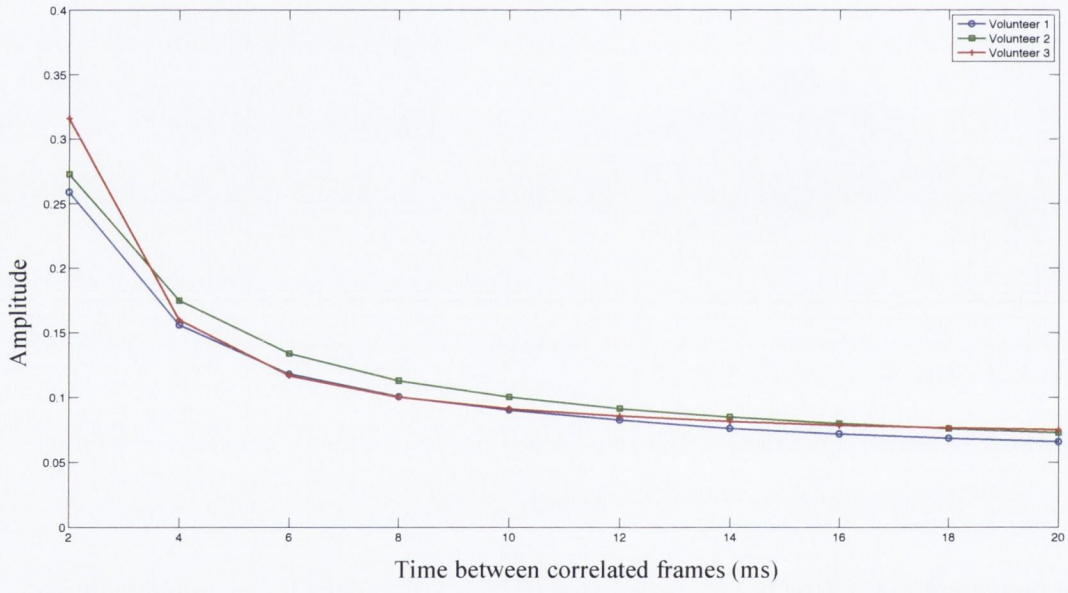

Figure 7. Dependence of peak height amplitude on the time between the reference frame and the tested frame. Frames were recorded 2 ms apart and the values shown are measured over 5 s.

3.2 Simulated Speckle

3.2.1 Biospeckle Characterisation

The speckle size of the *in-vivo* speckle images was calculated from the FWHM to be 1 pixel. Using speckle sizes of $\sigma_s = 2$ pixels and $\sigma_v = 0.8$ pixels, the speckle size seen *in-vivo* was replicated in the simulated biospeckle images. The standard deviation of the phase difference between speckle frames, $\sigma(\Delta\varphi)$, was found to provide the closest resemblance to the biospeckle seen *in-vivo* when $\sigma(\Delta\varphi)$ was set equal to 0.11 radians.

An *in-vivo* speckle image recorded from one volunteer and a mathematically generated speckle image are shown in figure 8. The image histograms of all frames from the *in-vivo* and simulated speckle sequence are shown alongside the speckle images. As evidenced, the simulated and *in-vivo* images appear similar in terms of the speckle size and distribution. Likewise, the histograms display similar features in terms of the spread of grey values, shape of the histogram and histogram skewness.

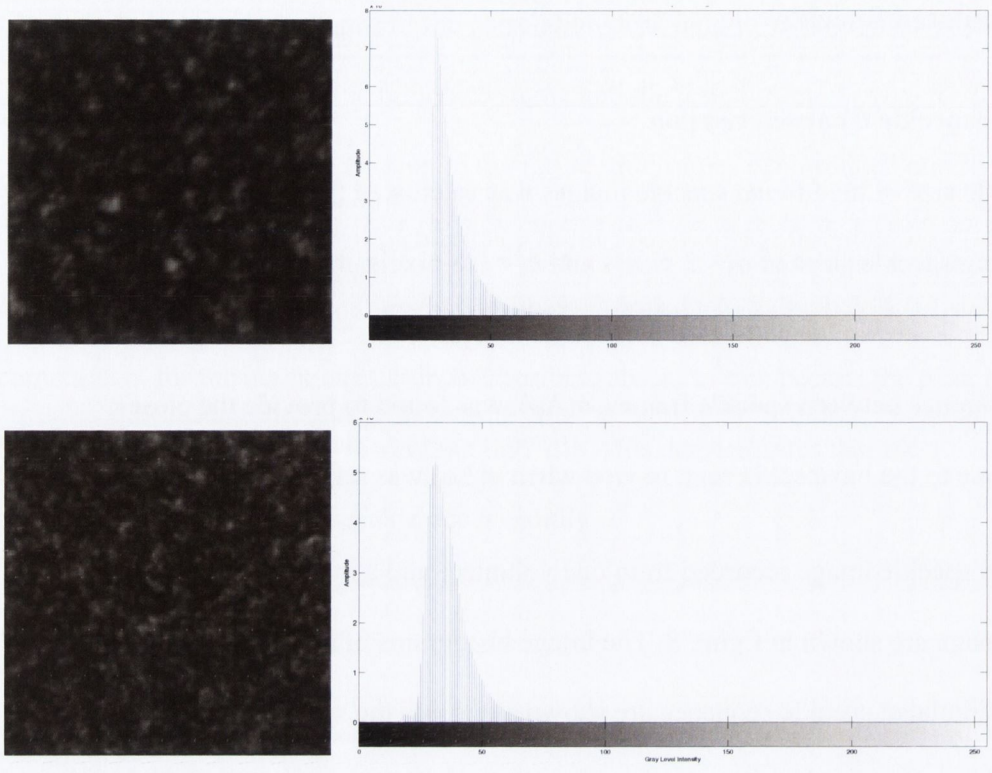

Figure 8. Simulated biospeckle pattern and the histogram created from all frames in the series (top) and biospeckle from *in-vivo* eye sclera and the histogram created from all frames in the series (bottom).

Figures 9 and 10 show the time history speckle patterns (THSP) and grey level co-occurrence matrices (GLCM) derived from the *in-vivo* and from the simulated biospeckle image sequences. Qualitatively, the THSPs and GLCMs appear comparable, displaying a high biospeckle activity through a fast change in pixel intensity over time.

Figure 9. THSP from simulated speckle (top) and from in-vivo eye (bottom).

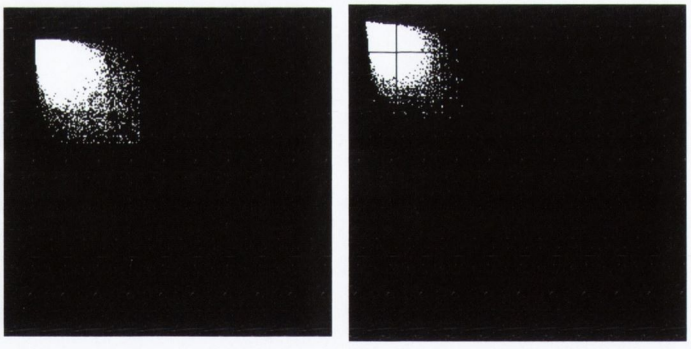

Figure 10. GLCM from simulated biospeckle (left) and from in-vivo eye (right).

Table 1 shows the quantative results of the second order statistics calculated from the GLCM of the THSP for (i) volunteers *in-vivo* and (ii) a series of simulated speckle patterns. The results of the simulated biospeckle agree with the results of the *in-vivo*

biospeckle from the sclera and the mathematically generated biospeckle images can be regarded as a good approximation to the *in-vivo* biospeckle.

	Mean *in-vivo* result from volunteers	Simulated result
Moment of Inertia	61.94 ± 17.78	63
Correlation	0.63 ± 0.10	0.53
Energy	0.003 ± 0.001	0.004
Homogeneity	0.29 ± 0.02	0.29

Table 1. Comparison of second order statistics calculated from the GLCM of the THSP from volunteers *in-vivo* and from a series of simulated speckle patterns.

3.2.2 Verification of OMT Signal Recovery from Cross-Correlation

Figure 11 displays both the resampled PZT trace inputted to translate the simulated biospeckle patterns and the unfiltered measured displacement trace using speckle correlation. The biospeckle was created using the same parameters that generated the patterns and results seen in section 3.2.1. The time between each frame was 2 ms.

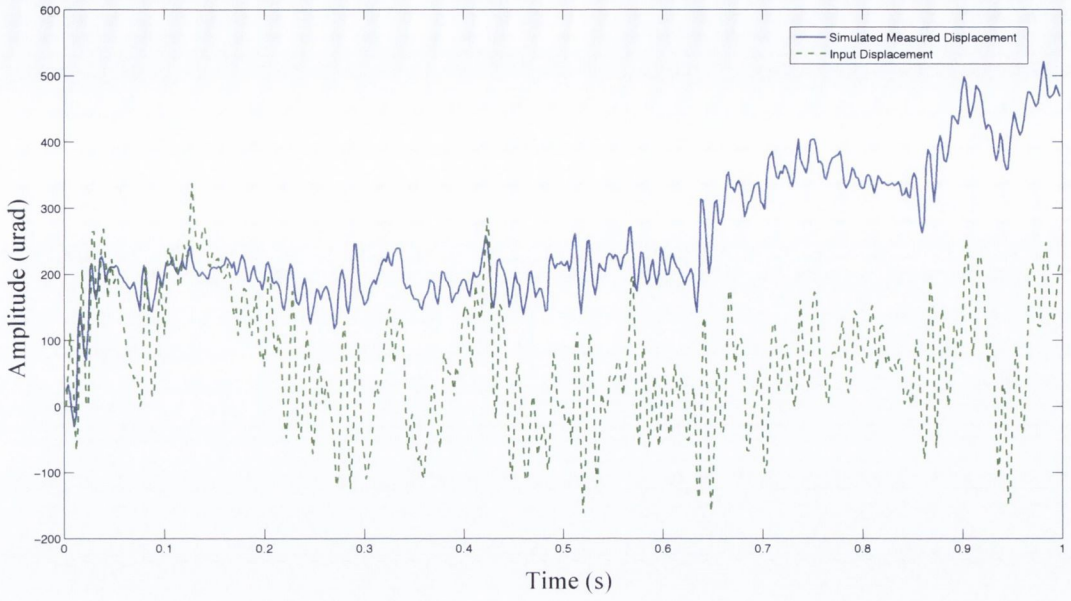

Figure 11. Inputted unfiltered OMT trace (green) and simulated measured displacement (blue).

Figure 12 displays the same data as figure 11 after it was filtered to remove noise outside the desired OMT frequency. The measured result was found to underestimate the amplitude by 62%. However, importantly, it was capable of tracking the displacement and recreating the general shape of the OMT trace.

The periodogram for the filtered recovered signal is shown in figure 13. The peak of the periodogram is at 80 Hz for both the inputted and the measured data. This shows that the frequency content of OMT can be recovered in the presence of biospeckle similar to that seen *in-vivo* using the speckle correlation algorithm designed for this work.

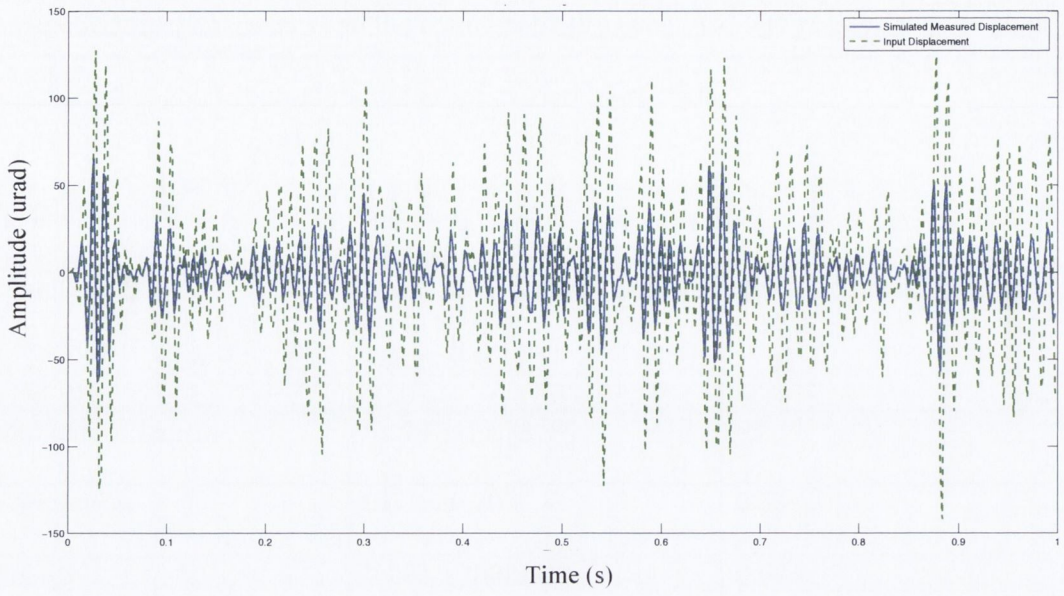

Figure 12. Filtered input data (green) and filtered displacement recovered from simulated biospeckle images (blue).

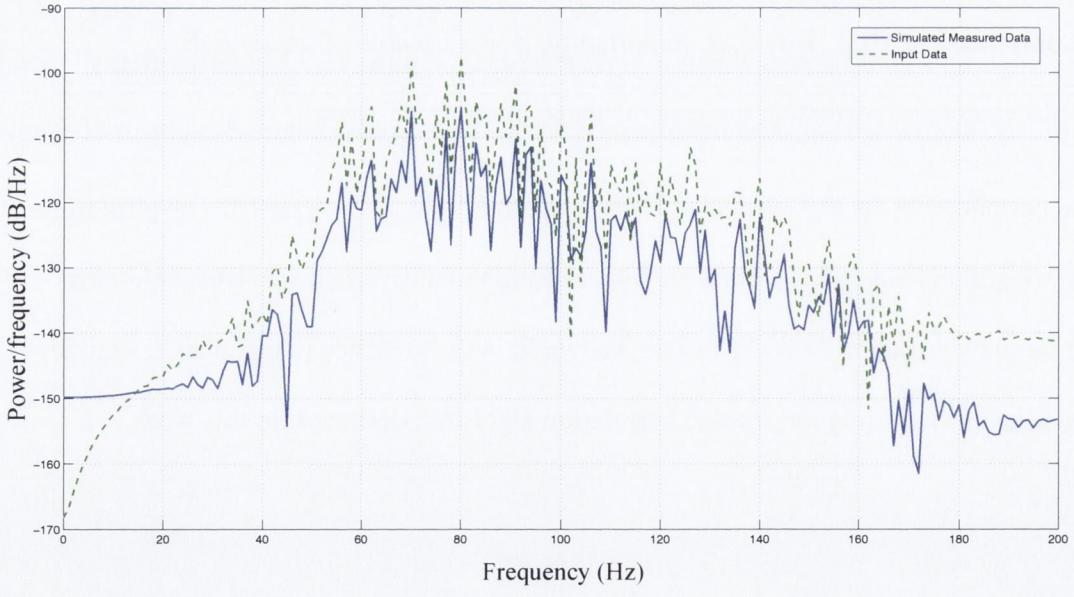

Figure 13. Periodogram of the recovered filtered signal (blue) and of the filtered input signal (green).

Table 2 shows the results of increasing $\sigma(\Delta\varphi)$ on simulated speckle frames. As expected, the mean stability of the images decreased with increasing $\sigma(\Delta\varphi)$. A plot of the correlation peak height-to-floor ratio against displacement error is shown in figure 14. A measurement error on the results was calculated using the equation:

$$Measurement\ error = \left(1 - \frac{Measured\ Amplitude}{Input\ Amplitude}\right) x\ 100$$

where the input amplitude was taken to be the mean peak-to-peak amplitude of the PZT signal used to translate the speckle images. The error increased drastically after the correlation peak height-to-floor ratio amplitude fell below 0.1 dB. This level of stability sets a lower limit on how stable the biospeckle images need to be to measure OMT displacement.

The correlation parameter, derived from the GLCM, showed a notable variation as $\sigma(\Delta\varphi)$ increased. The IM increased as the $\sigma(\Delta\varphi)$ increased, this was to be expected since a higher IM is indicative of higher biospeckle activity. The energy and homogeneity showed a slight change as $\sigma(\Delta\varphi)$ changed.

	Phase Change, $\sigma\Delta\varphi$ (radians)											
	0	**0.03**	**0.05**	**0.07**	**0.09**	**0.11**	**0.13**	**0.15**	**0.17**	**0.19**	**0.21**	**0.23**
Mean Peak Height-to-Floor Ratio (dB)	0.55	0.50	0.48	.43	.38	0.32	.27	.21	0.17	0.13	0.09	0.07
IM	12	18	28	36	56	63	76	91	102	113	121	122
Correlation	0.90	0.88	0.81	0.73	0.64	0.53	0.45	0.36	0.31	0.21	0.15	0.12
Energy	0.013	0.007	0.006	0.005	.004	0.004	.004	0.003	0.003	0.003	0.003	0.003
Homogeneity	0.57	0.44	0.38	0.34	0.3	0.29	0.27	0.26	0.25	0.24	0.24	0.24
Measurement Error (%)	65	64	63	63	63	62	62	63	64	57	597	2098

Table 2. Change in biospeckle parameters with increasing phase change. $\sigma\Delta\varphi$ = 0.11 was the actual value used in simulations. MSAF was equal to 0.

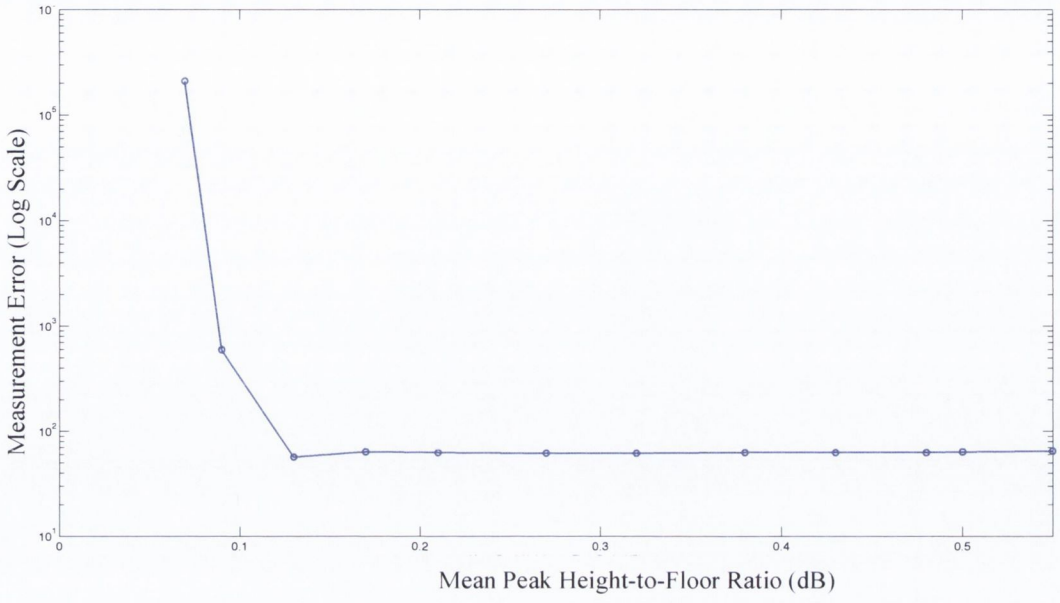

Figure 14. Mean peak height-to-floor ratio against measurement error for the simulated biospeckle images. The x-axis is a log scale.

Chapter three showed the multiple scattering factor (MSAF) to impact on measurement results by causing a calibration error. To investigate the impact of the MSAF in this chapter, another simulation of the measurements was performed, but with MSAF set to zero. The modeled case was equivalent to a surface scattering surface showing biospeckle but no volume scattering. Since there was no volume field interfering with the surface field, the speckle size was larger, as shown in figure 15.

Figure 16 displays the input and measured displacements for the simulated speckle with MSAF set to zero. As shown in the plot, the measured displacement was in good agreement with the input displacement. A measurement error of only 3% was calculated. This agrees with the results of chapter three, in that the time-varying

biospeckle alone does not disrupt the measurements. When multiple scattering is introduced, it causes systematic underestimation of amplitude.

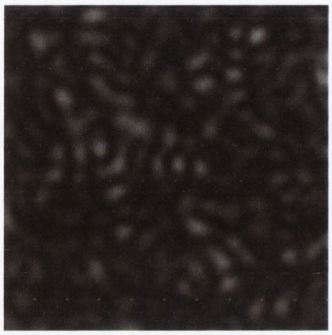

Figure 15. Simulated speckle pattern in the absence of volume scattering.

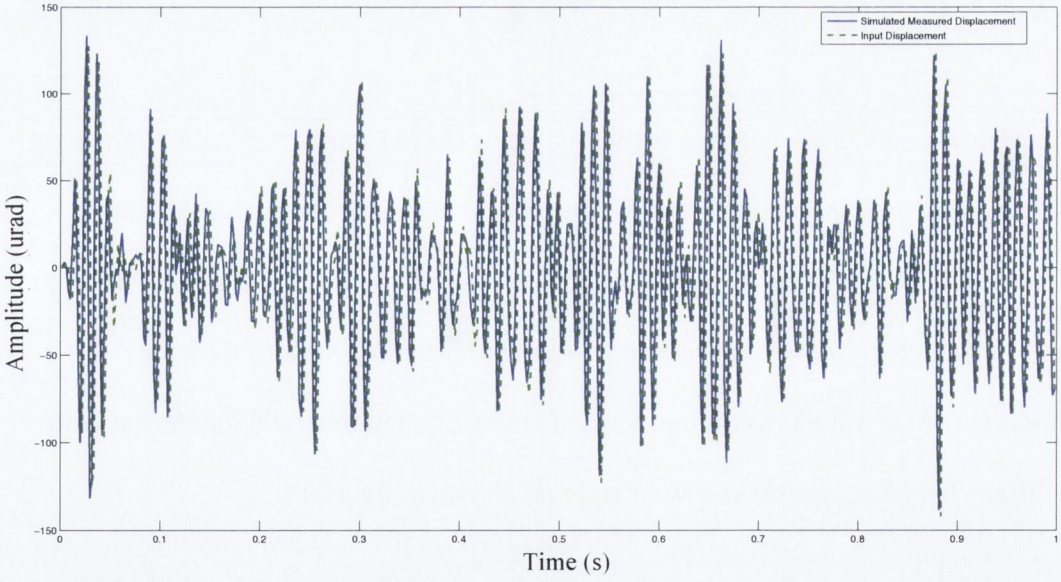

Figure 16. Filtered input data (green) and filtered displacement recovered from simulated biospeckle images (blue). MSAF was equal to zero.

4 Discussion

The reflected laser speckle pattern from a stationary, diffuse object is stable with time. However, any movement on or within the object will cause the speckle pattern to become time-dependent. *In-vivo* targets demonstrate time-dependent speckle, known as biospeckle. The aim of this work was to determine if *in-vivo* biospeckle images captured from the human sclera are sufficiently stable for speckle cross-correlation displacement tracking to be used for eye movement measurement and, in particular, for OMT measurement. The stability of the biospeckle images was investigated using metrics to characterize the correlation peak between frames.

In chapter two, the displacement of an inanimate diffuse object with a near ideal speckle surface was tracked. Results were taken for each frame correlated with an original undisplaced reference frame. Analysis of the results found that the speckle cross-correlation technique broke down at a displacement of about 5 mrad. In this chapter, the *in-vivo* speckle images were seen to become unstable rapidly. After five frames (10 ms), the correlation peak height-to-floor ratio was found to drop below 0.1 dB. A limitation of the results presented here is that as the *in-vivo* eye is moving, the decorrelation effects seen frame to frame cannot be definitively attributed completely to biospeckle. The decorrelation, and subsequent peak height drop, is caused in part by biospeckle and in part by any movement of the eye or head.

In chapter two, the maximum possible displacement of the sclera at a frame rate of 500 FPS was estimated to be 1.56 mrad per frame and it was shown that angular displacements in this range gave adequate correlation peaks to track speckle displacement. The rapid time-dependent decorrelation resulting from biospeckle is,

therefore, of a greater concern than the spatial decorrelation observed after an eye displacement.

Biospeckle destructs the temporal stability of speckle images. It acts as a source of noise and results in rapid decorrelation between image frames. To obtain the highest correlation peak *in-vivo* and keep decorrelation at a minimum, the time period between frame correlation needs to be short. In effect, this means tracking displacement using a frame-to-frame correlation rather than a tested reference frame. A drawback of this method is that as the displacement trace is generated by integrating all frame-to-frame displacements, any error that occurs during one correlation pair builds in to the displacement result and the error accumulates.

Frame-to-frame correlation places a high demand on the subpixel correlation algorithm because the movement between successive frames is such a tiny fraction of a pixel. Subpixel methods, such as Newton-Raphson [89] and gradient based [87, 88] techniques may have a higher accuracy than the technique used in this work but are more time consuming [134].

Biospeckle induced changes in a speckle pattern were numerically simulated in this work by creating a series of speckle matrices whose phase changes between speckle image frames. The simulated speckle images were shown to be qualitatively comparable to those found *in-vivo* and a quantative analysis of metrics derived from the GLCM also provided similar results. An OMT signal, previously recorded using a PZT system, was used to translate the simulated biospeckle images. The results of this showed that even in the presence of biospeckle, the OMT trace was recoverable. From this, it is expected that the OMT signal will be measureable from the eye sclera.

The mathematical biospeckle simulated in this work is a first order empirical model. Rather than attempting to present a theoretical model, this model was based on matching the temporal and spatial properties of the simulated speckle with the corresponding properties seen *in-vivo*. Limitations of the model are that it is based on results from a small (n = 3) number of volunteers and, rather than modeling 'pure biospeckle', the mathematical simulation also includes movements. However, the simulation of all possible movements is important so that all factors with potential to impact on frame-to-frame decorrelation can be identified.

To fully model biospeckle from the sclera would require an in-depth knowledge of the scattering properties of the sclera and of the temporal changes in these properties. A more precise understanding of the physics and statistics of the scattering interaction of these cells with laser light is also required. With a fuller understanding of these properties, other quantities such as the number of scatterers producing biospeckle and the rate of biospeckle could be included into the mathematical model.

Chapter three concluded that, when measuring speckle displacement, a material in which light is multiply scattered will give rise to a material-dependent calibration error. The results of the mathematical simulation in the current chapter show that biospeckle does not lead to a significant change in the measured angular displacement. Based on this, it is expected that biospeckle images captured *in-vivo* from the sclera will result in an OMT measurement that has a smaller than expected amplitude, due to multiple scattering of the laser light at the sclera, but that the biospeckle activity will be stable enough to track the displacement once a sufficiently high frame rate is used.

5 Conclusions

The aims of this work were (i) to assess how rapidly biospeckle frames from the *in-vivo* eye sclera decorrelate due to the time-dependent biospeckle and (ii) to establish if this decorrelation impacts on the feasibility of the proposed speckle correlation technique for OMT measurement.

It was found that decorrelation due to biospeckle was rapid and the method of cross-correlating each frame with an original reference frame is not suitable. To overcome the difficulties associated with biospeckle-induced decorrelation, each biospeckle image frame should be cross-correlated with the previous frame. With the technical optics available for this work, the shortest separation between frames was 2 ms.

A mathematical model to simulate biospeckle captured from the eye sclera at a frame rate of 500 Hz was presented and analysed. In the model, it was found that OMT-like displacements were recoverable from biospeckle images, provided the stability of the images remained at a level above 0.1 for the mean peak height-to-floor ratio. Based on speckle measurements recorded from volunteers in this study, it is expected that if *in-vivo* speckle images are correlated on a frame-to-frame basis then they will fulfil this requirement.

Chapter 5

OMT Measurement *in-vivo* by Laser Speckle Correlation Metrology

1 Introduction

Ocular microtremor (OMT) is the smallest and fastest of three fixational eye movements. Fixational eye movements (microsaccades, drift and OMT) are involuntary movements that occur even while the eye appears to be at rest. They were first described by Adler and Fliegelman [5] and have been studied extensively since [6-8, 10, 34]. Most studies on fixational eye movements concentrate on microsaccades [8, 50] and drift. Because of its small amplitude (12-216 μrad) and high frequency (mean of 84 Hz), OMT is difficult to measure.

To date, the most widely used tool to measure OMT has been a piezoelectric technique (PZT) [27, 31, 156]. Briefly, this technique involves the use of eye-contacting probes that are lowered onto the sclera of a subject. Movement of the eye causes a mechanical bend in the piezoelectric material that is converted to an electrical signal by the material. The signal is amplified and sent to a computer for off-line processing. The technique has a number of disadvantages including patient discomfort [17, 26] and possible bias of the measurement results by the eye-contacting probes [32]. Ideally, for clinical use, a non-contact method would be employed to record OMT.

OMT records are typically measured in the horizontal direction. The frequency content of the record is of most interest and is typically measured using a 'peak count' method. A reduction in OMT frequency has been shown to be of clinical importance in a number of medical circumstances, mostly associated with neurological disease [16, 19, 22, 42, 43, 45-48, 149, 157, 158].

Chapter two detailed and tested a straightforward non-contact technique to measure angular displacements in the range of OMT. The design was based upon an angular laser speckle correlation system with imaging in the Fourier plane of a lens [96, 97].

Speckle from an 'ideal' surface will exhibit surface scattering of the incoming light. However, speckle from laser light that penetrates into the volume of an object will exhibit multiple scattering. It was demonstrated in chapter three that this multiple scattering will lead to a bias error in the amplitude of measured displacement results.

In chapter four it was demonstrated that, in spite of the presence of time-varying speckle (biospeckle), the speckle captured from the eye sclera was reasonably stable between successive image frames at the frame rate of 500 Hz used. For the proposed speckle correlation metrology technique, the only constraint caused by the time varying speckle structure seen *in-vivo* was the need to leave a sufficiently short time between frame cross correlations. In practice, this means tracking frame-to-frame displacements when using a 500 Hz frame rate. The mathematical simulations in chapter four showed that translational motion was preserved in the presence of biospeckle and suggested biospeckle alone should have no systematic influence on the angular displacement measurement from the sclera. Biospeckle did, however, act as noise and result in a precision error in the displacement result. Based on these arguments, it is anticipated that OMT will be measureable from the sclera *in-vivo* using the proposed laser speckle

correlation system. The primary aim of this work was to determine whether useful OMT information can be recorded from the eye sclera *in-vivo* using the proposed laser speckle correlation system outlined in chapter two.

As outlined in chapter two, the maximum permissible exposure (MPE) outlined by international safety standards [135, 136] for a 10 s exposure of a 632.8 nm HeNe laser on a 7 mm pupil diameter is 388.65 μW. This value of MPE is calculated for exposure to the retina, here the laser will be directed at the sclera and will therefore pose less risk to the eye. In a study by Bolger [20], it was suggested that a five second recording is a "reasonable compromise between measurement precision and analytical effort". In this study, a 5 s recording will be taken from the eye sclera. While allowing for some exposure of the sclera to the laser during setup, this recording length will keep within eye-safe levels and give sufficient time to record a representative trace of OMT. The sclera was chosen as the target for the laser beam, because it reflects more light than the iris does. Additionally, the iris can change shape in response to incoming light, this would add a complication to laser speckle measurement from the iris.

1.1 Factors that Influence OMT Signal Measurement

Collins [11] investigated measures that can influence the characteristics of an OMT signal. In this study, it was reported that both acute intoxication of alcohol and moderate amounts of caffeine intake both independently resulted in a small, but significant increase in OMT peak frequency in healthy subjects. In the same study, time of day of testing was not found to have a significant effect on OMT parameters.

Age has been shown to influence OMT. A small but significant change in OMT parameters has been shown between subjects aged under 60 years and those aged over 60 years [23].

The peak frequency of OMT has been shown to increase when the eye is adducting (looking towards the nose) or abducting (looking away from the nose) [11]. This simple method of influencing OMT can be exploited as an indicator that recordings taken from the eye do in fact represent OMT.

In the largest study on OMT frequency, to date, Bolger *et al.* [14] found no significant difference in OMT parameteres between healthy males and females. Likewise, no significant difference in OMT parameters between the right and left eye has been found [17].

1.2 OMT Signal Identification

The recorded OMT signal is expected to be disrupted by microsaccades and drift. Drift causes a background movement in the measured signal, while microsaccades cause intermittent jumps in amplitude. OMT and drift occur together. Typically in OMT studies, a 20-150 Hz bandpass filter is used to effectively filter drift from the signal. Microsaccade removal presents more of a challenge.

In previous experiments, microsaccades were removed from the signal either by filtering [30], cutting [13, 22, 25, 31], adaptive time varying filter [27], multi resolution method [159] or by wavelet analysis [27]. Al-Kalbani [27] compared all five methods of microsaccade removal in terms of recovered simulated OMT signal in the time, frequency and joint time-frequency domains. The results showed the cutting and

wavelet methods to provide similar good reconstructions of an inputted test signal. An advantage of the wavelet method over the cutting method is that no information is lost and the time series signal can be reconstructed with minimal distortion to signal recovery. However, Al-Kalbani noted that the type of wavelet function and the number of levels chosen for reconstruction have to be defined *a priori* and that the chosen options influence the resulting recovered signal. Furthermore, Al-Kalbani noted that some abnormal OMT signals could not be reconstructed using the chosen parameters for the wavelet technique.

The primary purpose of the work here is to attempt to confirm the presence of OMT *in-vivo* using the proposed non-contact speckle correlation measurement system. OMT signals have never before been measured from the sclera using this laser speckle correlation technique. To gain an understanding of the recovered signal, a simple, visual extraction of microsaccades is preferable. For this reason, the cutting method of microsaccade removal will be implemented in this work, since no *a priori* information is required for its use.

The bulk of the OMT spectrum lies in the 40-80 Hz range. Sheahan [26] defined the shape of OMT spectra to be either 'type 1' or 'type 2' spectra. Type 1 consists of significant high frequency peaks, while in type 2, no significant high frequency peaks are found.

2 Methods

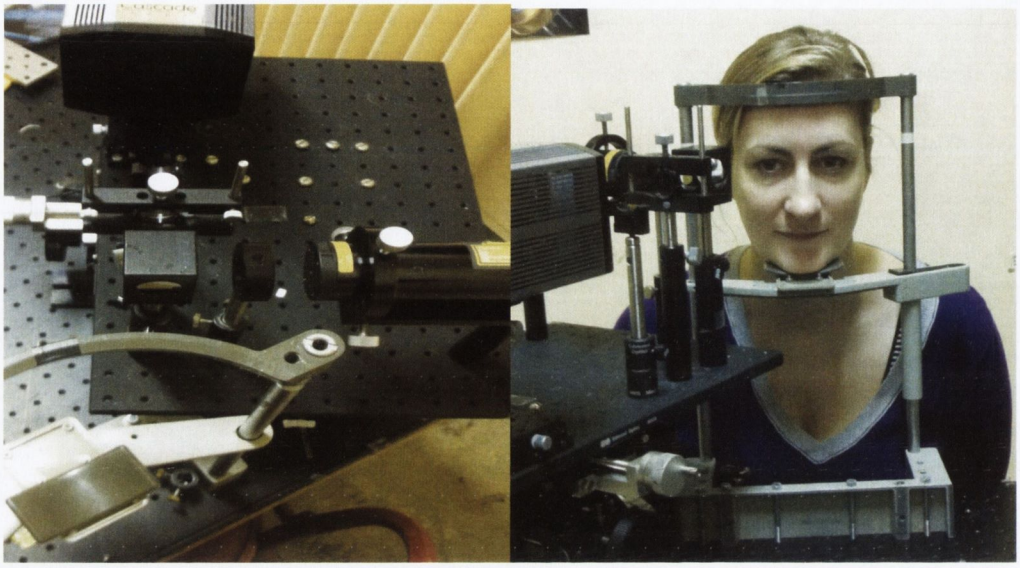

Figure 1. Equipment to measure OMT *in-vivo* (left). The subject placed their head in the headrest during measurement (right).

2.1 Equipment and Analysis

The equipment used to record OMT *in-vivo* is shown in figure 1. Speckle patterns were collected by an EMCCD camera (Cascade 128+, Roper Scientific [138]) operating at 500 Hz with a 128 x 128 array of 24 μm pixels and a 100% fill factor. The EMCCD sensor was placed in the Fourier plane of the lens. The equipment was mounted on an x-y-z stage that allowed for movement in all directions and precise alignment of the laser on the eye sclera.

After the speckle images were captured, the 8-bit uncompressed Audio Video Interleave (AVI) avi file was sent to the numerical software package Matlab [139] for processing. As detailed in previous chapters, a cross-correlation technique was used to measure the displacement between frames. To recover the input signal, each frame was cross-correlated with the previous frame.

Microsaccades were removed from the measured signal using the cutting technique described in section 1.2. An analysis programme was written in Matlab to identify microsaccades in the signal and remove them. The following steps were taken to remove a microsaccade;

(i) The difference (D) in pixels between each measured displacement and the previous measured displacement was calculated.

(ii) The mean (D_{mean}) and standard deviation (D_{stdev}) of that difference was then calculated.

(iii) Any displacement in the measured signal that was larger than the mean difference plus three standard deviations was considered to be a microsaccade, i.e. Microsaccade = $D_{mean} + (3 \times D_{stdev})$. The value of three standard deviations was found empirically to be a good confidence interval for microsaccade removal. A confidence interval of two standard deviations was found not to exclude enough data, while a confidence interval of four standard deviations was not sensitive enough to exclude microsaccade data.

(iv) The signal was resampled to exclude measurements that were part of a microsaccade.

(v) Since microsaccades cause a jump in the signal, the program then realigned the measured signal so that after a microsaccade, the trace continued on from the same time and amplitude it was at before the microsaccade.

Finally, to isolate the OMT signal and remove the 2-5 Hz drift artifact and other unwanted noise, the measured displacement signal was bandpass filtered between 20-150 Hz using a Butterworth filter of the 5^{th} order.

The peak frequency of the measurements was calculated using the peak counting method. A peak counting program was written in Matlab to automatically count the peaks of the filtered OMT signal.

A segment overlap periodogram was implemented to estimate the spectral content of the OMT data. For this, the filtered data was divided into 512 segments with a 0.9 Hz resolution. The power spectral density was then estimated using a Fourier transform, after a Hamming window was applied to each segment. To estimate the amplitude of the measured displacement over the measurement period, each local trough in the signal wave was subtracted from each subsequent peak and the mean of all values was taken to be the peak-to-peak amplitude of the measured signal.

2.2 Subjects

The protocol established for this study was approved by the local ethics committee (St James's/AMNCH Research Ethics Committee). All volunteers were provided with an information leaflet and educated about the purpose and nature of the study. The moderate risks were explained and candidates were given the opportunity to withdraw from the study at any time. Written informed consent was obtained from all volunteers.

In accordance with the findings and recommendations of Collins [11], volunteers in this study were asked to refrain from caffeine for two hours prior to testing. Due to lack of influence on OMT [11], no time of day constraint was implemented, though testing was mostly performed in the evening time.

The following measurement procedure was implemented for all trials in this work. Any deviations from the procedure are noted. In all cases, OMT was measured in the horizontal direction.

The laser was reduced down to an eye-safe power of 180 μW by the use of a neutral density filter and a beam splitter. The subject was seated and asked to place their head in a headrest. They were then asked to maintain as steady a position as possible, not to blink and to keep fixated in the straight ahead position. In contrast to other studies [11, 38], in this work the eyelids were not taped open. To protect the eye from accidental laser beam exposure, the subject closed their eye during precise alignment of the laser beam with the eye sclera. The sclera of the right eye was illuminated by a 632.8 nm plane polarized HeNe laser. Alignment of the laser beam at the eye sclera was reasonable easy and, given the ease of alignment and speed of measurement, if a subject blinked, the recording was stopped and another recording was taken. The beam was positioned approximately at the centre of the visible area of lateral sclera. The subject then opened their eye and the exact laser beam position was checked. If the position was suitably located on the sclera, they were asked to close their eye once more and then open it when ready for the measurement to be taken, otherwise the position of the laser was adjusted until accuracy was achieved. A 5 s recording was taken for each measurement.

The total time taken to record speckle images from a subject was approximately 1 minute, including set-up. The recordings were processed off-line.

2.3 *In-Vivo* Measurement of a Large Angular Displacement

As mentioned previously, multiple scattering is expected to cause a material-dependent systematic bias error in the speckle correlation measurement results. To check the accuracy of the measurement system *in-vivo* and to estimate the calibration error, an experiment was designed to measure a known displacement.

A small group of three healthy volunteers (2 male, 1 female, average age of 30) were recruited to investigate the ability of the system to follow a large angular movement in the presence of scattering *in-vivo*. Each volunteer was asked to follow a crosshair moving linearly across a computer screen. The screen was placed 100 cm away from the volunteer and the crosshair translated a distance of 4 cm in the horizontal direction. With this set-up the angular displacement of the eye is expected to be 40 mrad. The speckle patterns were recorded as described above, however, a 7 second (3500 image frames) recording was taken to allow time for the eye to comfortably follow the crosshair. For the analysis of the measured displacement, each speckle frame was correlated with the previous frame.

With this design, the mean velocity of the eye as it tracks the crosshair will be 5.71 mrad. Using a frame-to-frame measurement and a 500 Hz sample rate, this is equivalent to a displacement of 5.71 mrad ÷ 500 Hz = 11.4 μrad per frame (assuming all other eye movements cause a zero net displacement). As such, if the overall 'large' movement can be measured, then this will demonstrate that displacements close to the desired 12 μrad resolution necessary to measure OMT can be measured.

2.4 Measurements of OMT on a Group of Volunteers

In-vivo speckle measurements were captured from twenty healthy volunteers (7 males, 13 females, aged between 23-34 with a mean age of 27 years). In addition to calculating the signal spectral data and measuring amplitude, OMT speckle patterns were analyzed using the speckle contrast, peak height-to-floor ratio and time history speckle pattern (THSP).

2.5 Measurements while Adducting

To investigate whether the peak frequency of OMT changed with eye position, a small subgroup of the volunteers (6 total, 4 male and 2 female) had a second measurement taken. For this recording they were asked to look to their left so that their right eye was adducting. As explained previously, the peak frequency of OMT is expected to increase while the eye is adducting. The recordings were analysed with the same method as those taken with the eye in the straight ahead (primary) position. The change in frequency between each subject's OMT peak frequency in the primary and in the adducting eye position was calculated.

3 Results

3.1 *In-Vivo* Measurement of a Large Angular Displacement

Figure 2 displays the unfiltered measurement results from the three subjects. The mean of the three measured displacements was 13.12 mrad (equivalent to a mean velocity of 1.87 mrad). This mean measured result is much lower than expected 40 mrad displacement of the eye and gives an average measurement error:

$(\frac{Expected-Measured}{Expected}\ x\ 100)$ of 67.2%. The discrepancy between the measured results and the expected result is likely to be accounted for by the multiple scattering expected in the eye.

The spikes in the plot are consistent with the appearance of microsaccades. The microsaccades are seen to disrupt the trace and made the final displacement appear somewhat smaller. The trailing off seen on the green (dashed line) trace may be due an error in fixating by the subject.

Figure 3 displays the same results, but with the microsaccades removed. Because of the cutting technique used to remove the microsaccades, the traces were shorter than the original 7 s traces. In this case, the measured displacements were 20.27 mrad, 13.89 mrad and 9.98 mrad, giving a mean measured displacement of 14.71±5.2 mrad. Based on these results, the measurement error was reduced slightly to 63.22%.

Table 1 displays the measured displacement and mean velocity for each subject, calculated from the traces with microsaccades removed. The mean velocity from each subject (calculated from the average value of displacement per frame) was found to be 2.97 mrad, 1.44 mrad and 3.03 mrad with corresponding mean displacements per frame of 5.93μrad per frame, 2.88μrad per frame and 6.05μrad per frame (at a 500 frames per second (FPS) sampling rate).

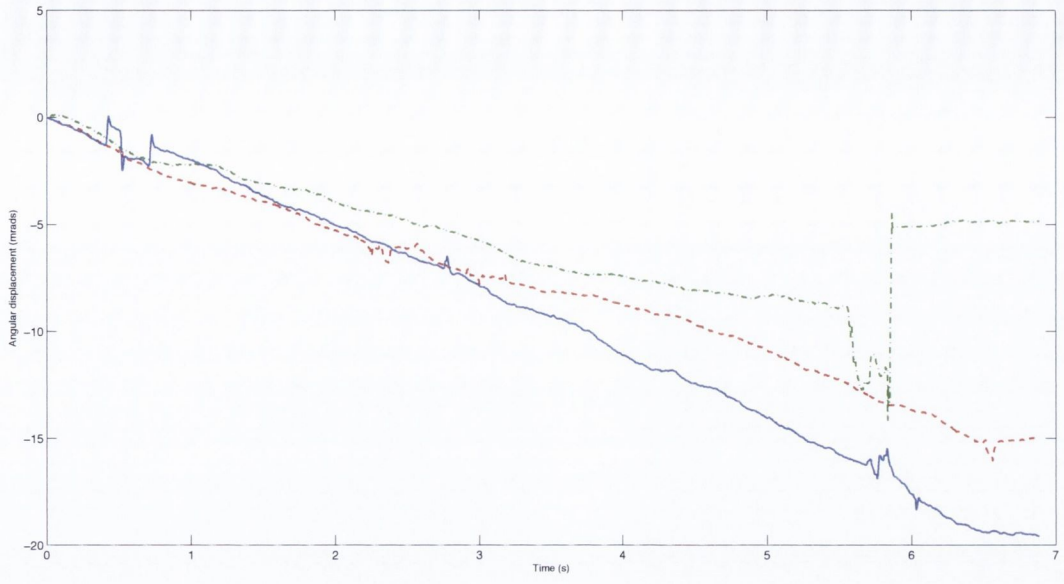

Figure 2. Measured large angle displacement from human sclera as it tracked a crosshair on a computer screen. The results from three different subjects are shown.

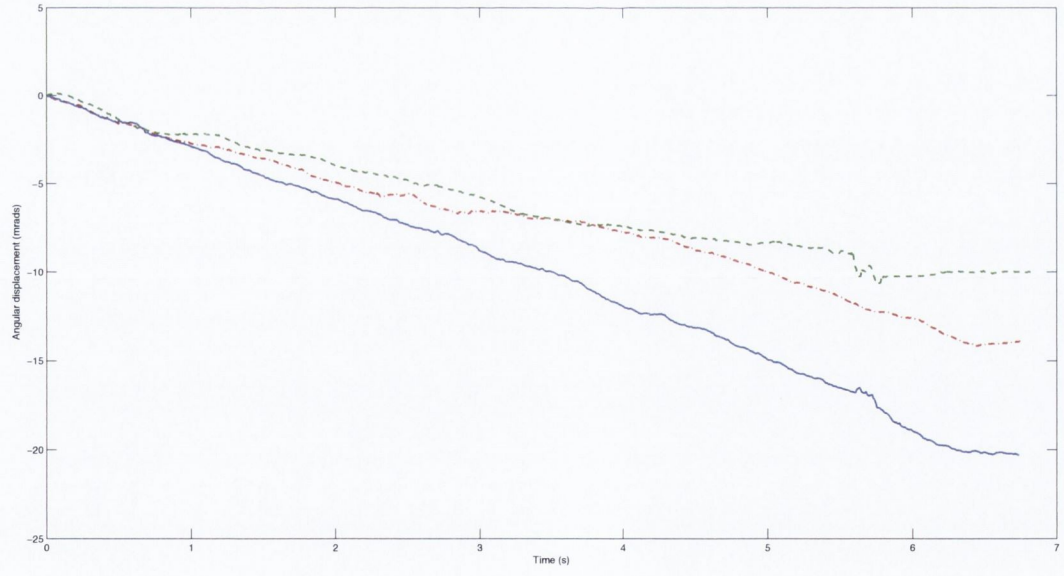

Figure 3. Measured large angle displacement from human sclera as it tracked a crosshair on a computer screen. Microsaccades were removed from the traces. The results from three different subjects are shown.

	Total Displacement (mrad)	Mean Displacement per Frame (μrad per frame)	Mean Velocity per Frame (mrad)	Expected Total Displacement (mrad)	Expected Mean Displacement per Frame (μrad per frame)	Expected Mean Velocity per frame (mrad)
Subject 1	20.27	5.93	2.97	40	11.4	5.71
Subject 2	13.89	4.05	2.03	40	11.4	5.71
Subject 3	9.81	2.88	1.44	40	11.4	5.71

Table 1. Measured displacement and mean velocity for each subject.

3.2 Measurements of OMT on a Group of Volunteers

3.2.1 Blinks

Any blinks in the measurement traces were immediately obvious. The effects of a blink on the measurement are shown in figure 4. They caused a lowering the speckle contrast, a jump in the unfiltered displacement trace and a dark area in the time history speckle pattern (THSP).

The affects of blinks on the THSP appeared distinctly different to change in the THSP caused by microsaccades. When a blink occurred, the THSP displayed blurred speckle, a dark area, more blurred speckle, another dark area and more blurred speckle before returning to the high-contrast speckle. It is supposed that the middle blurred speckle is speckle reflected from the closed eyelid, while the dark areas on either side are caused from the eyelid opening and closing. The outer blurred areas are likely to be due to an increase in tear flow prior to, and following a blink.

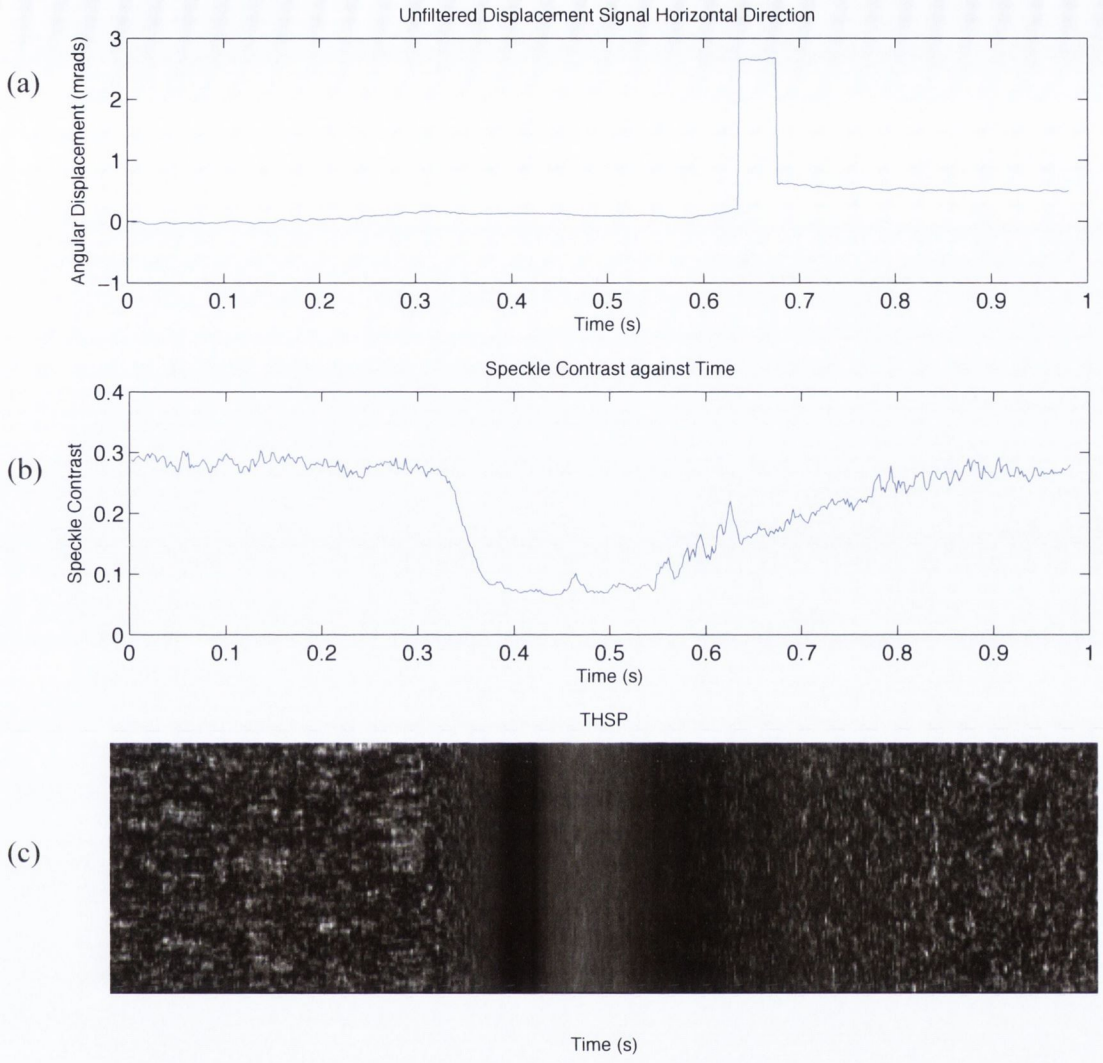

Figure 4. Effect of a blink on the measurement results of (a) the unfiltered measured displacement, (b) the speckle contrast and (c) the THSP.

3.2.2 Microsaccades

Most recorded eye traces showed evidence of irregular, large, sudden displacements consistent with microsaccades. Results recorded from a 5 s measurement of one subject are shown in figure 5. Locations where microsaccades occured are indicated with arrows. Evidence of the microsaccade-like displacements can be seen in the unfiltered and filtered displacement signals as well as in the speckle contrast, peak height-to-floor

ratio and THSP. Large amplitude microsaccades are easily visible in the displacement traces, where they distort the measured signal. The high velocity of the microsaccades caused a reduction in the speckle contrast of the recorded speckle patterns and led to blurred speckle patterns and a reduction in the signal peak height-to-floor ratio. This can be noted in the plots of speckle contrast and peak height-to-floor ratio over time. The blurred speckle can be noted in the THSP. In comparison to the blurring caused by blinks, the microsaccades do not cause the distinctive fully dark areas in the THSP and are of a shorter duration.

The measured values for the microsaccade-like displacements are consistent with values for microsaccades in the literature (frequency of 1-2 microsaccades per second and an amplitude of 1.45 mrad). The peak-to-peak amplitudes of the microsaccades varied, with a range of 0.058-7.89 mrad and a mean of 1.4 ±1.8 mrad. The number of microsaccades per unit time in the recorded traces also varied between subjects. The range across subjects was found to be between 0–2.6 microsaccades per second with a mean of 0.65 ±0.75 microsaccades per second. A similar variability of between 0 - 2.73 microsaccades per second was reported by Collins [11]. Figure 6 shows an example of an unfiltered OMT measurement both before and after microsaccade removal.

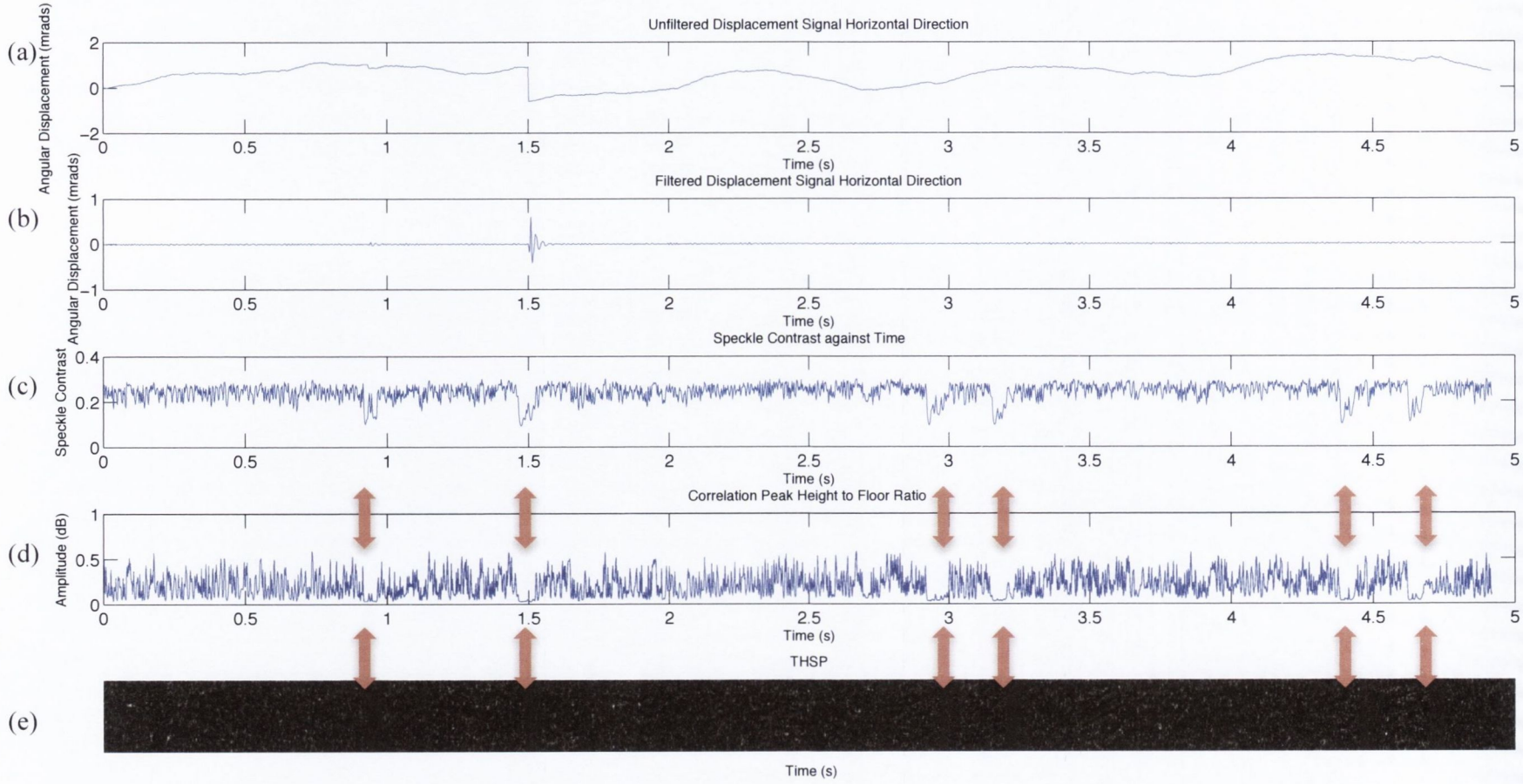
(a)
Unfiltered Displacement Signal Horizontal Direction
Angular Displacement (mrads)
2
0
−2
0
0.5
1
1.5
2
2.5
3
3.5
4
4.5
5
Time (s)
(b)
Filtered Displacement Signal Horizontal Direction
Angular Displacement (mrads)
1
0
−1
0
0.5
1
1.5
2
2.5
3
3.5
4
4.5
5
Time (s)
(c)
Speckle Contrast against Time
Speckle Contrast
0.4
0.2
0
0
0.5
1
1.5
2
2.5
3
3.5
4
4.5
5
Time (s)
(d)
Correlation Peak Height to Floor Ratio
Amplitude (dB)
1
0.5
0
0
0.5
1
1.5
2
2.5
3
3.5
4
4.5
5
Time (s)
(e)
THSP
Time (s)

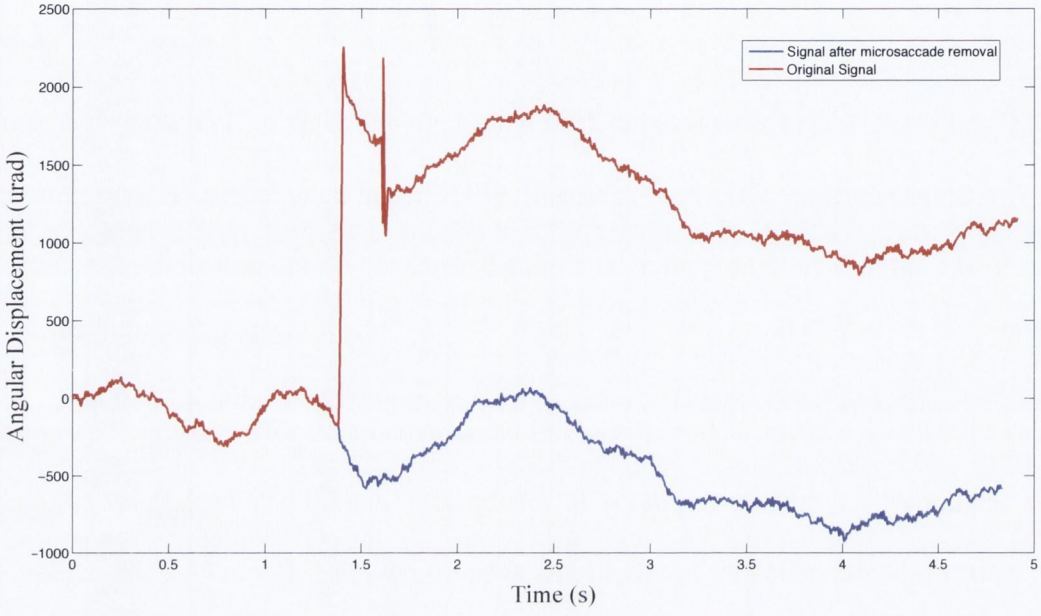

Figure 6. A 5 s unfiltered signal measured from a subject *in-vivo* showing the trace before microsaccade removal (red) and after microsaccade removal (blue).

3.2.3 Drift

The slow drifting background of figure 6 is indicative of drift. The plot shows a high frequency component overlaid on the drift component. As can be seen in the OMT signals in figures 8 and 9, the drift component of the signal was effectively filtered out by the 20-150 Hz bandpass filter.

3.2.4 OMT

Figures 7 and 8 show filtered OMT records. Microsaccades were removed from the trace prior to bandpass filtering. The mean peak frequency for the 20 subjects, estimated from peak counting, was 78.27 ±3.86 Hz. These peak frequencies are in agreement with the peak count values reported from both the largest OMT frequency study (84 Hz) [14] and the most recent report of OMT peak frequency (87.3 Hz) [11].

The mean peak-to-peak amplitude of OMT was found to be 21.42 ±7.01 μrad. This is within the same order of the expected range of 12-200 μrad peak-to-peak. However, from the results of section 3.1 for a large angular displacement, the measured amplitude is expected to be approximately 63% lower than the true value. The 'calibration' error may be non-linear and change with amplitude. It was shown in chapter three that calibration errors arise from multiple scattering in a material.

The mean frame-to-frame displacements measured in the crosshair tracking study were of the same order of OMT. Therefore, it is reasonable to assume that the 63% measurement error found in the experiment, also applies to the measurements recorded for OMT and that the true mean value for the amplitude might be about 35 μrad.

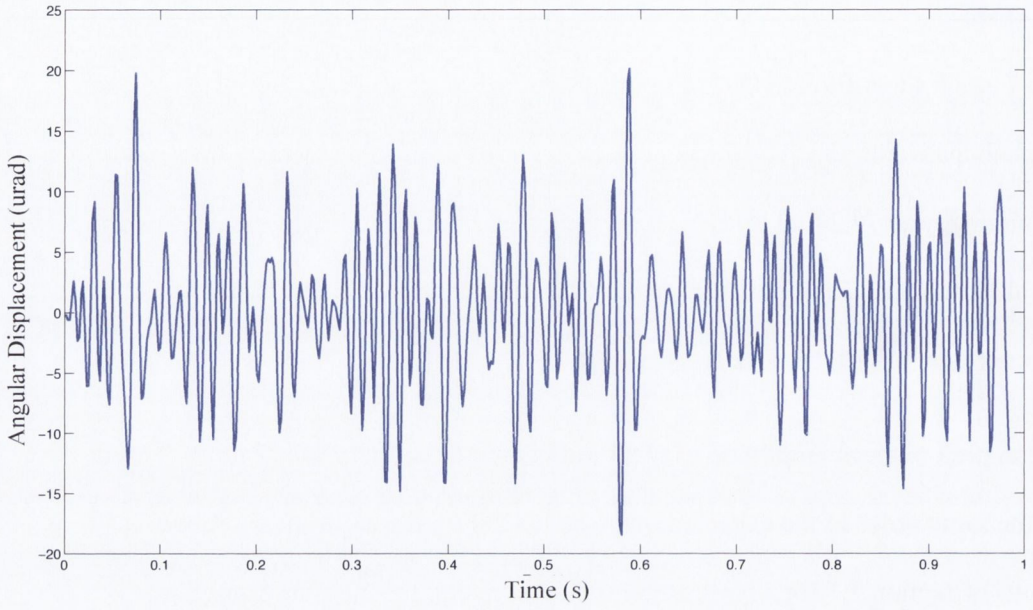

Figure 7. One second of a measured OMT signal from a subject. Microsaccades were removed from the signal and it was bandpass filtered between 20-150 Hz to remove any drift artefact.

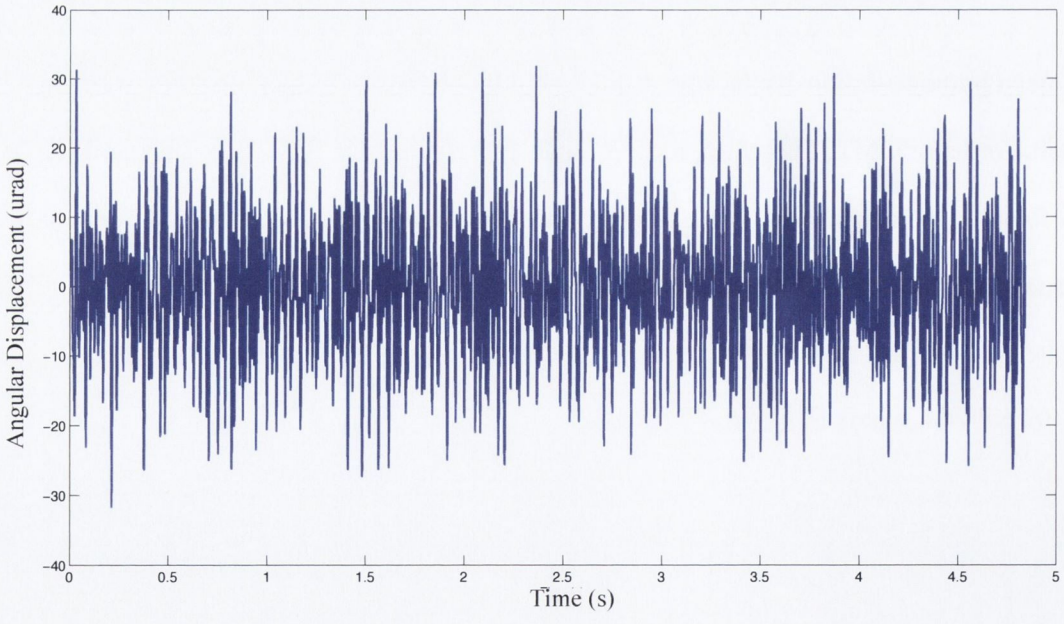

Figure 8. A five second measurement of OMT recorded from a subject. Microsaccades were removed from the signal and it was bandpass filtered between 20-150 Hz to remove any drift artefact.

The periodograms of the OMT spectra recorded for all 20 subjects displayed shapes that were consistent with those defined by Sheahan [26]. Figures 9 and 10 show an example of each type of measured spectra.

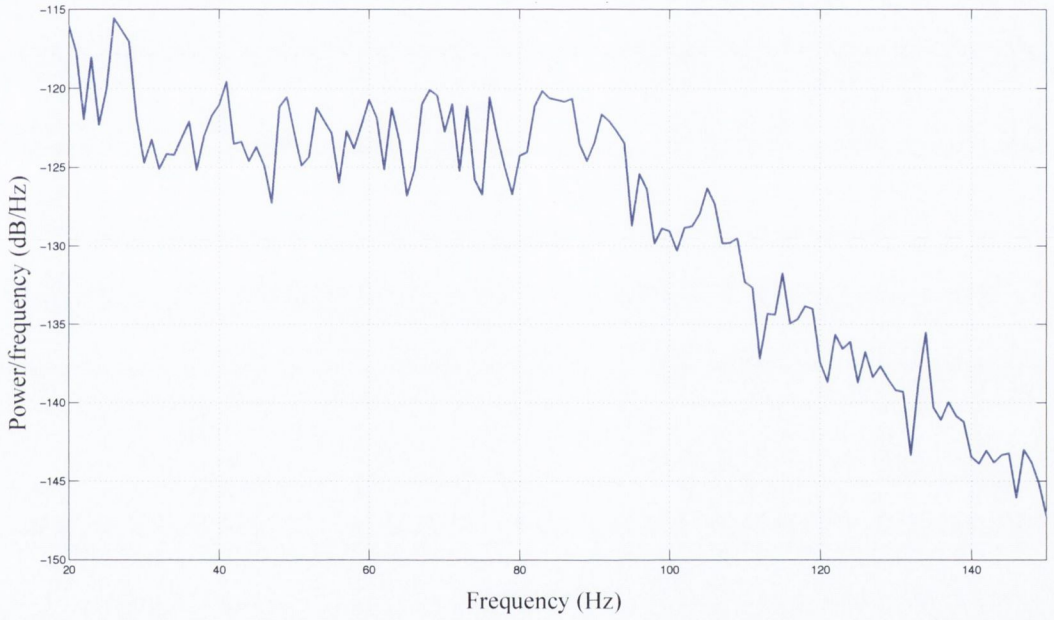

Figure 9. Periodogram displaying 'type 1' OMT spectra.

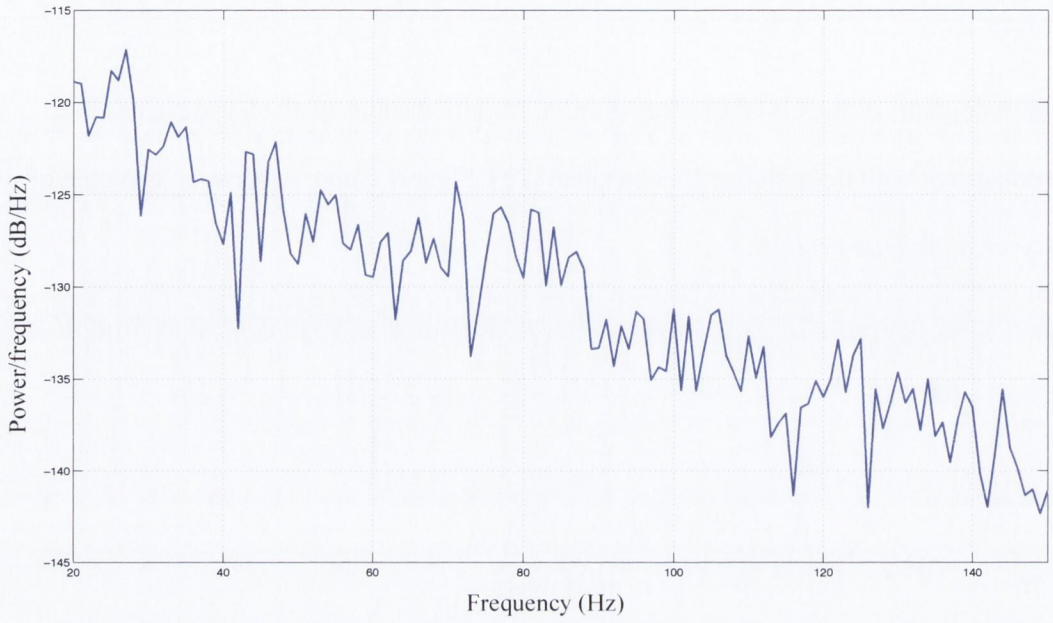

Figure 10. Periodogram displaying 'type 2' spectra.

3.3 Measurements while Adducting

The mean of the six calculations for the difference in peak frequency between the eye in the primary position and the eye in the adducting state gave an increase in peak frequency of 10±6.2 Hz, using the peak counting estimate. This value of increased peak frequency in adduction is of the same order as that reported by Collins [11] (a 9.5 Hz increase). A mean peak-to-peak amplitude of 17.76 μrad was calculated for adducting subjects. This mean amplitude is lower than that found for OMT recorded in the primary position (21.42 ±7.01 μrad) but within the standard deviation of the measurements.

It should be noted that the high standard deviation in the peak frequency measurements is indicative of the fact that in some cases the peak frequency did not always increase. In two

cases, the peak frequency decreased. A limitation of the results of this study is the small (n = 6) number of subjects tested.

4 Discussion

A non-contacting device to record OMT is essential to extend its feasibility as a clinical tool and to provide a means to allow for further research into OMT's role in vision. The non-contact nature would allow for visual tasks to be performed while OMT recordings are taken. This form of research is impossible with the current, eye-contacting, piezoelectric technique (PZT) [27, 31] for OMT measurement. This chapter aimed to investigate whether a reliable OMT signal could be recorded using a non-contact laser speckle correlation system.

It was established in this study that parameters consistent with known OMT values could be recorded using the proposed speckle correlation system. A mean peak frequency of 78±3.86 Hz, established from the peak counting method, was calculated for the 20 subjects tested in the study. This is in the same order of the mean peak value of 83.68±5.78 Hz calculated by Bolger *et al.* [14] in the largest study performed on OMT frequency. Discrepancies between the two mean peak values could be due to the different measurement techniques used and the small number of subjects in this study.

Since there is no way to verify the true value of OMT in a subject, the values reported here can only be compared to values reported elsewhere in the literature.

The *in-vivo* measurement of a large angular displacement from the sclera showed that while the speckle correlation system is capable of tracking eye-movement from the sclera, the amplitude of the angular displacement had a measurement error of about 63%. The frame-to-frame displacement being measured was 11.4 μrad. Importantly, despite the error in amplitude accuracy, this showed that the proposed system does have the resolution necessary to measure displacements in the range of OMT (12-216 μrad).

A laser beam does penetrate into the scleral surface and suffers from multiple scattering before emerging again. It is likely that multiple scattering contributes to the error seen *in-vivo*. A limitation on the error estimation is that it is unclear as to what range of calibration errors to expect from the small numbers studied in this work. The error may vary for different individuals and it is unknown whether the calibration error is linear or if the error changes with amplitude. The results of the simulation in chapter three suggest a possible non-linearity in the amplitude response for frame-to-frame displacements larger than a speckle size. It is unclear whether the same non-linearity is also applicable to the *in-vivo* eye measurements in this study.

Measurements that contained blinks were not processed for the results of this study since if a subject blinked, a new measurement was recorded. Nonetheless, processing of the discarded measurements did show instances of signal loss due to blinks and their corresponding build up of tears. The cutting method used to remove microsaccades was also capable of removing parts of the signal that contained blinks. Taping the eye open can lead to discomfort for a subject and drying out of the eye. Since blinks can be easily removed from the signal (with only the same limitations as those for microsaccade

removal), it is reasonable to assume that OMT measurement can be performed without taping the eyes open.

Future refinements to the optical setup would include making it more compact so that it could be developed into a handheld device. Laser diodes could be used to reduce the size of the optics. However, to produce good quality speckle, the laser diodes would need to be highly coherent. Any change in the wavelength of the laser used for speckle correlation would have the effect of changing the speckle size and the scattering properties on the target.

Infra-red lasers are typically used in other eye-tracking systems. These lasers have the benefit of having power levels that can be about five times higher than for a HeNe laser without increasing the hazard to the eye from the laser. A higher power level will result in a higher signal-to-noise ratio at the image detector.

Multiple scattering in a material is dependent on the absorption coefficient of the material, which in turn is dependent on the wavelength of the incoming light. To keep multiple scattering at a minimum at short penetration of the incoming light is desired. In the infra-red range of the electromagnetic spectrum ($\lambda \geq 2000$ nm), light is mostly absorbed and penetrates only to a depth of about one or two cell layers in tissue [160]. In the 600 – 1600 nm wavelength range, scattering prevails over absorption and the percentage of backscattered incident light increases to 35 - 70%. In this range, light penetrates to a depth of about 8 -10 mm [160]. For these reasons, development of the laser speckle correlation technique to include an infra-red laser may be worthwhile.

5 Conclusions

A novel technique to measure ocular microtremor *in-vivo* from the eye sclera in a non-contact manner was tested. It was found that, even in the presence of other eye and head movements, tear flow and time-varying speckle, that the OMT signal could be tracked. Motion consistent with OMT, drift and microsaccades was detected by the technique. Some uncertainty is noted in the amplitude measurement. Nonetheless, a peak frequency of 78.27 ±3.86 Hz and mean peak-to-peak amplitude of 21.42 ±7.01 μrad was measured from OMT measurements of 20 subjects. Although a small number of subjects was used, the study has shown evidence that OMT can be recorded in a non-contact manner using laser speckle correlation.

Chapter 6

Thesis Discussion and Conclusions

The primary aim of the work in this thesis was to investigate and develop a non-contact method to measure ocular microtremor (OMT). A laser speckle correlation technique was shown to have the technical requirements needed to measure OMT and it was tested *in-vivo*. The results showed that OMT could be measured using the system. The work in this thesis is the first report of laser speckle correlation used to measure OMT.

The OMT measurement device designed in this thesis had a resolution of 4 μrad and a dynamic range of 4-5000 μrad. The system was shown to be insensitive to linear displacements along the optical axis. The system was also shown to be invariant to changes in target beam locations of within ±25 mm along the optical axis. The significance of these performance characteristics is that angular displacements of OMT can be measured even in the presence of some head movement by a subject and no strict target beam positioning is required.

When a 'non-ideal' speckle surface was used, the system was found to have a material dependent bias error with displacement. This error was not foreseen since not much literature on speckle displacement of non-ideal surfaces exists. The calibration error is likely to be due to a multiple scattering component of scatter interfering with a surface

component. The results are supportive of a concept that speckle from a volume field does not carry displacement information.

The measured bias error was found to be fairly consistent for each type of material tested and was linear within the range of 4-197 μrad. However, there was some evidence that the error becomes non-linear at higher displacements and that this non-linearity is related to the speckle size relative to the displacement.

Some reference to a material dependent decorrelation factor is made in the paper by Rose *et al.* upon which the optical set-up in this work is based. The decorrelation factor is used to differentiate partially developed speckle from fully developed speckle and it is noted that their setup is applicable to both types of speckle. Further work is required to explore the relationship between the decorrelation factor in their work and the calibration error seen in this work.

A mathematical model was created to investigate the influence of the multiple scattering component on the measurement system. Through the model, it was shown that multiple scattering led to a reduced accuracy in the measurement results. This was consistent with the differences in the experimental measurement results seen for surface and volume scattering materials.

Limited information in the literature was suggestive that the sclera may be a suitable target from which to record speckle. The novelty of this work was that two-dimensional images of speckle from the sclera were collected and their spatial and temporal evolutions were investigated. The stability of the *in-vivo* speckle was also examined. Previously unknown

information on the speckle contrast and the properties of the time history speckle pattern from the *in-vivo* speckle images was collected.

The design of the optical system was found be sufficient to measure stable speckle patterns of high speckle contrast on a frame-to-frame basis. Importantly, the effects of time-varying biospeckle were minimized by sampling the speckle patterns at a high frame rate (500 Hz) with the highly light-sensitive camera used in this work. This is the first time a value has been reported for a sampling rate adequate to capture speckle images from the sclera for metrology purposes.

A limitation on the investigation into biospeckle from the *in-vivo* sclera is that the recorded images included eye movement in addition to biospeckle. Ideally, to fully characterize biospeckle-only variations in the speckle patterns, it would be necessary to separate it from other movement in some way. Only one wavelength laser was implemented in this study and it is unclear whether a different wavelength would give rise to biospeckle with different properties, e.g. speed of speckle fluctuations. Similarly, it is unclear whether eye condition will influence the *in-vivo* speckle images in any way.

When measurements of the eye rotating through a large angle were taken, the results showed a bias error similar to that seen for the inanimate materials in chapter three. This suggests that the concept outlined in chapter three of a multiple scattering field interfering with a surface scattering field and producing a bias error was also plausible for the eye. Furthermore, the results showed that the frame rate of 500 Hz was adequate to measure displacements of the eye.

Measurements of speckle recorded from the *in-vivo* sclera were shown to provide good evidence that OMT was recorded. The peak frequency was within the expected range and the spectra displayed shapes characteristic of OMT. Similarly, the measured waveform displayed OMT-like features and the amplitude was within the OMT range. It was noted that the reported amplitude is likely to be lower than the true amplitude due to the calibration error discussed above. Blinks, tear flow, drift and microsaccades were all found to disrupt OMT measurement, but were easily removed from the signal through filtering and cutting of the signal.

Future work on this research could include development of a handheld device and a miniaturization of the optical design. The overall bulk of the system is mostly occupied by the laser and the imaging camera. The laser could simply be replaced with a laser diode. New imaging sensors with high light sensitivity and smaller pixel sizes are emerging. A smaller pixel size would allow for a better resolution for the measurement system.

Ideally, the measurement device would report the true measured amplitude. Further work to quantify and establish the cause of the calibration error seen in the results of this study is needed. The system could be tested using a laser with a different wavelength. Since different lasers penetrate to different depths within a material, the use of a different wavelength laser for a given material should produce a different calibration error to that of a 632 nm laser. Whether the calibration error is linear with amplitude remains to be determined. The work in this thesis suggests that the error may be non-linear, though evidence for this is more strongly supported through the mathematical model than it is for the experimental results. Further work is required to investigate why there was a difference between the modeled and experimental results.

The mathematical model created in this thesis was used to investigate the effects of multiple scattering and of biospeckle on the speckle correlation system. The model could be enhanced by refining the speckle patterns generated for volume scattering materials and living objects. Parameters relating to the number and velocity of scatterers representing biospeckle could be added.

The benefit of OMT as a clinical indicator of neurological disorders has been shown in the literature. It is anticipated that a non-contact device to measure OMT, such as the device developed in this work, would encourage its acceptance into routine clinical practice. Futhermore, the system could be used in a research setting in attempt to gain a more thorough understanding of OMT and its role in vision.

References

1. Beers, M.H., et al., *The Merck Manual of Medical Information: Home Edition* 2008: Paw Prints.

2. Tuchin, V.V., *Handbook of Optical Biomedical Diagnostics*2002: SPIE Press.

3. Kaufman, P.L., et al., *Adler's Physiology of the Eye.* 11 ed2011: Saunders/Elsevier. 795.

4. Gilroy, A. and B. MacPherson, *Atlas of Anatomy*2012: Thieme New York.

5. Adler, F.H. and M. Fliegelman, *Influence of Fixation on the Visual Acuity.* Arch Ophthal, 1934. **12**(4): p. 475-483.

6. Ratliff, F. and L.A. Riggs, *Involuntary motions of the eye during monocular fixation.* Journal of Experimental Psychology\, 1950. **40**\: p. 687\-701\.

7. Ditchburn, R. and B. Ginsborg, *Involuntary eye movements during fixation.* The Journal of Physiology, 1953. **119**(1): p. 1-17.

8. Martinez-Conde, S., S.L. Macknik, and D.H. Hubel, *The role of fixational eye movements in visual perception.* Nat Rev Neurosci, 2004. **5**(3): p. 229-240.

9. Pansell, T., et al., *Slow oscillatory eye movement during visual fixation.* Experimental Brain Research, 2011. **209**(1): p. 1-8.

10. Coakley, D., *Minute eye movement and brain stem function*1983: CRC Press.

11. Collins, N., *Ocular Microtremor as a Clinical and Scientific Tool in Neurologic Disease; Validation and Application of a Generalised Discovery Protocol*, 2011, University of Dublin, Trinity College.

12. Yarbus, A.L., *Eye movements and vision*1967, New York: Plenum Press.

13. Spauschus, A., et al., *The origin of ocular microtremor in man.* Experimental Brain Research, 1999. **126**(4): p. 556-562.

14. Bolger, C., et al., *Dominant frequency content of ocular microtremor from normal subjects.* Vision Research, 1999. **39**(11): p. 1911-1915.

15. Bolger, C., et al., *High-Frequency Eye Tremor - Reliability of Measurement.* Clinical Physics and Physiological Measurement, 1992. **13**(2): p. 151-159.

16. Coakley, D. and J.G. Thomas, *Ocular microtremor: a neurogenic phenomenon.* Electromyography and clinical neurophysiology, 1979. **19**(4): p. 325-8.

17. Sheahan, N.F., et al., *Sources of Variance in Ocular Microtremor* Physiological Measurement, 1994. **15**(1): p. 101-106.

18. Ciuffreda, K.J. and B. Tannen, *Eye movement basics for the clinician*1995: Mosby.

19. Bolger, C., et al., *Ocular microtremor in oculomotor palsy.* Journal of Neuro-Ophthalmology, 1999. **19**(1): p. 42-45.

20. Bolger, C., *Ocular microtremor : reliability of measurement physiological variation and neurogenetic origin* in *Medicine*1995, University of Dublin, Trinity College.

21. Boyle, G., D. Coakley, and J.F. Malone, *Interferometry for ocular microtremor measurement.* Appl. Opt., 2001. **40**(1): p. 167-175.

22. Bolger, C., et al., *Ocular microtremor (OMT): a new neurophysiological approach to multiple sclerosis.* Journal of Neurology Neurosurgery and Psychiatry, 2000. **68**(5): p. 639-642.

23. Bolger, C., et al., *Effect of age on ocular microtremor activity.* Journals of Gerontology Series a-Biological Sciences and Medical Sciences, 2001. **56**(6): p. M386-M390.

24. Kevin, L.G., A.J. Cunningham, and C. Bolger, *Comparison of ocular microtremor and bispectral index during sevoflurane anaesthesia.* British Journal of Anaesthesia, 2002. **89**(4): p. 551-555.

25. Heaney, M., et al., *Ocular microtremor during general anesthesia: Results of a multicenter trial using automated signal analysis.* Anesthesia and Analgesia, 2004. **99**(3): p. 775-780.

26. Sheahan, N., *Ocular Microtremor Measurement Technique and Biophysical Analysis*, 1991, University of Dublin, Trinity College.

27. Al-Kalbani, M., *Ocular Microtremor Measurement, Characterization & Analysis*, 2009, University of Dublin, Trinity College.

28. Instruments, N., *LabView.*

29. Robinson, D.A., *A Method of Measuring Eye Movement Using a Scleral Search Coil in a Magnetic Field.* Ieee Transactions on Biomedical Engineering, 1963. **BM10**(4): p. 137-&.

30. Bengi, H. and J.G. Thomas, *Three Electronic Methods for Recording Ocular Tremor.* Medical & Biological Engineering, 1968. **6**(2): p. 171-&.

31. Sheahan, N., et al., *Ocular microtremor measurement system: Design and performance.* Medical and Biological Engineering and Computing, 1993. **31**(3): p. 205-212.

32. McCamy, M.B., et al., *Simultaneous recordings of ocular microtremor and microsaccades with a piezoelectric sensor and a video-oculography system.* PeerJ, 2013. **1**: p. e14.

33. Barlow, H.B., *Eye movements during fixation.* J Physiol, 1952. **116**(3): p. 290-306.

34. Ditchburn, R.W., *Eye-movements and visual perception*1973: Clarendon Press. 421.

35. Eizenman, M., R.C. Frecker, and P.E. Hallett, *Precise non-contacting measurement of eye movements using the corneal reflex.* Vision Res, 1984. **24**(2): p. 167-74.

36. Clark, M.R., *A two-dimensional Purkinje eye tracker.* Behavior Research Methods & Instrumentation, 1975. **7**(2): p. 215-219.

37. Cornsweet, T.N. and H.D. Crane, *Accurate two-dimensional eye tracker using first and fourth Purkinje images.* J. Opt. Soc. Am., 1973. **63**(8): p. 921-928.

38. Boyle, G., *Ocular Microtremor Non-Contacting Measurement and Biophysical Analysis*, 1999, University of Dublin, Trinity College.

39. Ryle, J.P., *Optical engineering applications in biomedical and bioprocess engineering : ocular microtremor (OMT) sensor and digital in-line holographic microscopy (DIHM)*, in *Engineering* 2010, University College Dublin: Dublin. p. 313.

40. Ryle, J.P., et al., *Compact portable ocular microtremor sensor: design, development and calibration.* Journal of Biomedical Optics, 2009. **14**(1).

41. Rabal, H.J. and R.A. Braga, *Dynamic Laser Speckle and Applications*2008: CRC Press.

42. Coakley, D. and J.G. Thomas, *Ocular Microtremor Record and Prognosis of Unconscious Patient.* Lancet, 1977. **1**(8010): p. 512-515.

43. Bojanic, S. and C. Bolger, *Ocular microtremor (OMT): A useful indicator of outcome in coma?* British Journal of Anaesthesia, 1999. **82**(5): p. 795P-796P.

44. Bojanic, S., T. Simpson, and C. Bolger, *Ocular microtremor (OMT): a tool for measuring depth of anaesthesia?* British Journal of Anaesthesia, 2001. **87**(2): p. 364P-365P.

45. Coakley, D. and J.G. Thomas, *The ocular microtremor record as a potential procedure for establishing brain death.* Journal of the Neurological Sciences, 1977. **31**(2): p. 199-205.

46. Bolger, C., et al., *Ocular microtremor in brain stem death.* Neurosurgery, 1999. **44**(6): p. 1201-1206.

47. Coakley, D., J.G. Thomas, and J.N. Lunn, *Effect of Anesthesia on Ocular Microtremor* British Journal of Anaesthesia, 1976. **48**(11): p. 1122-1123.

48. Bolger, C., et al., *Ocular microtremor in patients with idiopathic Parkinson's disease.* Journal of Neurology Neurosurgery and Psychiatry, 1999. **66**(4): p. 528-531.

49. Bengi, H. and J.G. Thomas, *Studies on Human Ocular Tremor*, in *Perspectives in biomedical engineering*, R.M. Kenedi, Editor 1973, University Park Press.

50. Martinez-Conde, S., J. Otero-Millan, and S.L. Macknik, *The impact of microsaccades on vision: towards a unified theory of saccadic function.* Nat Rev Neurosci, 2013. **14**(2): p. 83-96.

51. Coakley, D., *Ocular Microtremor Record During Sleep.* Transactions of the Ophthalmological Societies of the United Kingdom, 1976. **96**: p. 436-438.

52. Goodman, J.W., *Speckle phenomena in optics: theory and applications*2007: Roberts & Company Publishers. 406.

53. Dainty, J.C., *The Statistics of Speckle Patterns*, in *Progress in Optics*, E. Wolf, Editor 1976: North-Holland, Amsterdam.

54. Goodman, J., *Statistical properties of laser speckle patterns*, in *Laser Speckle and Related Phenomena*, J.C. Dainty, Editor 1975. p. 9-75.

55. Hecht, E., *Optics*2002: Addison-Wesley.

56. Oulamara, A., G. Tribillon, and J. Duvernoy, *Biological-activity measurement on botanical specimen surfaces using a temporal decorrelation effect of laser speckle.* Journal of Modern Optics, 1989. **36**(2): p. 165-179.

57. Arizaga, R., M. Trivi, and H. Rabal, *Speckle time evolution characterization by the co-occurrence matrix analysis.* Optics & Laser Technology, 1999. **31**(2): p. 163-169.

58. Nobre, C.M.B., et al., *Biospeckle laser spectral analysis under Inertia Moment, Entropy and Cross-Spectrum methods.* Optics Communications, 2009. **282**(11): p. 2236-2242.

59. Haralick, R.M. and L.G. Shapiro, *Computer and robot vision*1993: Addison-Wesley Pub. Co.

60. Erf, R.K., *Speckle metrology*1978: Academic Press.

61. Françon, M., *Laser speckle and applications in optics* 1ed1979, New York: Academic Press.

62. Ohtsubo, J., *Velocity measurement using the time-space cross-correlation of speckle patterns.* Optics Communications, 1980. **34**(2): p. 147-152.

63. Asakura, T. and N. Takai, *Dynamic laser speckles and their application to velocity measurements of the diffuse object.* Applied physics, 1981. **25**(3): p. 179-194.

64. Sánchez-Arévalo, F.M., et al., *Use of digital speckle pattern correlation for strain measurements in a CuAlBe shape memory alloy.* Materials Characterization, 2009. **60**(8): p. 775-782.

65. Feiel, R. and P. Wilksch, *High-resolution laser speckle correlation for displacement and strain measurement.* Applied Optics, 2000. **39**(1): p. 54-60.

66. Amodio, D., et al., *Digital speckle correlation for strain measurement by image analysis.* Experimental Mechanics, 2003. **43**(4): p. 396-402.

67. Fujii, H. and T. Asakura, *Effect of surface roughness on the statistical distribution of image speckle intensity.* Optics Communications, 1974. **11**(1): p. 35-38.

68. Leger D Fau - Mathieu, E., J.C. Mathieu E Fau - Perrin, and J.C. Perrin, *Optical surface roughness determination using speckle correlation technique.* Appl. Opt., 1975. **14**(0003-6935 (Print)): p. 872-7.

69. Asakura, T., *Surface roughness measurement.* Speckle Metrology, 1978. **1**: p. 11-49.

70. Dhanasekar, B., et al., *Evaluation of surface roughness based on monochromatic speckle correlation using image processing.* Precision Engineering, 2008. **32**(3): p. 196-206.

71. Archbold, E., J.M. Burch, and A.E. Ennos, *Recording of In-plane Surface Displacement by Double-exposure Speckle Photography.* Optica Acta: International Journal of Optics, 1970. **17**(12): p. 883-898.

72. Chu, T.C., W.F. Ranson, and M.A. Sutton, *Applications of digital-image-correlation techniques to experimental mechanics.* Experimental Mechanics, 1985. **25**(3): p. 232-244.

73. Sutton, M.A., et al., *Determination of displacements using an improved digital correlation method.* Image and Vision Computing, 1983. **1**(3): p. 133-139.

74. Pan, B. and K. Li, *A fast digital image correlation method for deformation measurement.* Optics and Lasers in Engineering, 2011. **49**(7): p. 841-847.

75. Pan, B., *Reliability-guided digital image correlation for image deformation measurement.* Applied Optics, 2009. **48**(8): p. 1535.

76. Lu, H. and P.D. Cary, *Deformation measurements by digital image correlation: Implementation of a second-order displacement gradient.* Experimental Mechanics, 2000. **40**(4): p. 393-400.

77. Kirugulige, M.S., H.V. Tippur, and T.S. Denney, *Measurement of transient deformations using digital image correlation method and high-speed photography: application to dynamic fracture.* Appl. Opt., 2007. **46**(22): p. 5083-5096.

78. Hung, P.-C. and A.S. Voloshin, *In-plane strain measurement by digital image correlation.* Journal of the Brazilian Society of Mechanical Sciences and Engineering, 2003. **25**: p. 215-221.

79. Sjodahl, M., *Accuracy in electronic speckle photography.* Appl. Opt., 1997. **36**(13): p. 2875-2885.

80. Pan, B., et al., *Two-dimensional digital image correlation for in-plane displacement and strain measurement: a review.* Measurement Science and Technology, 2009. **20**(6): p. 062001.

81. Pan, B., et al., *Study on subset size selection in digital image correlation for speckle patterns.* Opt. Express, 2008. **16**(10): p. 7037-7048.

82. Lecompte, D., et al., *Quality assessment of speckle patterns for digital image correlation.* Optics and Lasers in Engineering, 2006. **44**(11): p. 1132-1145.

83. Hua, T., et al., *Evaluation of the quality of a speckle pattern in the digital image correlation method by mean subset fluctuation.* Optics & Laser Technology, 2011. **43**(1): p. 9-13.

84. Kirkpatrick, S.J., D.D. Duncan, and E.M. Wells-Grey, *Detrimental effects of speckle-pixel size matching in laser speckle contrast imaging.* Opt. Lett., 2008. **33**(24): p. 2886-2888.

85. Sjodahl, M. and L.R. Benckert, *Electronic Speckle Photography - Analysis of an Algorithm Giving the Displacement with Subpixel Acuracy* Applied Optics, 1993. **32**(13): p. 2278-2284.

86. Sjodahl, M., *Electronic Speckle Photography - Increased Accuracy by NonIntegral Pixel Shifting.* Applied Optics, 1994. **33**(28): p. 6667-6673.

87. Zhou, P. and K.E. Goodson, *Subpixel displacement and deformation gradient measurement using digital image/speckle correlation (DISC).* Optical Engineering, 2001. **40**(8): p. 1613-1620.

88. Zhang, J., et al., *Application of an improved subpixel registration algorithm on digital speckle correlation measurement.* Optics & Laser Technology, 2003. **35**(7): p. 533-542.

89. Bruck, H., et al., *Digital image correlation using Newton-Raphson method of partial differential correction.* Experimental Mechanics, 1989. **29**(3): p. 261-267.

90. Cofaru, C. and et al., *Evaluation of digital image correlation techniques using realistic ground truth speckle images.* Measurement Science and Technology. **21**(5): p. 055102.

91. Pan, B., et al., *Performance of sub-pixel registration algorithms in digital image correlation.* Measurement Science and Technology, 2006(6): p. 1615.

92. Yamaguchi, I., *Automatic measurement of in-plane translation by speckle correlation using a linear image sensor.* Journal of Physics E: Scientific Instruments, 1986. **19**(11): p. 944.

93. Schnell, U., J. Piot, and R. Dandliker, *Detection of movement with laser speckle patterns: statistical properties.* J. Opt. Soc. Am. A, 1998. **15**(1): p. 207-216.

94. Bhaduri, B., et al., *Simultaneous measurement of translation and tilt using digital speckle photography.* Applied Optics, 2010. **49**(18): p. 3573-3579.

95. Tiziani, H.J., *A study of the use of laser speckle to measure small tilts of optically rough surfaces accurately.* Optics Communications, 1972. **5**(4): p. 271-276.

96. Rose, B., H. Imam, and S.G. Hanson, *Non-contact laser speckle sensor for measuring one- and two-dimensional angular displacement.* Journal of Optics, 1998. **29**(3): p. 115.

97. Rose B., et al., *Laser-speckle angular-displacement sensor: theoretical and experimental study.* Appl. Opt., 1998. **37**(11): p. 2119.

98. Sjodahl, M. and L. Larsson. *Speckle correlation used for measuring microstructural changes in paper*. in *Speckle Metrology 2003*. 2003. International Society for Optics and Photonics.

99. Sjodahl, M. and L. Larsson, *Monitoring microstructural material changes in paper through microscopic speckle correlation rate measurements.* Optics and Lasers in Engineering, 2004. **42**(2): p. 193-201.

100. Sankaran, V., et al., *Polarization Discrimination of Coherently Propagating Light in Turbid Media.* Appl. Opt., 1999. **38**(19): p. 4252-4261.

101. Briers, J.D., *Wavelength dependence of intensity fluctuations in laser speckle patterns from biological specimens.* Optics Communications, 1975. **13**(3): p. 324-326.

102. Briers, J.D., *A note on the statistics of laser speckle patterns added to coherent and incoherent uniform background fields, and a possible application for the case of incoherent addition.* Optical and Quantum Electronics, 1975. **7**(5): p. 422-424.

103. Goodman, J.W., *Some fundamental properties of speckle.* J. Opt. Soc. Am., 1976. **66**(11): p. 1145-1150.

104. Pajuelo, M., et al., *Bio-speckle assessment of bruising in fruits.* Optics and Lasers in Engineering, 2003. **40**(1,Äì2): p. 13-24.

105. Wang, L.V. and H. Wu, *Biomedical Optics: Principles and Imaging*, 2007, Wiley.

106. Piederrière, Y., et al., *Backscattered speckle size as a function of polarization: influence of particle-size and- concentration.* Opt. Express, 2005. **13**(13): p. 5030-5039.

107. Xu, Z., C. Joenathan, and B.M. Khorana, *Temporal and spatial properties of the time-varying speckles of botanical specimens.* Optical Engineering, 1995. **34**(5): p. 1487-1502.

108. Zakharov, P., et al., *Multiple-scattering suppression in dynamic light scattering based on a digital camera detection scheme.* Appl. Opt., 2006. **45**(8): p. 1756-1764.

109. Lu, B., et al., *Comparison of Methods for Reducing the Effects of Scattering in Spectrophotometry.* Appl. Spectrosc., 2006. **60**(10): p. 1157-1166.

110. Tuchin, V.V., *Optical Clearing of Tissues And Blood*2006: SPIE Press.

111. Briers, J.D., *Speckle fluctuations and biomedical optics - implications and applications.* Optical Engineering, 1993. **32**(2): p. 277-283.

112. Braga Jr, R.A., et al., *Biological feature isolation by wavelets in biospeckle laser images.* Computers and Electronics in Agriculture, 2007. **58**(2): p. 123-132.

113. Romero, G.G., E.E. Alan*f*±¬¥s, and H.c.J. Rabal, *Statistics of the dynamic speckle produced by a rotating diffuser and its application to the assessment of paint drying.* Optical Engineering, 2000. **39**(6): p. 1652-1658.

114. Rabelo, G.F., R.A. Braga Júnior, and I.M.D. Fabbro, *Laser speckle techniques in quality evaluation of orange fruits.* Revista Brasileira de Engenharia Agrícola e Ambiental, 2005. **9**: p. 570-575.

115. Romero, G.G., et al., *Bio-speckle activity applied to the assessment of tomato fruit ripening.* Biosystems Engineering, 2009. **103**(1): p. 116-119.

116. Cardoso, R.R., et al., *Frequency signature of water activity by biospeckle laser.* Optics Communications, 2011. **284**(8): p. 2131-2136.

117. Braga, R.A., et al., *Assessment of Seed Viability by Laser Speckle Techniques.* Biosystems Engineering, 2003. **86**(3): p. 287-294.

118. Aizu, Y. and T. Asakura, *Coherent Optical Techniques for Diagnostics of Retinal Blood Flow.* Journal of Biomedical Optics, 1999. **4**(1): p. 61-75.

119. Aizu, Y. and T. Asakura, *Bio-speckle phenomena and their application to the evaluation of blood flow.* Optics & Laser Technology, 1991. **23**(4): p. 205-219.

120. Briers, J.D., *Laser Doppler, speckle and related techniques for blood perfusion mapping and imaging.* Physiological Measurement, 2001. **22**(4): p. R35.

121. Briers, J.D., G. Richards, and X.W. He, *Capillary Blood Flow Monitoring Using Laser Speckle Contrast Analysis (LASCA).* Journal of Biomedical Optics, 1999. **4**(1): p. 164-175.

122. Yuan, S., et al., *Determination of optimal exposure time for imaging of blood flow changes with laser speckle contrast imaging.* Appl. Opt., 2005. **44**(10): p. 1823-1830.

123. Fujii, H., et al., *Blood flow observed by time-varying laser speckle.* Opt. Lett., 1985. **10**(3): p. 104-106.

124. Briers, J.D. and S. Webster, *Laser speckle contrast analysis (LASCA): a nonscanning, full-field technique for monitoring capillary blood flow.* Journal of Biomedical Optics, 1996. **1**(2): p. 174-179.

125. Briers, J.D. and S. Webster, *Quasi real-time digital version of single-exposure speckle photography for full-field monitoring of velocity or flow fields.* Optics Communications, 1995. **116**(1,Äì3): p. 36-42.

126. Yokoi, N. and Y. Aizu, *Improvement of estimation parameters in bio-speckle blood flow imaging.* Optical Review. **17**(3): p. 230-238.

127. Duncan, D.D. and S.J. Kirkpatrick, *The copula: a tool for simulating speckle dynamics.* J. Opt. Soc. Am. A, 2008. **25**(1): p. 231-237.

128. Rabal, H., et al., *Numerical model for dynamic speckle: an approach using the movement of the scatterers.* Journal of Optics A: Pure and Applied Optics, 2003. **5**(5): p. S381.

129. Federico, A., et al., *Simulation of dynamic speckle sequences and its application to the analysis of transient processes.* Optics Communications, 2006. **260**(2): p. 493-499.

130. Sendra, G.H., et al., *Numerical model for simulation of dynamic speckle reference patterns.* Optics Communications, 2009. **282**(18): p. 3693-3700.

131. Reulen, J.P.H., et al., *Precise Recording of Eye-Movement - The IRIS Technique .1.* Medical & Biological Engineering & Computing, 1988. **26**(1): p. 20-26.

132. Kasprzak, H.T. and D.R. Iskander, *Ultrasonic Measurement of Fine Head Movements in a Standard Ophthalmic Headrest.* Instrumentation and Measurement, IEEE Transactions on, 2010. **59**(1): p. 164-170.

133. Greenwood, R., *Neurological Rehabilitation*, 1997, Psychology Press. p. 173.

134. Bing, P. and et al., *Performance of sub-pixel registration algorithms in digital image correlation.* Measurement Science and Technology, 2006. **17**(6): p. 1615.

135. IEC, *Safety of laser products*, 2007, International Electrotechnical Commission: Geneva.

136. Institution, A.N.S., *American National Standard for Safe Use of Lasers*, in *ANSI Z136.1*, A.N.S. Institution, Editor 2007.

137. ANSI, *American National Standard for Safe Use of Lasers*, 2007, American National Standards Institute.

138. Photometrics. Available from: http://www.photometrics.com/.

139. Mathworks, T., *Matlab*, 2010.

140. Braga, R.A., et al., *Reliability of biospeckle image analysis.* Optics and Lasers in Engineering, 2007. **45**(3): p. 390-395.

141. Tuchin, V.V., *Light scattering study of tissues.* Physics-Uspekhi, 1997. **40**(5): p. 495.

142. Ennos, A.E., *Speckle interferometry*, in *Laser Speckle and Related Phenomena*1975, Springer Berlin Heidelberg. p. 203-253.

143. Piederrière, Y., et al., *Scattering through fluids: speckle size measurement and Monte Carlo simulations close to and into the multiple scattering.* Opt. Express, 2004. **12**(1): p. 176-188.

144. Meyer, W.V., et al., *Multiple-scattering suppression by cross correlation.* Appl. Opt., 1997. **36**(30): p. 7551-7558.

145. Semenov, D., I. Sidorov, and E. Nippolainen, *Distance sensing to rough semitransparent and multiscattering materials using dynamic speckles.* Appl. Opt., 2009. **48**(28): p. 5266-5273.

146. Tuchin, V.V. and S.o.P.-o.I. Engineers, *Tissue optics: light scattering methods and instruments for medical diagnosis* 2007: SPIE/International Society for Optical Engineering.

147. Bland, J. and Altman, D., *Statistical methods for assessing agreement between two methods of clinical measurement.* The Lancet 1986. **327** (8476) p. 307-310.

148. Bland, J. and Altman, D., *Measuring agreement in method comparison studies.* Stat Methods Med Res 1999. **8** (2) p. 135-160.

149. Coakley, D. and J. Phillips, *Ocular Microtremor of Patients with Brain-Stem Injury.* Journal of Neurology Neurosurgery and Psychiatry, 1984. **47**(10): p. 1146-1146.

150. Leahy, M.J., *Microcirculation Imaging*2012: Wiley.

151. Acharya U, R., E.Y.k. Ng, and J.S. Suri, *Image Modeling of the Human Eye*2008: Artech House.

152. King, P., *Low level laser therapy: A review.* Lasers in Medical Science, 1989. **4**(3): p. 141-150.

153. Kumar, B.V.K.V. and L. Hassebrook, *Performance measures for correlation filters.* Appl. Opt., 1990. **29**(20): p. 2997-3006.

154. Kumar, B.V.K.V., A. Mahalanobis, and R.D. Juday, *Correlation Pattern Recognition*2005: Cambridge University Press.

155. Rabal, H.J., *Numerical model for dynamic speckle: an approach using the movement of the scatterers.* Journal of Optics A: Pure and Applied Optics, 2003. **5**(5): p. S381.

156. Thomas, J.G. and d. Coakley, *Transducer for recording fine eye movement through the closed eyelid.* Medical and Biological Engineering and Computing, 1977. **15**(6): p. 705-706.

157. Bojanic, S., T. Simpson, and C. Bolger, *Ocular microtremor: a tool for measuring depth of anaesthesia?* British Journal of Anaesthesia, 2001. **86**(4): p. 519-522.

158. Coakley, D., et al., *Ocular Microtremor and Brain-Stem Function - Recording Methods and Physical Characterization.* Clinical Physics and Physiological Measurement, 1986. **7**(4): p. 395-396.

159. Ramdane-Cherif, Z., et al., *An Autoregressive (AR) Model Applied to Eye Tremor Movement, Clinical Application in Schizophrenia.* Journal of Medical Systems, 2004. **28**(5): p. 489-495.

160. Tuchin, V.V., *Handbook of Optical Biomedical Diagnostics*, 2002, SPIE Press.

Appendix (I)

1 Simulator Calibration

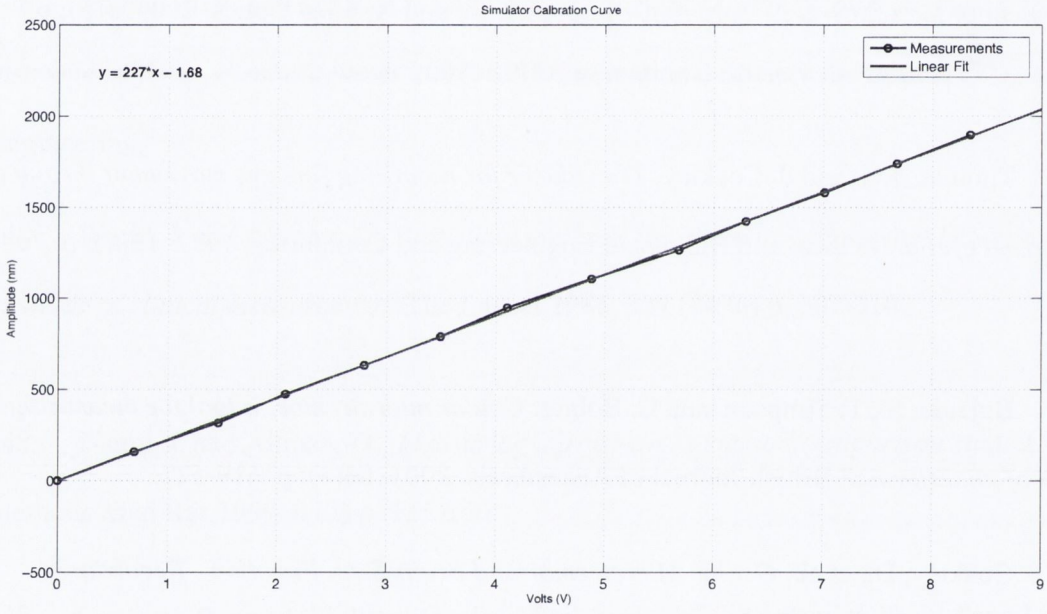

Figure 1. Amplitude calibration of the OMT simulator.

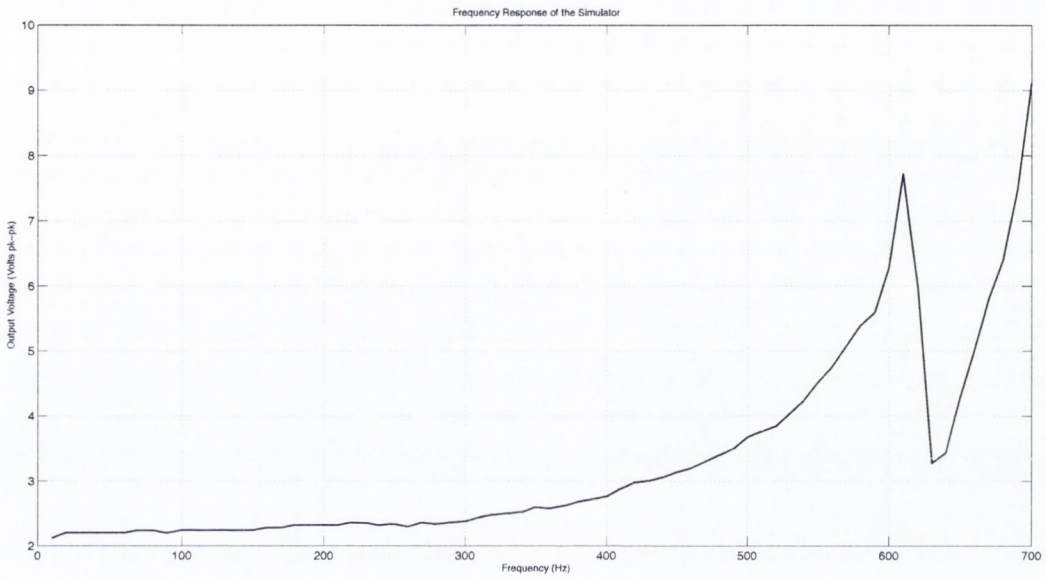

Figure 2. Frequency Calibration of the OMT simulator.

Appendix (II)

1 *In-Vivo* Results: Type 1 Spectra

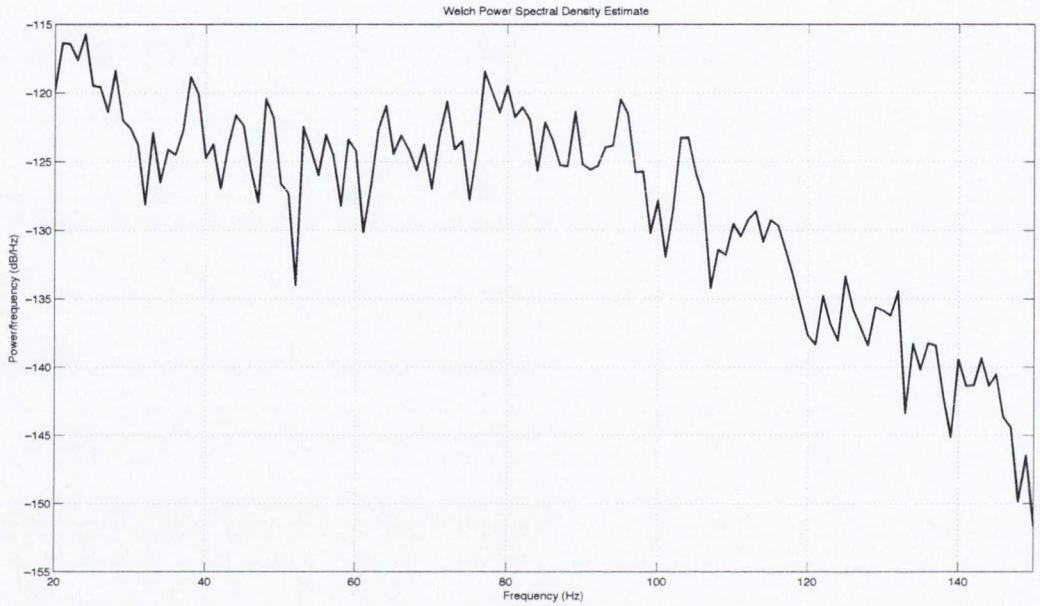

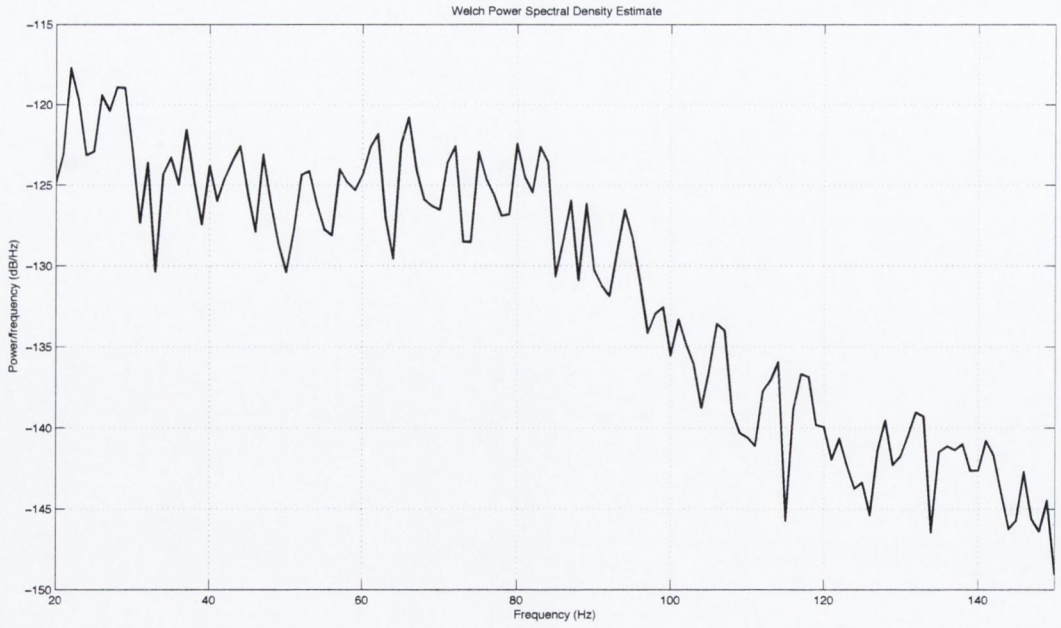

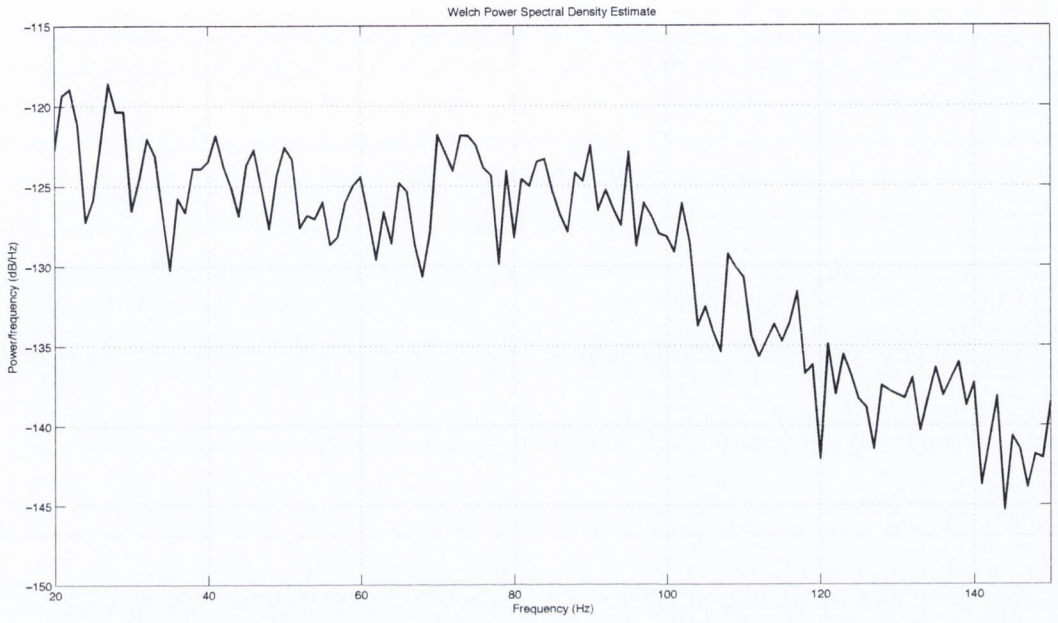
Welch Power Spectral Density Estimate
Power/frequency (dB/Hz)
Frequency (Hz)
−115
−120
−125
−130
−135
−140
−145
−150
20
40
60
80
100
120
140

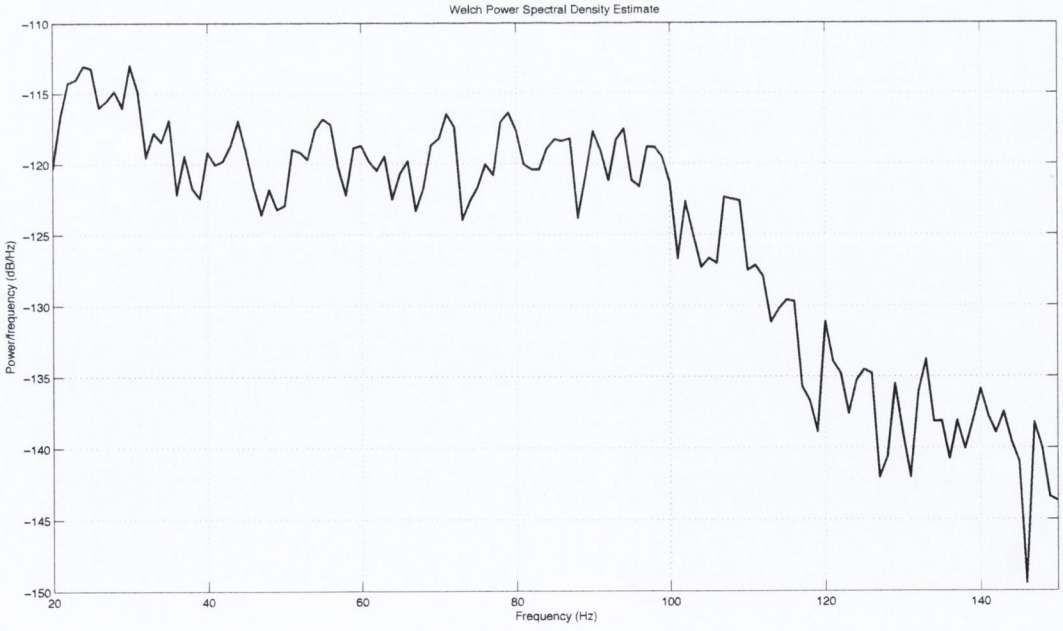
Welch Power Spectral Density Estimate
Power/frequency (dB/Hz)
Frequency (Hz)
−110
−115
−120
−125
−130
−135
−140
−145
−150
20
40
60
80
100
120
140

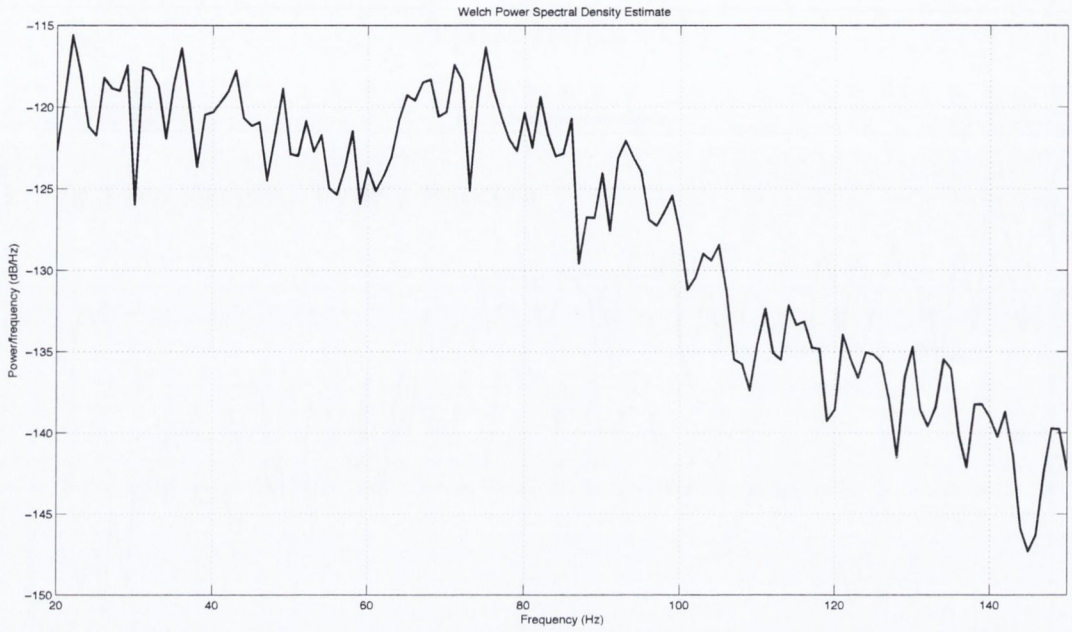
Welch Power Spectral Density Estimate
Power/frequency (dB/Hz)
Frequency (Hz)
−115
−120
−125
−130
−135
−140
−145
−150
20
40
60
80
100
120
140

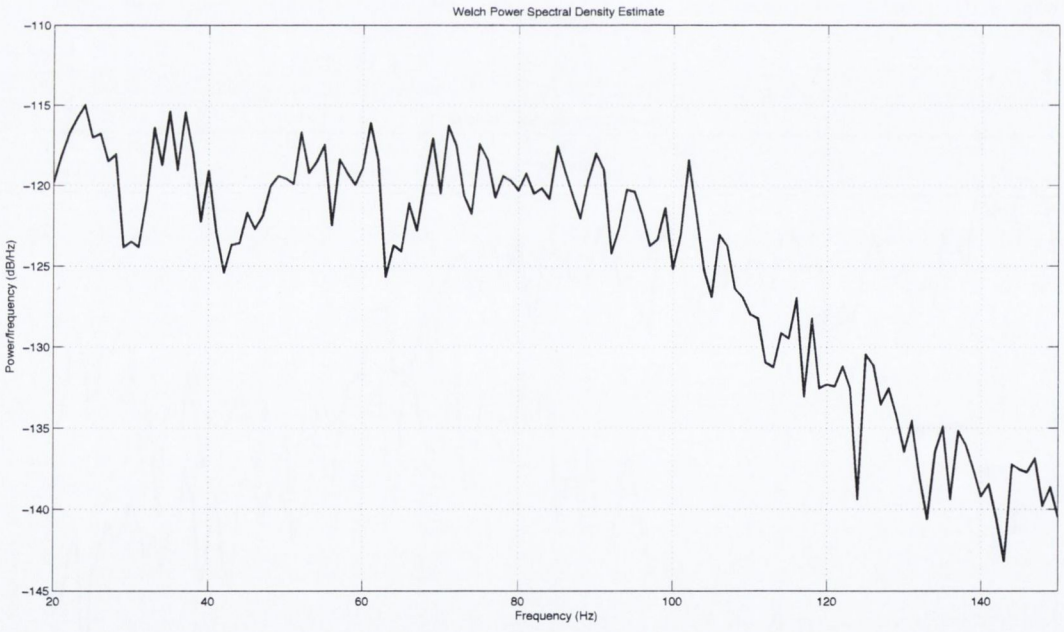
Welch Power Spectral Density Estimate
Power/frequency (dB/Hz)
Frequency (Hz)
−110
−115
−120
−125
−130
−135
−140
−145
20
40
60
80
100
120
140

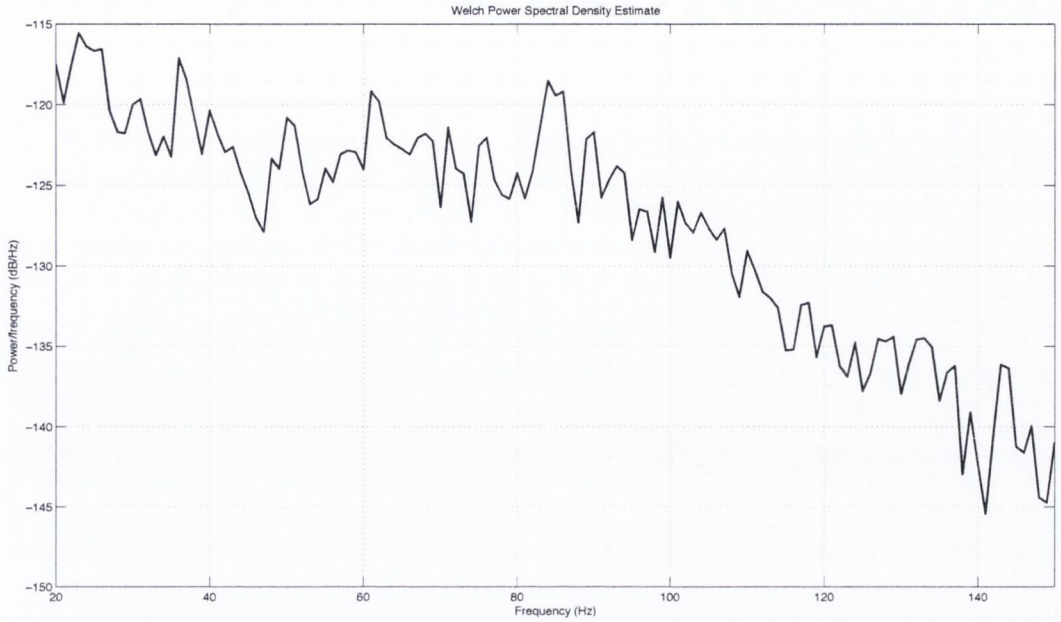
Welch Power Spectral Density Estimate
Power/frequency (dB/Hz)
Frequency (Hz)
−115
−120
−125
−130
−135
−140
−145
−150
20
40
60
80
100
120
140

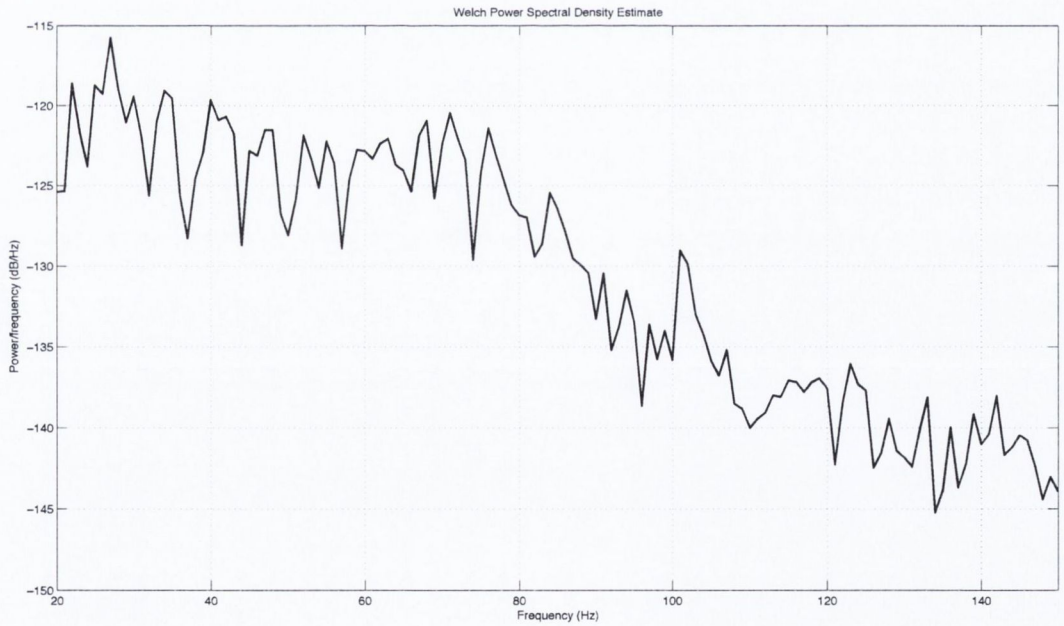
Welch Power Spectral Density Estimate
Power/frequency (dB/Hz)
Frequency (Hz)
−115
−120
−125
−130
−135
−140
−145
−150
20
40
60
80
100
120
140

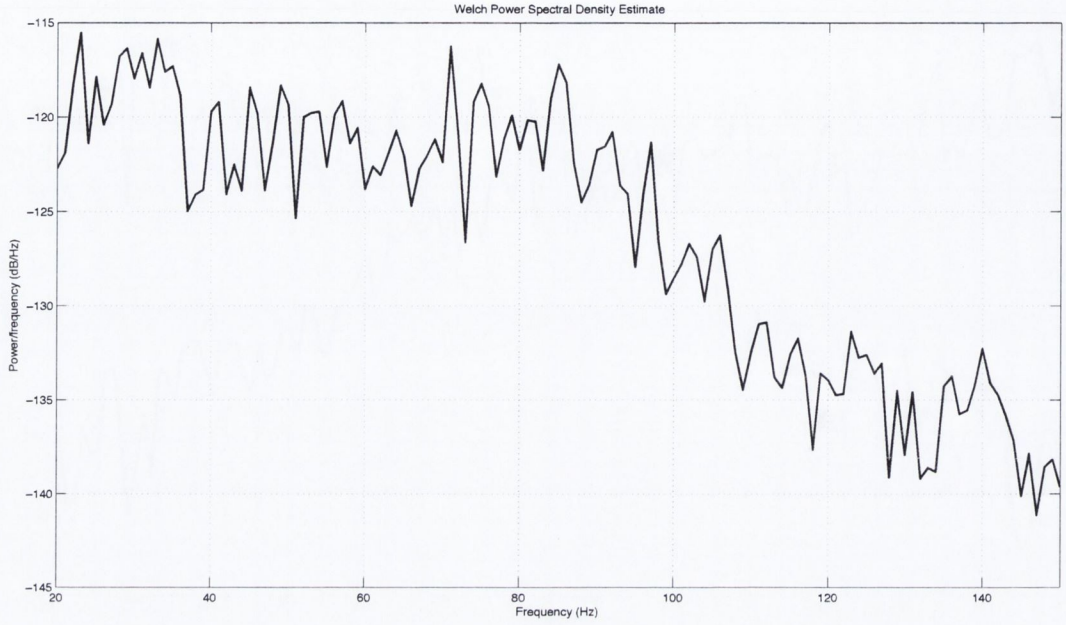
Welch Power Spectral Density Estimate
Power/frequency (dB/Hz)
Frequency (Hz)
−115
−120
−125
−130
−135
−140
−145
20
40
60
80
100
120
140

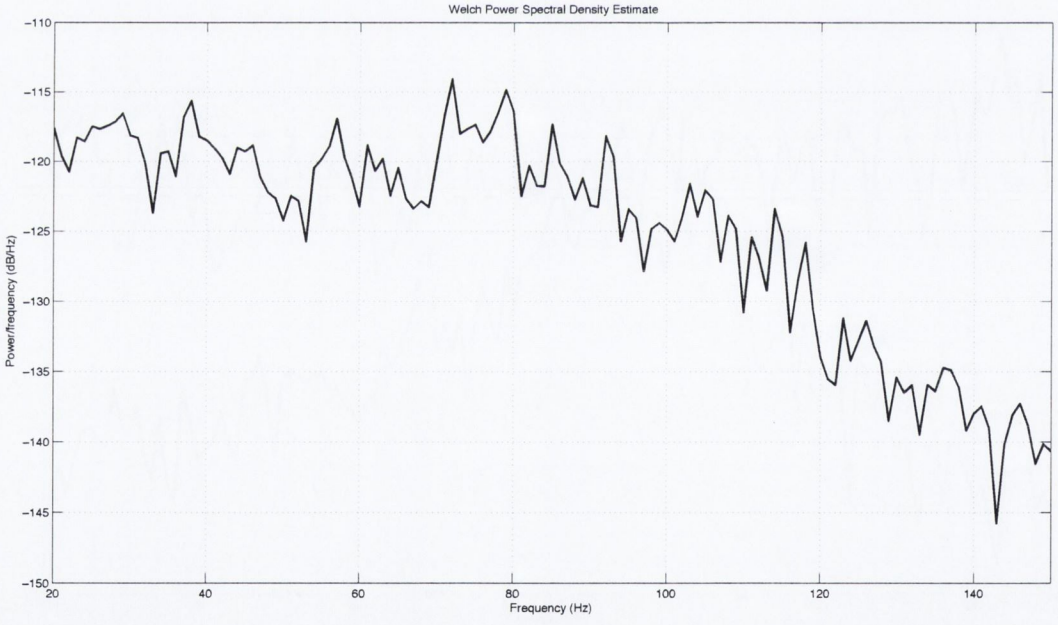
Welch Power Spectral Density Estimate
Power/frequency (dB/Hz)
Frequency (Hz)
−110
−115
−120
−125
−130
−135
−140
−145
−150
20
40
60
80
100
120
140

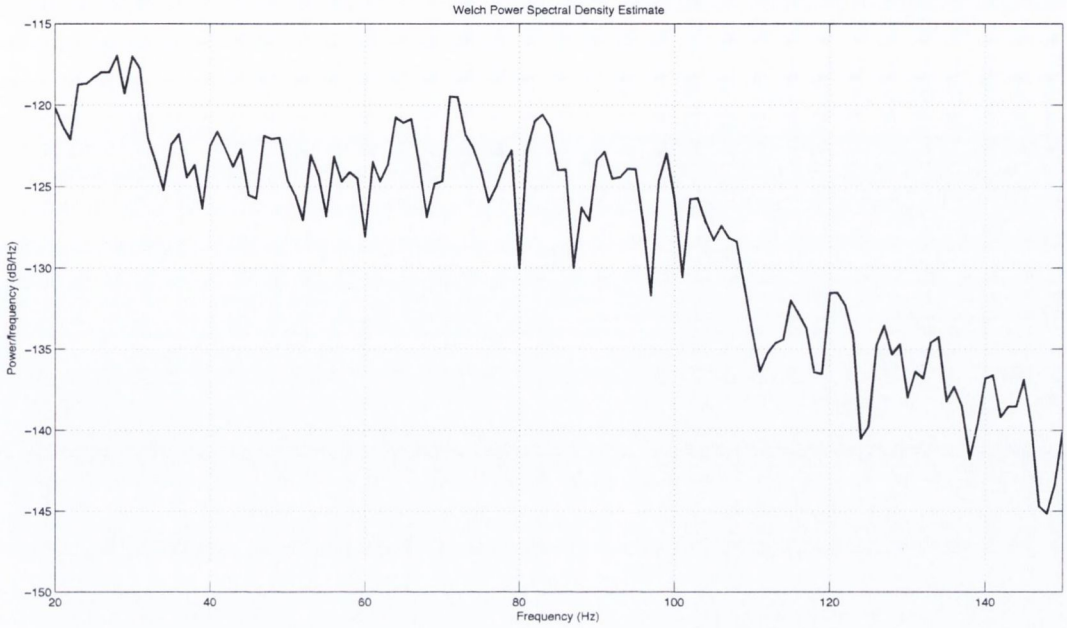
Welch Power Spectral Density Estimate
Power/frequency (dB/Hz)
Frequency (Hz)
−115
−120
−125
−130
−135
−140
−145
−150
20
40
60
80
100
120
140

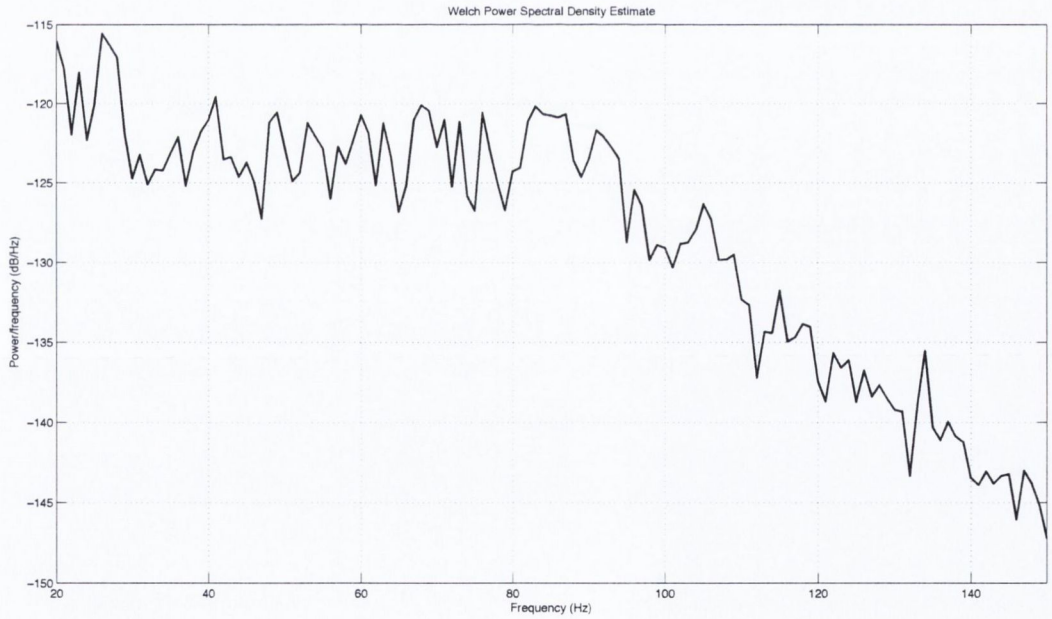
Welch Power Spectral Density Estimate
Power/frequency (dB/Hz)
Frequency (Hz)
−115
−120
−125
−130
−135
−140
−145
−150
20
40
60
80
100
120
140

2 *In-Vivo* Results: Type 2 Spectra

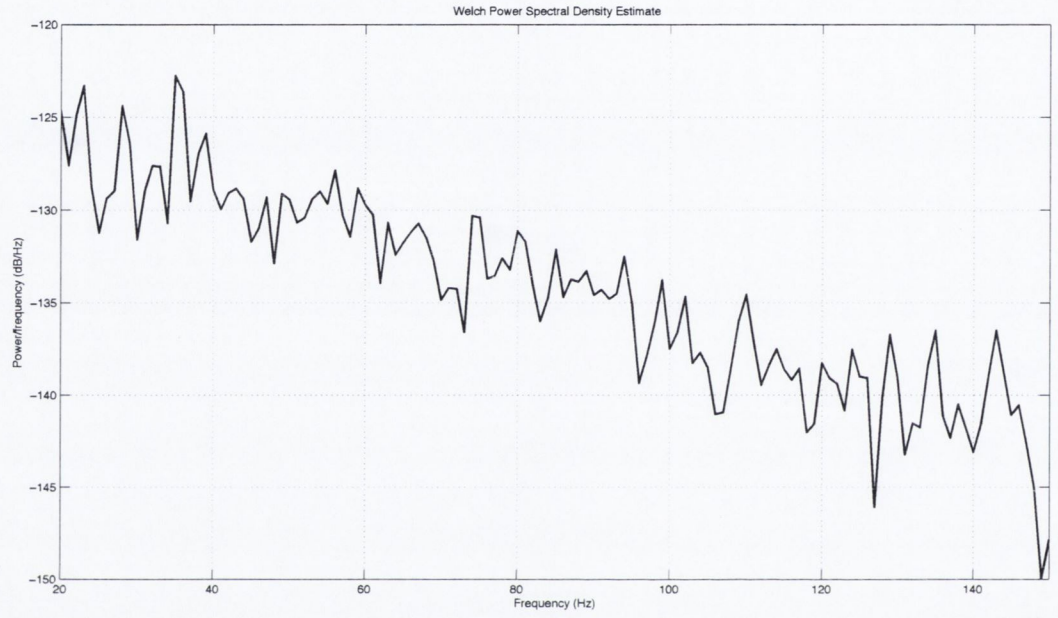

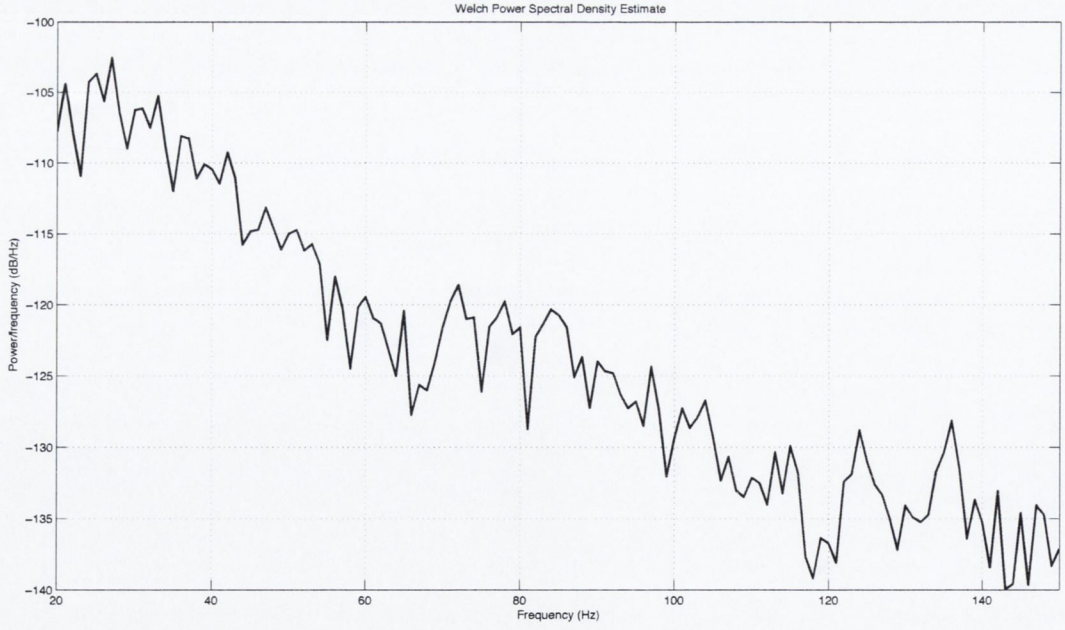

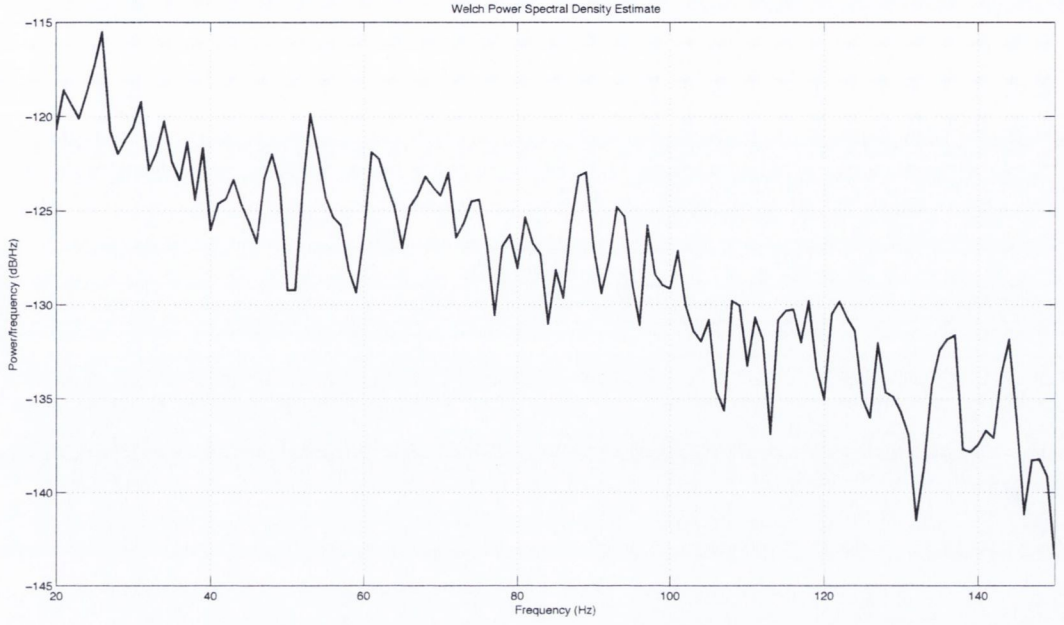
Welch Power Spectral Density Estimate
Power/frequency (dB/Hz)
Frequency (Hz)
−115
−120
−125
−130
−135
−140
−145
20
40
60
80
100
120
140

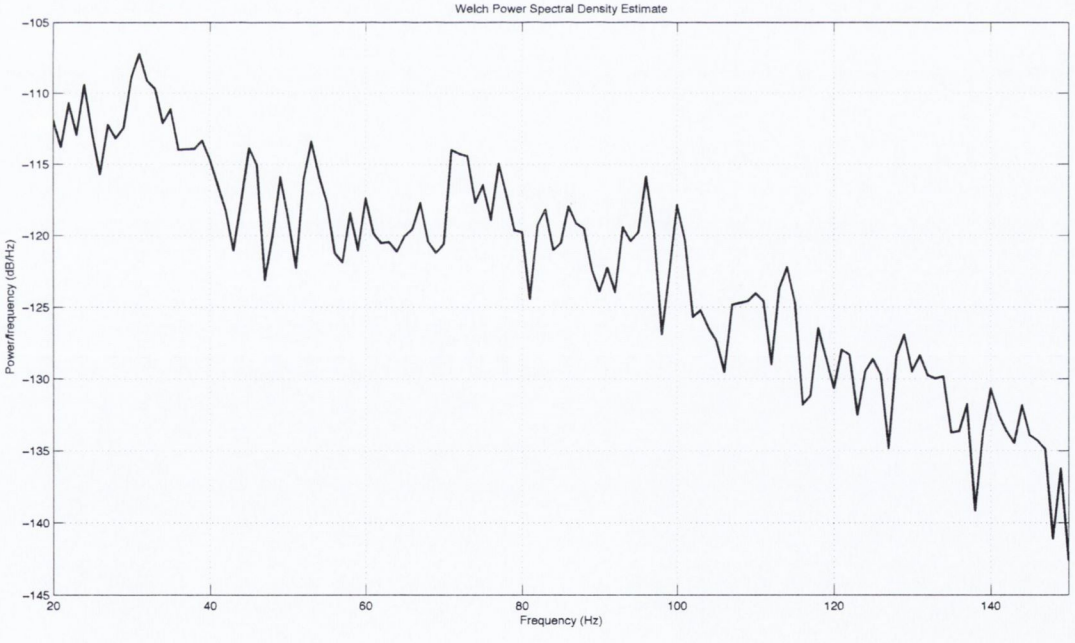
Welch Power Spectral Density Estimate
Power/frequency (dB/Hz)
Frequency (Hz)
−105
−110
−115
−120
−125
−130
−135
−140
−145
20
40
60
80
100
120
140

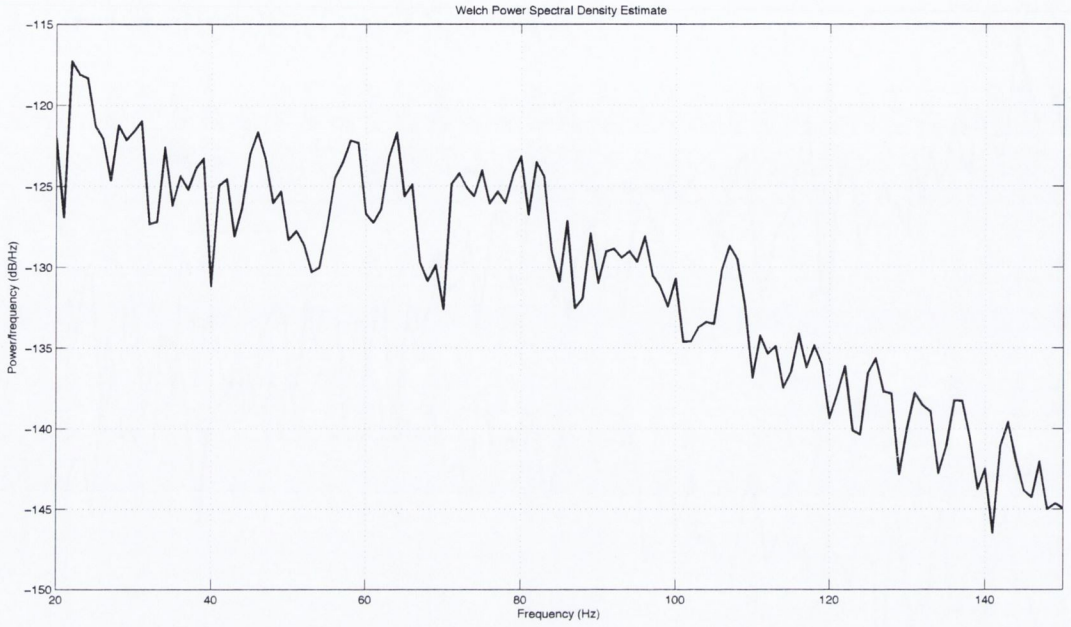
Welch Power Spectral Density Estimate
Power/frequency (dB/Hz)
Frequency (Hz)
−115
−120
−125
−130
−135
−140
−145
20
40
60
80
100
120
140

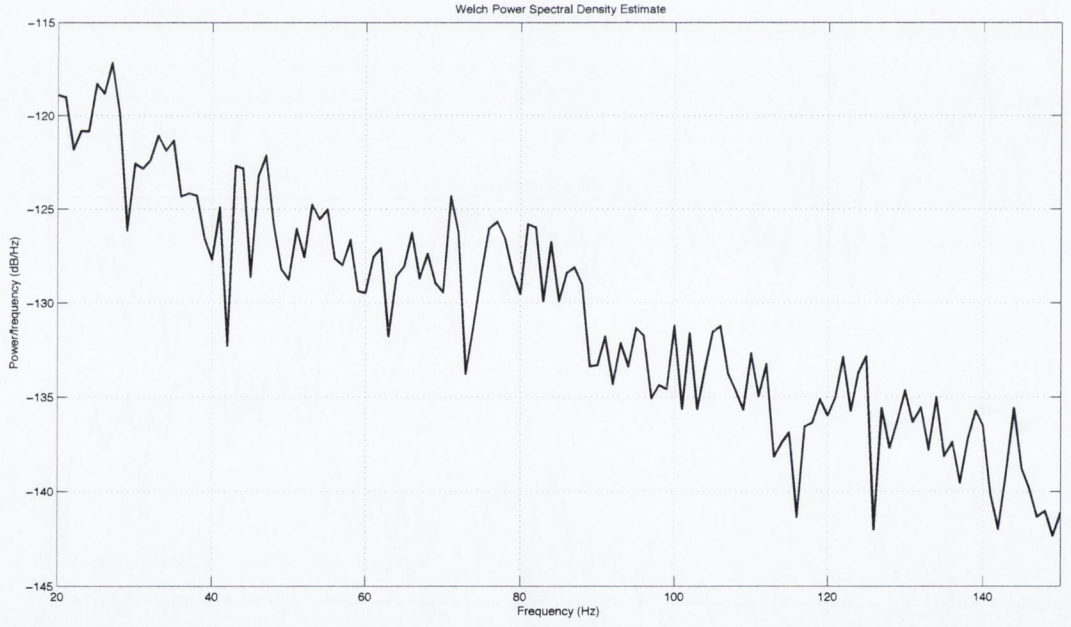
Welch Power Spectral Density Estimate
Power/frequency (dB/Hz)
Frequency (Hz)
−115
−120
−125
−130
−135
−140
−145
20
40
60
80
100
120
140

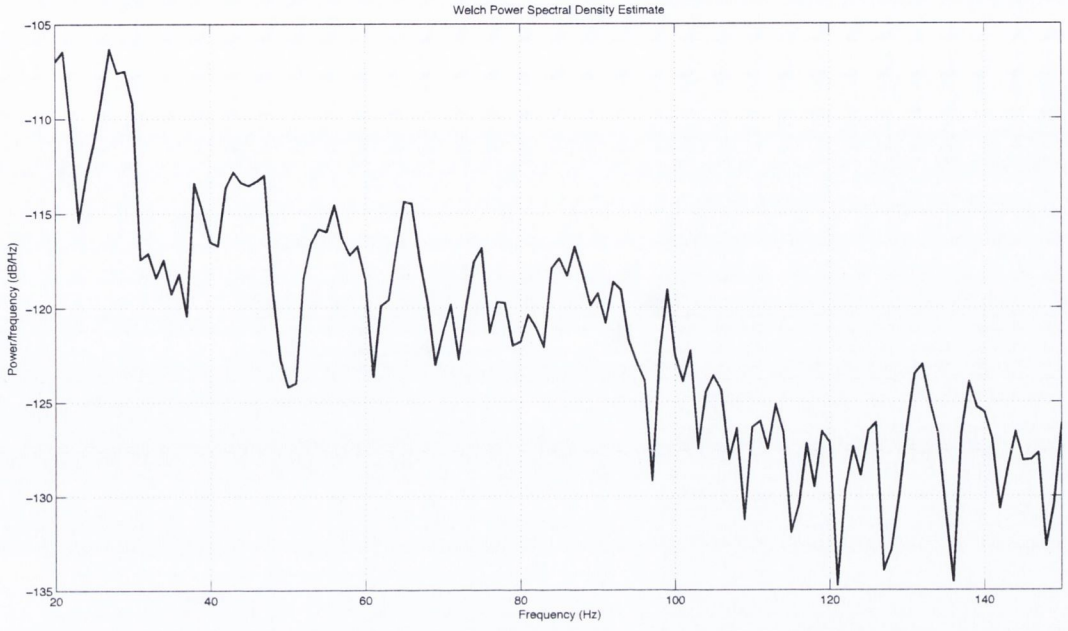
Welch Power Spectral Density Estimate
Power/frequency (dB/Hz)
Frequency (Hz)
−105
−110
−115
−120
−125
−130
−135
20
40
60
80
100
120
140

Laser Speckle Correlation as a Non-Contact Ocular Microtremor Measurement Technique

Emer Kenny

Abstract

Ocular microtremor (OMT) is high frequency (about 84Hz), low amplitude (between 12-216μrad) fixational eye movement present in all healthy people. Benefits of measuring OMT have been proven in a number of clinical conditions. To date, the most widely used research tool to measure OMT has been an eye-contacting piezoelectric probe technique (PZT). Ideally, for practical clinical use, a device to measure OMT would be non-contact. The aim of this thesis is to investigate and develop a non-contact laser speckle correlation method to measure OMT in the human eye. The proposed system is tested and validated both *in-vitro* and *in-vivo*. The system was found to have a resolution of 4μrad and a dynamic range of 4-5000μrad. The results of testing the speckle correlation system on a group of 20 healthy subjects found an average OMT peak frequency of 78±3.86Hz and a mean amplitude of 21.42 ±7.01μrad peak-to-peak.